Interactions between cement and combined concrete admixtures

The influence on cement paste rheology

Karel Lesage

Examination committee:
Prof. dr. ir. J. Berlamont, chair (KU Leuven)
Prof. dr. ir. L. Taerwe, chair (UGent)
Prof. dr. ir. L. Vandewalle, supervisor (KU Leuven)
Prof. dr. ir. G. De Schutter, supervisor (UGent)
Prof. dr. ir.-arch. Ö. Cizer (KU Leuven)
Prof. dr. M. Smet (KU Leuven)
Prof. dr. B. Goderis (KU Leuven)
Prof. dr. ir. V. Boel (UGent)
Prof. dr. ir. N. De Belie (UGent)
Prof. dr. ir. T. De Mulder (UGent)
Dr. N. Roussel (IFSTTAR)

Dissertation presented
in partial fulfillment
of the requirements
for the degree of
Doctor of Engineering

June 2014

Legal depot D/2014/7515/82
ISBN 978-94-6018-858-9

Acknowledgement

I like to thank my supervisors prof. dr. ir. Lucie Vandewalle and prof. dr. ir. Geert De Schutter (Ghent University) who both facilitated this joint doctorate at their university. I especially appreciate the liberty that was entrusted to me by these experts in going into more depth in the different fields of science concerning the multidisciplinary topic.

A special word of thanks to my assessor prof. dr. ir.-arch. Özlem Cizer, who's daily practice I was allowed to follow from nearby. This appeared to be a useful guide in exploring the scientific and academic world from within. I am very grateful for the many reading and commenting, not only on this book, but also on all my papers.

The examination committee is greatly acknowledged for their effort, especially prof. Mario Smet for the guidance in the superplasticizer synthesis and dr. Nicolas Roussel (IFSTTAR, France) for the fruitful discussions at several international conferences.

The Research Foundation – Flanders is acknowledged for the funding of the research project "Controlling the rheology of concrete for the combined use of plasticizers/retarders and accelerators", wherein this doctorate is embedded. In this respect, I also like to show my gratitude to the project partners at the Royal Military Academy in Brussels: prof. dr. John Vantomme, Cdt. ir. Bram Desmet, Jun and Peter.

For the technical aspects of this research I am thankful for the expertise within Reyntjens laboratory and the helpful hands of Stephan, Gerda, Filip, Iris, Luc W. and Frank. Furthermore, I also want to express my appreciation for the efficiency and care of the KU Leuven departmental support by Paul, Rita, Danny and Freddy. Similarly, I need to extend my gratitude to the

different other labs and departments which I visited for conducting parts of my research:

- At the KU Leuven department of Materials Engineering, I like to thank Bram, Lubica, Remus, Yiannis, Silviana and Lieven for technical support and fruitful discussions on material properties and characterization.
- At the SMaRT division of the KU Leuven department of Chemical Engineering, great rheological instruments and appreciated technical support was provided by Anja, Ruth, Jeroen, Bob, Bruke and Ward.
- For the work on the polymer synthesis, I am grateful for the practical help of Stijn and Joice from the KU Leuven Chemistry Department and from Veerle Boterberg from Ghent University.
- Mineralogical studies were performed at the department of Geology at KU Leuven where I want to thank Ruben, Gilles, Rieko and Elvira.
- I like to thank Jeroen, Pieter and Serge from Magnel Laboratory (Ghent University) for the enlightened discussions and enjoyable moments.

For the non-technical aspects of the last four and a half years, I owe many thanks to several people. Sitting at the first row, my girlfriend Tess has continuously supported me and I am thankful for the lovely live that we have built together in-between the periods of hard work. My support and energy are now fully with her for the remaining of her doctorate in economics. It is also with sincere gratitude that I like to thank my parents, sister and close family for their tremendous amount of patience and positive support. The enjoyable moments with family and friends are highly appreciated as energizing and fun.

Finally, I like to thank my colleagues at the Building Technology division in Leuven for the nice talks and friendly atmosphere. The collegiality with Kristof, Salman, Els, Joren, Rutger, Iveta, Nicho, Roel and our secretary Kristine and the partly shared mission with most of them was truly inspirational to me. With the windows pointed at the beautiful Arenberg castle, our buzzing offices were a nice place to work.

Thanks to you all!

Karel

Abstract

During the last decades, innovative concrete applications have been the result of technological developments as new processing techniques, the use of concrete admixtures and advanced materials. All these improvements increase the demand for better performing concrete with enhanced workability. However, the lack of reliable engineering tools in traditional concrete production methods has led to some inconsistent control of the workability. Therefore, today's research is increasingly investigating advanced models that capture the flow behavior of fresh concrete as accurately as possible. These models are continuously improving but generally keep facing problems which are linked to the agglomeration of the cement particles and to the implementation of combined concrete admixtures.

The objective of this work is to investigate the rheological mechanism in cement paste for the combined use of superplasticizer, retarder and accelerator. In particular, an effect on the particle agglomeration is aimed for in order to contribute to a more fundamental understanding of the concrete's flow behavior.

Concerning the superplasticizer impact on cement paste, thermodynamic modelling and mineralogy studies led to the conclusion that the superplasticizer can change the hydrate morphology to such an extent that the interparticle contact forces are modified. The extra addition of retarder led to a densified polymer layer at the cement grain surface which contributed to the steric stabilization of the cement paste. An additional electrostatic effect and the induced changes in hydrate morphology are also demonstrated to contribute to the low paste viscosity. With the extra addition of a calcium salt accelerator to the cement paste, an interstitial structure was assumed to diminish the rheological effect of the polymer layer.

All the developed conceptual mechanisms were implemented in a coherent agglomeration model, based on measurable parameters. In this model, the internal and external hydrates in a cement agglomerate were defined and quantified. Generally, the cumulative amount of hydrates within the agglomerates influenced the agglomerate stability and the amount of external hydrates determined the reagglomeration rate. For the superplasticizer only, a proportional relation was found between the change in agglomeration rate and the external agglomerate connectivity while, for the extra addition of retarder and accelerator, a reverse relation was found. The latter was attributed to a mechanical contribution of the interstitial volume. On the one hand, the retarder creates a source of slowly hydrating nuclei and particles in that volume and, on the other hand, these particles are expected to coagulate due to the accelerator addition. In the second case, the interstitial volume also delivered a contribution to the stress resistance of the cement paste at rest.

This fundamental research combines dedicated analytical methods and conceptual models to improve the understanding of particle agglomeration and contributes to a more extensive insight into the concrete rheology.

Samenvatting

In de laatste decennia werden innovatieve betontoepassingen ontwikkeld door nieuwe productiemethoden, het gebruik van hulpstoffen, geavanceerde materialen, etc. Deze technologische vooruitgang heeft geleid tot een toenemende vraag naar performanter beton met een verbeterde verwerkbaarheid. Echter, de gebruikelijke productiemethoden hebben al aangetoond de controle over de verwerkbaarheid van het vers beton niet volledig te beheersen. Daarom legt het hedendaags wetenschappelijk onderzoek zich toe op geavanceerde modellen om het vloeigedrag zo goed mogelijk te begrijpen. Deze modellen worden continu verder uitgewerkt maar ondervinden over het algemeen grote moeilijkheden om de agglomeratie van cementdeeltjes en het effect van gecombineerde hulpstoffen in rekening te brengen.

Het doel van dit onderzoek is om het reologisch mechanisme in cementpasta's te onderzoeken met inbegrip van de combinatie van een superplastificeerder, vertrager en versneller. In het bijzonder wordt het effect op de deeltjesagglomeratie beoogd om bij te dragen tot een beter fundamenteel begrip van het vloeigedrag van beton.

Met betrekking tot de impact van de superplastificeerder, werd door thermodynamische modellering en analyse van de mineralogie geconcludeerd dat de superplastificeerder in staat is om de morfologie van de hydraatfasen zodanig te wijzigen dat de deeltjesinteractie verandert. De extra toevoeging van de vertrager bleek te leiden tot een verdicht polymeernetwerk op de cementpartikels, wat bijdraagt tot de sterische stabilisatie van de cementpasta. Een bijkomend elektrostatisch effect en geïnduceerde veranderingen in de morfologie werden eveneens aangetoond bij te dragen tot de lage viscositeit van de pasta. Met de extra toevoeging van een calciumzout als versneller, werd de interstitiële structuur verondersteld om het polymeereffect te verminderen.

Al deze conceptuele mechanismen werden ingebouwd in een coherent agglomeratiemodel gebaseerd op meetbare parameters. In dit model werden interne en externe hydraatfasen in een cementagglomeraat gedefinieerd en gekwantificeerd. Over het algemeen wordt de stabiliteit van de agglomeraten beïnvloed door de cumulatieve hoeveelheid interne hydraten en de agglomeratiesnelheid beïnvloed door de externe hydraten. Voor enkel de superplastificeerder werd een proportionele relatie gevonden tussen de verandering in agglomeratiesnelheid en de externe connectiviteit van de agglomeraten terwijl, voor de extra toevoeging van vertrager en versneller, eerder een omgekeerde relatie werd gevonden. Deze laatste werd toegekend aan een mechanische bijdrage van het interstitieel volume. Enerzijds, creëert de vertrager een bron van fijne hydraterende partikeltjes in dit volume en, anderzijds, coaguleert de versneller deze fijne partikeltjes nadien. Dit gecoaguleerd volume wordt geacht een bijdrage te leveren aan de structuuropbouw in de cementpasta.

Dit fundamenteel onderzoek combineert diepgaande analytische methoden en conceptuele modellen om het begrip van de deeltjesagglomeratie te vergroten en bij te dragen tot een dieper inzicht in de reologie van beton.

Nomenclature

A_i	Hysteresis area
C	CaO
CN	Calcium nitrate
C1	dry cement powder of cement 1
C1REF	paste of water and C1 without superplasticizer
C1SP	paste of water, C1 and SP
C1SPSG	C1SP paste with additional retarder (SG)
C1SPSGCN	C1SPSG paste with additional accelerator (CN)
CH	portlandite
C-S-H	calcium silicate hydrate
EDX	X-ray spectrometry
ESEM	Environmental Scanning electron microscopy
F	Fe_2O_3
FBRM	Focused Beam Reflectance Measurement
G'_{min}	minimal storage modulus
G'_{max}	maximal storage modulus
H	H_2O
ICP-OES	Inductive Coupled Plasma – Optical Emission Spectroscopy
M	MgO
OPC	ordinary Portland cement
PCE	Polycarboxylate ether

QXRD	Quantitative X-ray diffraction
R_i	agglomeration rate
S	SiO_2
$\overline{S}$	SO_3
SAc	Sodium Acetate
SCC	Self Compacting Concrete
SG	Sodium gluconate
SI	Saturation Index
SP	Superplasticizer
TOC	Total Organic Content
XRD	X-ray diffractometry
XRF	X-ray fluorescence

Contents

Chapter 1 - General introduction

1.1 Subject of the research

Concrete is the largest volume material used by man and it has proven to be indispensable for large infrastructure projects. The produced volume of 10km³ of concrete per year is tremendous, compared with fired clay, timber, and steel used in construction, representing respectively about 2, 1.3 km³ and 0.1 km³/yr [1]. The main reasons for its success are the wide availability and low cost of its components (cement, sand, aggregates and water) but also the ease of production and the durable properties of the final product. Moreover, the ability to shape a flowable slurry into a load bearing, durable rock-like material creates exceptional construction opportunities. For all these reasons, concrete is often the most economical and ecological building material for large scale construction projects [1].

Because of the high production volume of concrete, its total energy and CO_2 footprint becomes increasingly important. Therefore, any improvement that contributes to the material properties or performance can have a big impact on costs and environment [1]. To that end, it is expected that the use of environmentally responsible binders and recycled aggregates will increase in the near future. A further reduction of the paste quantity would also beneficially lower the binder content without affecting the hardened properties too much. However, all these measures have minor to severe consequences for the concrete's flowability [1].

During the last decades, processing techniques, admixtures, supplementary cementitious materials, mixing technology, etc. have led to innovative concrete applications such as self-compacting concrete (SCC), environmentally responsible concretes and many others. Particularly the arrival of plasticizing admixtures was essential in improving the flow properties of concrete while contributing to the durability and the strength

enhancement. It allowed a reduced porosity of the hardened material and a partly substitution of cement with industrial-waste materials [2]. Furthermore, the smaller category of hydration controlling admixtures has created the possibility to extend the workable life of fresh concrete and to advance the control on its hardening. These admixtures allow returning unused plastic concrete back to the production plant, preventing unnecessary construction waste.

All the mentioned improvements increase the demand for better performing concrete with enhanced workability. However, as the requirements for higher performance rise, the robustness of the mix design becomes a more critical issue [2]. The traditional production method and the variations in components have proven to be vulnerable in some advanced applications. For example, in few cases, the impact of admixtures on rheology has appeared to be hard to control and sometimes even treacherous. Lack of rheology control has led to defects like incomplete formwork filling (Fig.1.1), honey combing (Fig.1.2), excessive air voids, segregation, etc. This foreclosed a prosperous strength development and targeted durability and, in worst case, it involved a total reconstruction.

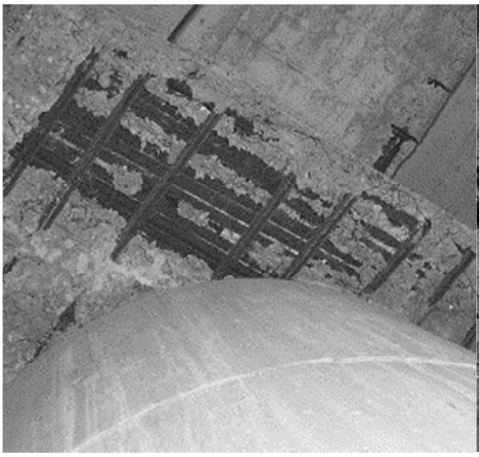

Fig.1.1 Dense reinforcement congested the flowing concrete [3]

Fig.1.2 Insufficient homogenization led to clustering of large aggregates (called honeycombs) [3]

The lack of reliable processing tools to face the evolving performance requirements results from the widely developed empirical practice in construction industry. If one compares the engineering tools for hardened concrete with the ones available for fluid concrete in Fig.1.3, a major discrepancy is detected. In contrast to widely understood and educated construction technology for hard concrete, the relation between material characteristics and properties of interest for fluid concrete is described

only by practical tests. This allows a classification of descriptive flow parameters in function of the mix design but it does not generate predictable fluid performance based on material selection. This practice is longstanding but it now shows limited acceptance to the recent technological advancements because of the increasing complexity.

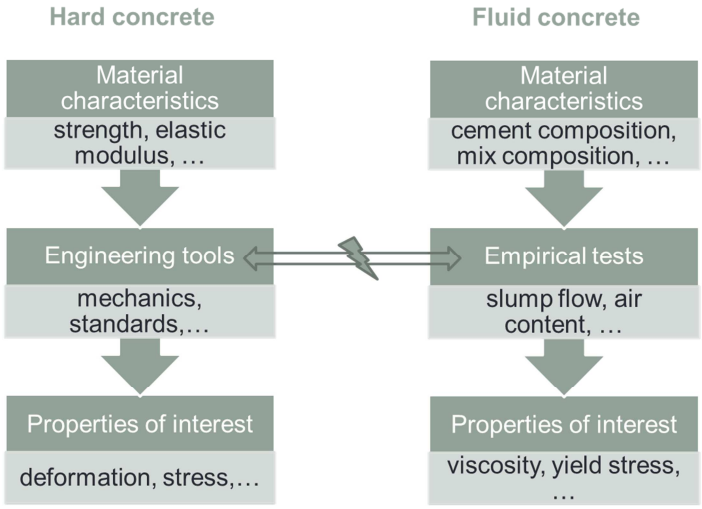

Fig.1.3 The different approach in engineering practice for hard and fluid concrete

The need for more detailed engineering tools is inevitable but requires a "bottom-up" micro- mechanistic theory (e.g. [4, 5]). This theory would have to include a full description of the macroscopic properties of fresh concrete in function of meso -, micro - and nanoscopic features that are introduced in a physical or chemical way during the concrete processing. Implementation of this theory in practice through user-friendly tools would reduce the risks during processing or at least mitigate the inflicted damage. One example of predicted concrete flow during casting is illustrated in Fig.1.4. It can be seen how the experimental casting of concrete (top) compares with the numerical simulations (bottom) for two SCC's with a yield stress equal to 120 Pa (left) and 60 Pa (right). It is observed how the concrete with low yield stress is better able to flow around the steel profile and fill the formwork more consistently.

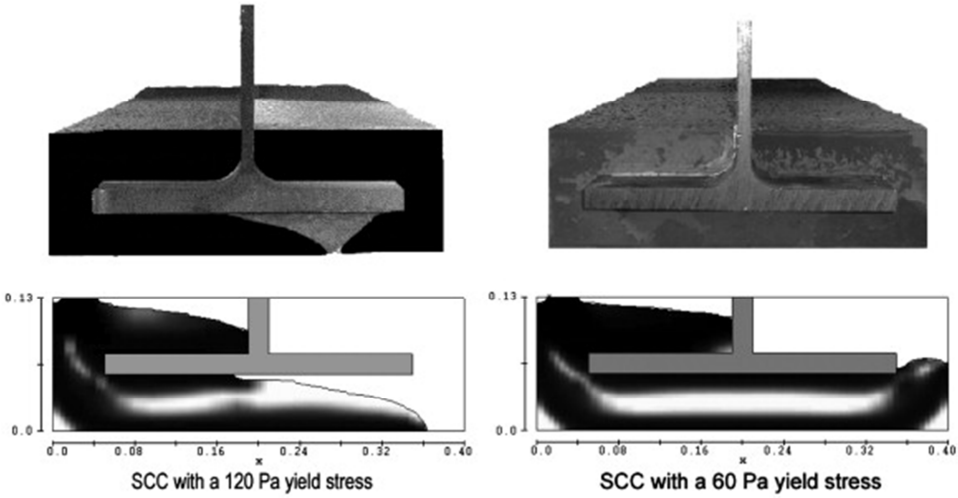

Fig.1.4 Schematic comparison of experimental (top) and computational (bottom) concrete casting [6, 7]

Despite increasing progress in computational and micromechanical modelling, a truly detailed simulation of concrete rheology is nearly impossible with today's ordinary computers and therefore remains unfeasible for practice. To that end, researchers incorporate the motion of the broadly sized particles (cement, sand and aggregates) in simulations through multi-scale or homogenization modelling [2]. These models are continuously improving but generally keep facing problems linked to agglomeration of the particles [8]. Agglomeration makes the particle sizes evolve continuously, making it virtually impossible for the material parameters to remain constant. This remarkable feature that coagulates flowing particles together into an eventually hard and strong building material, remains a major scientific challenge in current concrete rheology research and will be further explored in this thesis.

The present research is embedded in a funded project from the Research Foundation – Flanders entitled "Controlling the rheology of concrete for the combined use of plasticizers/retarders and accelerators". Considering all the above, the subject of this research might seem twofold: On the one hand, one could pursue a better rheological control of any concrete which asks for mature micromechanical models and the underlying fundamental understanding. On the other hand, one might focus on the rheological implications of concrete admixtures which are also not fully understood. The subject of this research has actually been approached from both sides and it is located exactly on the intersection of these two areas of interest: By addressing an important need in model improvement (i.e.

agglomeration), the influence of combined admixtures can be investigated in terms of the obtained model parameters only. This strengthens the bridge between the concrete composition and the rheological performance and thereby contributes to a bottom-up understanding of concrete rheology.

1.2 Research strategy

The scope of this thesis is to perform fundamental research on the physico-chemical interactions between cement particles and concrete admixtures with a complementary set of experiments and analyses. The aim is to assess the micromechanical impact of combined admixtures on cement paste rheology in order to ultimately understand concrete rheology.

Several correlations between mix design and rheological performance have been found in earlier work but only few address the actual inter-particle connection rate, let alone the influence of combined admixtures. Therefore, the cement particle agglomeration will be put at the center of discussion in this thesis for two reasons. First, to identify potential rheological mechanisms that elaborate our conceptual understanding, and second, to channel the rheological influence of combined admixtures towards these mechanisms.

It is the objective of the experimental research to correctly employ the suitable techniques and to quantify all supportive information to achieve the research goals. This experimental part of the research focuses particularly on the effect of admixtures on the physical and chemical state of the cement paste. The rheologically relevant parameters are extracted and applied in conceptual discussions that feed the fundamental model. Encountered research boundaries, like material sensitivity, are pinpointed and concisely handled with more specific experiments.

Based on the experimental research and the available literature, the fundamental research concentrates on the development of a sound understanding of the micromechanical mechanism in cement paste. This objective has resulted in an agglomeration model that links chemical with rheological consequences. In its current state, the model allows a classification of the active micromechanical mechanism based on macroscopic experimental observations for several admixture combinations. In this way, a new instrument is developed to address a

major scientific challenge in concrete rheology and a potential foundation is laid for future engineering tools.

1.3 Outline

The outline of the thesis is visualized in Fig.1.5. After the introduction, a dedicated bibliographical research is presented, introducing all the required research parameters and indicating the current state of the art about the subject of research. The third chapter contains all the applied research materials and methods. The following part of the thesis consists out of three mainly parallel chapters, each one built up around one specific admixture combination. Within these chapters, it is always started with experimental observations that are also useful in determining the right agglomeration parameters. In the following section of each chapter, further experimental analysis and fundamental discussion is provided with the aim to feed the conceptual understanding of cement agglomeration. In every final section of each chapter, the gained insights are implemented in the developing agglomeration model. In this way, the agglomeration model and our fundamental understanding are gradually improved over the three chapters.

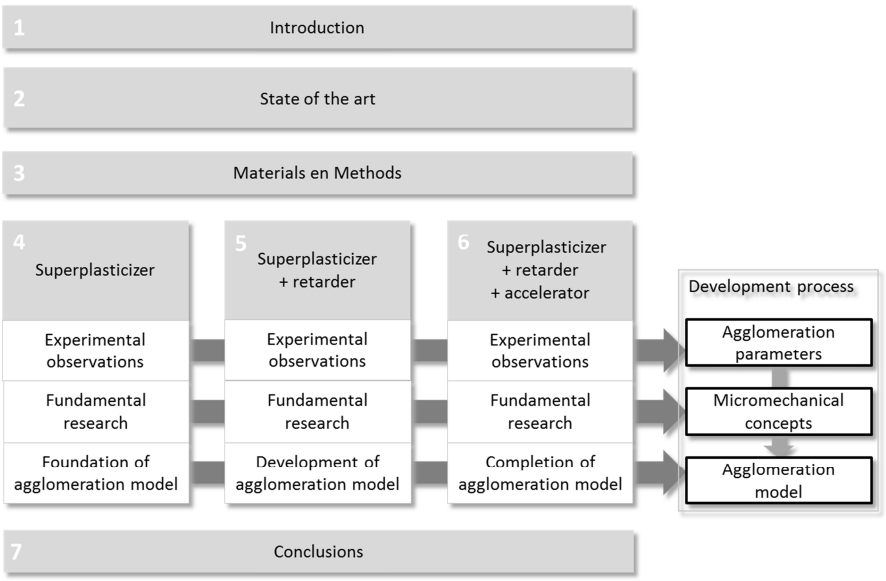

Fig.1.5 Outline of the thesis

Chapter 2 – State of the art After introducing concrete rheology, a comprehensive overview of all materials composing cement paste is given. For each material, the primary relation to rheology is briefly discussed. In the following section, the relevant forces and other rheological parameters are clarified to explain the complexity of the cement paste system. An up-to-date literature status is presented for the application of combined admixtures and the experienced difficulties. Finally, the available literature on the relation between specific cement properties and the consequences for rheology are summarized.

Chapter 3 – Materials and Methods This chapter starts with the description of the selected materials and their characteristics. The particular cement and admixtures are handled after which the mixing procedure of the cement pastes is described. In the second part of this chapter, the analytical methods and instrumentation are elaborated. Special attention is devoted to the different rheological measuring procedures that will be applied in the next chapters of experimental research.

Chapter 4 – Superplasticizer The first section contains the experimental determination of hydration kinetics, oscillatory and hysteresis rheology for cement pastes with and without superplasticizer. The origin of the observed differences is addressed in the second section by the use of additional chemical data and thermodynamic modelling. Finally, in the last section, the basic parameters of the agglomeration model are developed to formalize the relation in-between the experimental observations for the use of superplasticizer.

Chapter 5 – Retarder Parallel to the fourth chapter, the influence of the retarder-superplasticizer combination will be determined by similar experiments as for the pastes with only superplasticizer. The origin of the retarder influence is investigated by different experiments, allowing a more comprehensive view on the retarder action mechanism. After that, again in the third section, all findings are implemented in the agglomeration model that was initiated in the previous chapter. By completing this model, the active micromechanical mechanism of the current admixture combination can be identified.

Chapter 6 – Accelerator Closing the series of three parallel chapters, the experiments are performed here for the admixture combination of superplasticizer, retarder and accelerator. The contribution of the accelerator to the changes in experimental observations is discussed in

terms of literature progress on the calcium influence. Subsequently, the accelerator interference is incorporated in the agglomeration model in the final section.

Chapter 7 – Conclusions and outlook In this final chapter, the general conclusions are summarized and the original contributions and outlook for future research are given.

Chapter 2 - State of the art

In this state of the art, the multifaceted problem of concrete rheology for the use of combined concrete admixtures will be introduced in section 2.1. An essential part of the solution situates itself at the level of the cement paste and the interactions with admixtures. Therefore, an up-to-date elaboration of cement and admixture material properties will be given first in section 2.2. Afterwards, these facets will be integrated in a rheological approach of the cement admixture interactions. Finally, in section 4, the possibilities in modelling the cement paste rheology in function of relevant parameters are explored and further elaborated.

2.1 Introduction to concrete rheology

The term rheology stems from the Greek words “panta rhei” meaning literally “everything flows” which entailed both the obvious flow of river water and landslides but also the slow progression of glaciers and dunes. Today, we attribute flow properties to liquids while solid-like materials are said to deform. A material like concrete can be liquid initially (called *fresh*) and subsequently evolves to its hardened state according to the cement hydration. Therefore, the current use of “concrete rheology” automatically refers to the science of flow and deformation of the concrete in its fresh state.

To characterize concrete rheology, a quantifiable relation should be obtained between the applied stress (e.g. gravitational force during pouring) and the resulting concrete deformation (e.g. concrete flow). This relation can also be investigated for an applied deformation (e.g. vibrating) and the corresponding stress response (e.g. consolidation). Either way, the result is called the flow curve and is often plotted in a stress-strain diagram

(see Fig.2.1), with the measured shear stress in the vertical axis and the speed of deformation (or *shear rate*) in the horizontal axis.

In Fig.2.1, different flow curves can be found, each referring to a material with specific properties. For ordinary materials, like water, we expect a linear relation between the applied shear rate and the measured stress response (i.e. Newtonian). The harder we stir, the more resistance we feel. For other materials, like ketchup, we experience a relatively lower resistance for harder stirring. This corresponds to a flow curve for which the positive increment in shear stress gradually decreases for increasing shear rate which is referred to as shear thinning. For a shear thickening material, like a corn starch solution, the situation is reversed and more stress is caused by higher shearing.

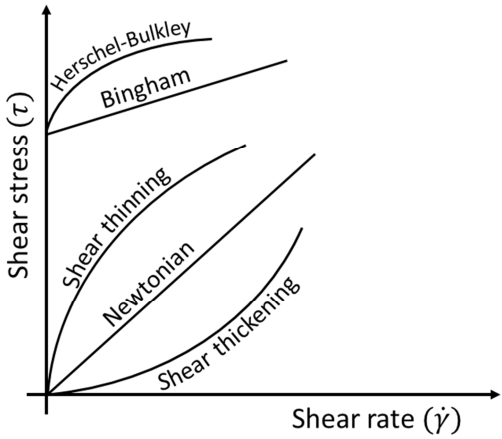

Fig.2.1 Different evolutions of shear stress
in function of applied velocity

Materials that show a stress response for an applied deformation but that do not flow until a critical stress level is reached, are called *yield stress* fluids. Below this critical yield stress, the material will respond as a solid and show a steeply rising elastic stress response. For concrete, having a yield stress, this means that a lot of energy might be required to make the material flow on command. Therefore, practical tools have been developed to apply this energy or to prevent the concrete from resting. For example, by vibrating the poured concrete, it fills the formwork more completely. Similarly, by keeping the mixing drum slowly rotating during transport, more powerful tools are prevented at the building site to make the - otherwise stiffened - concrete flow out of the drum upon arrival.

Once a material is flowing, the speed of flow is determined by its resistance to the flow itself and, for concrete, this will greatly affect the time needed to fill up the casting mold. The resistance to flow is quantified by the tangential *viscosity* which is expressed as the ratio of an increment in shear stress for an increment in shear rate or, alternatively, the slope of the flow curve in Fig.2.1. For example, it can be seen in Fig.2.1 that the slope of the flow curve decreases for increasing shear rate, for shear thinning materials. This corresponds with a decreasing viscosity which can be felt as a lower resistance to stirring of ketchup, for example.

For materials that have a yield stress, like concrete, the slope of the flow curves is called the plastic viscosity. To describe the relation between the yield stress and the plastic viscosity evolution, the following models are most frequently mentioned in case of cement paste:

The power-law model: $\tau = K \cdot \dot{\gamma}^n$ (2.1)

The Bingham model: $\tau = \tau_y + \mu_p \cdot \dot{\gamma}$ (2.2)

The Herschel-Bulkley model: $\tau = \tau_y + K \cdot \dot{\gamma}^n$ (2.3)

In the above models, τ_y is a yield stress parameter, μ_p is a plastic viscosity, K is called the "consistency-factor" [Pa·s^n] and n is the power law index (Eq.2.1) or consistency index (Eq.2.3). It is clear from Fig.2.1 and the equations (2.1) to (2.3) that knowing the yield stress and the viscosity (evolution) of a flowing concrete is a quite complete description of its rheological performance. To that end, considering a certain concrete mix, the viscosity and yield stress can be plotted in a rheograph as in the center of Fig.2.2 (i.e. 'Ref.'). When changes are made to the concrete composition, the rheological effect is comprehensively visualized in this diagram. This tool allows the changes in mix composition to be deduced or implemented in function of a specific rheological performance.

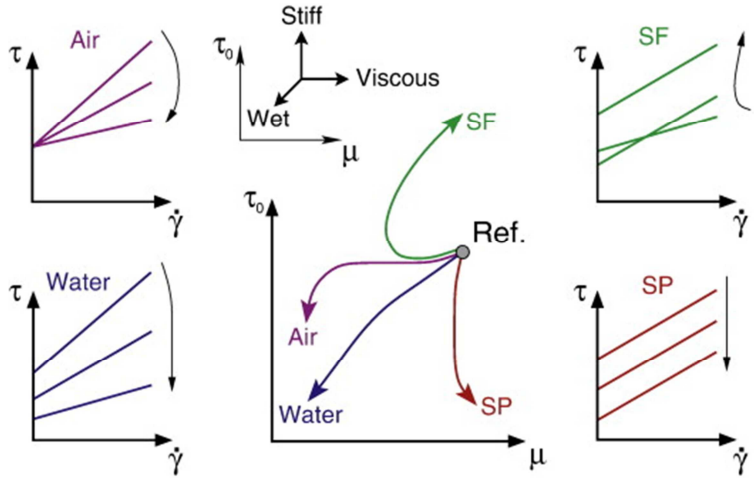

Fig.2.2 A principal rheograph showing the effect of water, air entrainer, silica fume (SF) and superplasticizer (SP) [9, 10]

As can be observed in Fig.2.2, many component dosages can be varied for directing the concrete's rheology along a certain path. For example, the addition of more water will reduce the yield stress, so that flow is easier started and it will similarly lower the plastic viscosity so that the concrete flows faster. The downside of having more water is that the strength of the hardened concrete will be influenced negatively. To that end, superplasticizers (SP) have been developed to cope with this problem. These chemical admixtures can lower the yield stress and control the viscosity without negatively affecting the concrete strength.

The use of superplasticizers aims for a change in rheology but also admixtures with other purposes have an effect on the general concrete rheology. For example, air can be added to improve the durability of the hardened concrete but it appears also to lower the viscosity of the fresh concrete (see Fig.2. 2). These kind of collateral effects are forming important artifacts for prescribing the concrete composition that relates best to the building requirements.

In this thesis, the rheological consequences of the use of combined admixtures in cement paste will be investigated thoroughly. It concerns the combined addition of superplasticizer, retarder and accelerator. The latter two admixtures are intended for changing the hydration speed and not the rheology itself. The existing knowledge on combined admixtures has mostly focused on only two kinds of admixtures and never on three of them. The studied combination is of interest when one would consider long transport of concrete for which the hydration should be retarded and

subsequent pouring conditions for which the hydration should be accelerated, like the construction of long tunnels or remote infrastructure projects in cold weather environment. It is in the scope of this work to find out to what extent these admixtures influence the cement paste rheology and what the exact mechanism is.

The influence of the used chemical admixtures on rheology will be investigated primarily for cement pastes as this removes the collateral effects of granulates and other powders present in concrete. This is a more effective method because the chemical admixtures are active on the level of the cement grain, in contrast to mineral additions, like silica fume or fly ash. Cement paste can also be rheologically characterized by a yield stress and plastic viscosity, just like concrete, as both liquids are suspensions. In the case of concrete we find granulates suspended in cement paste and in the case of cement paste, the cement particles are suspended in water. In this way, the investigated cement paste rheology will contribute to future understanding of the concrete rheology.

2.2 Cement and admixtures

In order to explore the cement-admixture interaction, it is important to know the material properties and the latest state of knowledge concerning their interactions. In this section, the cement material properties will be discussed first, followed by the hydration behavior and some cement related features that are relevant for the rheology. At the end, the admixture material properties will be explained, together with their direct consequences for cement-admixture interactions.

2.2.1 Cement

Cement is known as the most frequently used binder in today's mortar and concrete production. In contact with water, it forms a workable cement paste that eventually stiffens and hardens due to chemical reactions of the cement powder (i.e. hydration). In construction practice worldwide, approximately five types of cement are frequently used, depending on the required properties of the fresh or hard construction element. All types contain a substantial amount of Portland clinker and the most important cement type is a mixture of only Portland clinker and gypsum, called ordinary Portland cement (OPC).

The Portland clinker is the source of metal oxides that hydrate in contact with water. It is produced by heating a mixture of limestone, clay and other materials with similar bulk composition to a temperature of 1450°C [11]. Afterwards, the cooled clinker is ground to a particle diameter smaller than 75µm under the rigorous addition of gypsum to control the final setting and hardening properties of the cement. During grinding the different metal oxides can end up together in one grain of cement powder. Their local relative proportion results in four main individual mineral phases heterogeneously spread out over the particle surface. The average metal oxide composition of the global particle surface contains around 67% CaO (C), 22% SiO_2 (S), 5% Al_2O_3 (A) and 3% Fe_2O_3 (F)[1]. Foreign ions and alkali or metal sulfates are also incorporated in the solid solution. In the following table the clinker phases are listed with their trivial phase name, notation, their frequency, chemical name and formula, average composition and hydration behavior [11].

Table 2.1 Overview of cement minerals and properties (based on [11, 12])

Phase name	**Notation**	**Freq.**	**Chemical name**	**Chemical formula**	**Composition**	**Hydration behavior**
alite	C_3S	50-70%	Tricalcium silicate	$3CaO.SiO_2$	74%CaO 26%SiO_2	Quick hydration (of 3-5%)
belite	C_2S	15-30%	Dicalcium silicate	$2CaO.SiO_2$	65% CaO 35% SiO_2	Slow hydration
aluminate	C_3A	5-10%	Tricalcium aluminate	$3CaO.Al_2O_3$	62% CaO 38% Al_2O_3	Quick hydration
ferrite	$C_4(A,F)$	5-15%	Calcium aluminate ferrite	$3CaO.Al_2O_3.Fe_2O_3$	46% CaO 21% Al_2O_3 33% Fe_2O_3	Slow hydration

Hydration of clinker minerals

The cement hydration includes the chemical reactions between the individual clinker minerals, gypsum and water. These reactions can occur successively and simultaneously, creating a complex chemical system of high ionic strength. To elucidate its evolution, the hydration reaction of the separate mineral phases is discussed first:

[1] In cement chemistry, the following abbreviations are used for the oxides: C=CaO, S=SiO_2, A=Al_2O_3, F=Fe_2O_3, M=MgO, $\overline{S}$ =SO_3, H=H_2O

Tricalcium silicate (C_3S)

In literature, the progress in hydration of C_3S and even of OPC has been defined to occur in four or five stages. These stages are bounded by somewhat arbitrary points in the plot of the heat of hydration versus time, as can be seen in Fig.2.3. In order to discuss the kinetic mechanisms, we distinguish (1) initial reaction, (2) period of slow reaction (also dormant or induction period), (3) acceleration period, and (4) deceleration period. The distinction between the stages is not sharply defined and the timing given in Fig.2.3 serves as an example of average alite.

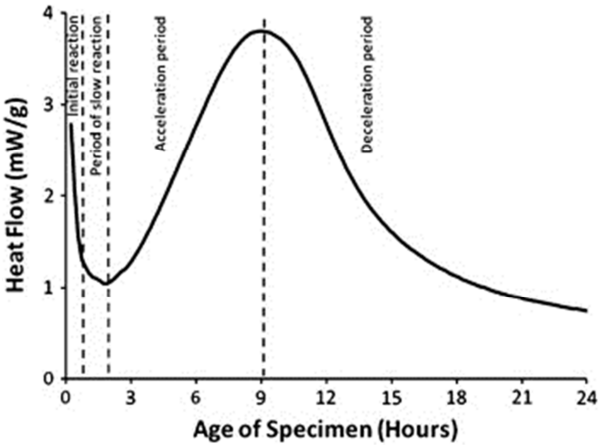

Fig.2.3 Rate of alite hydration as a function of time given by isothermal calorimetry measurements [13]

The heat release in the initial period is dominated by the wetting of the particle surface and the immediate start of the dissolution of C_3S (see Eq.2.4). This dissolution decelerates fast within the first hour while the solution remains undersaturated. The exact mechanism behind this remarkable behavior is still subject of discussion.

$$C_3S + 3H_2O \rightarrow 3Ca^{2+} + H_2SiO_4^{2-} + 4OH^- \qquad (2.4)$$

At the end of the initial period, the hydration of alite reaches a dormant period, further called induction period, with a very low rate of hydration. This period can last 1 to 2 hours after which the dissolution and the hydration reaction restarts during the acceleration period. The actual hydration reaction of alite is described in Eq.2.5 and shows how the hydration products calcium silicate hydrate (C-S-H) and portlandite (CH) are formed. The stoichiometry of the C-S-H phase depends on the local availability of water, calcium and silica ions and it even changes with age

and temperature. The dashes within the abbreviation indicate that no particular composition is implied but a generic name for any amorphous or poorly crystalline calcium silicate hydrate is implied.

$$3CaO \cdot SiO_2 + (3+m-n)H_2O = nCaO \cdot SiO_2 \cdot mH_2O + (3-n)Ca(OH)_2 \qquad (2.5)$$

Several mechanisms have been proposed to explain the transition from the initial period to the induction period and the postponed start of the acceleration period. Historically, this involves the following theories [14]:

Protective membrane

A protective layer is formed on the C_3S surface by the initial reaction products. The layer hinders immediate further hydration until this layer is degraded by ageing or phase transformation [14]. The phase transformation appears to be the conversion from intermediate silicate hydrate phases into C-S-H when the calcium concentration becomes sufficiently high. Despite difficulties in detecting this early layer, a direct correlation between the length of the slow reaction period and rate of surface hydrate development has been indicated frequently [13].

Semi-permeable membrane

A semi-permeable layer is formed by the initial reaction product, partly sealing of the particle surface for most ions and with limited particle dissolution underneath it. The membrane breaks when the osmotic pressure reaches a certain threshold [14].

Double layer theory

Dissolved ions lower the undersaturation close to the particle surface and hinder further dissolution. This layer is removed once supersaturation with respect to the hydrates is obtained and massive nucleation and growth take place [14]. According to several authors [15-17], a superficially hydroxylated layer forms on the C_3S surface and the dissociation of ions from this layer occurs much more slowly than would be otherwise expected for a mineral in highly undersaturated solutions [13].

Crystallographic defects

Dislocations are crystallographic defects that can give rise to so-called etch pits in the alite surface. The material defect facilitates rapid dissolution, far from equilibrium conditions, and induce deeper pits in the surface. Closer to equilibrium conditions, the pits tend to grow in lateral direction at a

much lower rate. The material density of dislocations is related with the length of the induction period which ends when the supersaturation is reached with respect to the hydrates [14].

Nucleation of calcium hydroxide (CH)

The CH nucleation is poisoned by silicates and cannot grow further which disables further C-S-H formation and onsets the induction period. Once the level of supersaturation with respect to CH is sufficiently high, this effect is overcome and the induction period ends by the renewed C-S-H formation [14].

Nucleation of C–S–H

The initial formation of C-S-H is controlled by the CH concentration in solution and is slowed down as it reaches saturation. This initial rate controls the reaction rate during the induction period until the renewed C-S-H growth occurs [14]. The growth of C-S-H can be seen as an aggregation process of anisotropic particles around the initial seeds [18]. For mature pastes, the Jennings colloid model [19] envisions two stable morphologies of C–S–H with different packing densities, known as high density and low density C-S-H [13, 19].

Once the dissolution of C_3S and the growth of C-S-H and CH have restarted, the induction period of C_3S is finished. During the acceleration stage, the small particles will have reacted completely, while the larger particles will react steadily thereafter. The extent of reaction for C_3S is about 70% in 28 days and almost all hydratable material reacts in one year [11].

Dicalcium silicate (C_2S)

The hydration kinetics of belite is very similar to that of alite but the reaction rate is much slower. The hydration products are also C-S-H and in lesser extent CH. About 30% of the belite reacts within the first 28 days of hydration and almost 90% has reacted within one year [11].

Tricalcium aluminate (C_3A)

Next to alite, the cement phase that is dominant in the hydration kinetics is the aluminate phase. Unlike alite, there is no immediate deceleration of this fast reacting product. For the isolated phase, the reaction is started by

immediate formation of poorly crystallized aluminum hydroxide or AFm phase, represented by C_2AH_8 and C_4AH_{13}. After about 25 minutes, these metastable phases transform into the stable hydrogarnet (C_3AH_6) [13]. This rapid exothermic reaction leads to fast setting of the aluminate paste and is referred to by *flash set*.

In ordinary Portland cement, the high initial reaction rate of the aluminate phase is prevented by the addition of calcium sulfate to extend the workability time of the cement paste. This calcium sulfate might be added as gypsum ($CaSO_4 \cdot 2H_2O$), anhydrite ($CaSO_4$) or hemihydrate ($CaSO_4 \cdot 0.5H_2O$). The latter is formed due to partial dehydration of gypsum during grinding and its mineral name is bassanite.

With sulfate in the pore solution of ordinary Portland cement, the initial rapid reaction of the aluminate phase is decelerated within tens of minutes as visualized by the initial steep decrease in Fig.2.4 [20]. In this first stage, the initial reaction product of aluminate, calcium sulfate and water is ettringite (Eq.2.6) . This needle-like crystal belongs to the broad group of AFt phases with the general formula $[Ca_3(Al, Fe)(OH)_6]X_3 \cdot xH_2O$, where X represents a formula unit of a doubly charged anion [11].

$$C_3A + 3C\bar{S}H_2 + 26\,H_2O \rightarrow C_6A\bar{S}_3H_{32} \qquad \text{(AFt)} \quad (2.6)$$

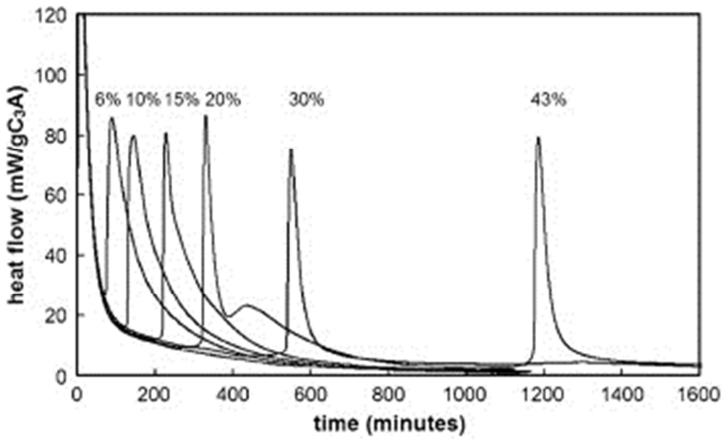

Fig.2.4 Heat evolution rate curves during the hydration of C_3A in solutions saturated with respect to portlandite for increasing quantities of gypsum (wt.%) [20]

After the initial deceleration, a period of low heat flow occurs for which the length depends on the dosage of calcium sulfate in the system. When all

calcium sulfate is consumed, the aluminate reaction restarts and forms mainly monosulfoaluminate (AFm) as fewer sulfate is available now to incorporate. Also the initially formed ettringite reacts with available C_3A and forms a lower sulfate containing mineral of the AFm family (Eq.2.7). In OPC the restart of the reaction should be postponed until after the alite hydration peak to ensure correct setting and hardening [13].

$$2C_3A + C_6A\bar{S}_3H_{32} + 4\,H_2O \rightarrow 3\,C_4A\bar{S}H_{12} \qquad \text{(AFm)} \quad (2.7)$$

Similar to the induction period of alite, the rapid slowdown of the C_3A hydration in presence of calcium sulfate is not fully understood. Three possible explanations are returning in literature, but only the last one seems feasible according to recent research [13, 20]:

- Ettringite slows down further hydration by forming a diffusion barrier at the C_3A surfaces
- Some other phases, for example AFm, slow the reaction down in the same way
- The reaction is slowed down directly by adsorption of some solute species provided by dissolution of calcium sulfate.

Due to the porosity of an ettringite layer and the observed disability of AFm to slow down hydration, it seems that sulfate ions build up at the defect sites of the C_3A surface. Similar to a potential mechanism for alite, this would inhibit the formation of etch pits, slowing down the rate of dissolution. Over time, the depletion of sulfate ions in the pore solution will cause desorption of these sulfate ions to re-establish the dynamic equilibrium. This will lead to a change in aluminate dissolution rate and a re-initiation of the aluminate hydration [13]. After a few months, all aluminate is supposed to be reacted [11].

Calcium aluminoferrite (C_4(A, F))

Calcium aluminoferrite is referred to by the ferrite phase and its hydration reaction delivers similar product as the aluminate hydration reaction but at considerably lower rate. When calcium sulfate is present, the AFt phase C_6(A, F)$\overline{S}_3H_{32}$ is the main hydration product which is later converted into AFm (C_4(A, F)$\bar{S}H_{12}$) [11].

Hydration of Portland cement

As mentioned before, a grain of Portland cement can contain the different clinker phases. As a consequence, the hydration of OPC includes the

described hydration reactions of the individual phases and their interactions. Furthermore, the alkalis, gypsum and changing amounts of calcium, hydroxide and sulfate ions influence this complex system. The most important phase, as can be seen in Table 2.1, is alite and therefore its hydration behavior has a big impact on the hydration of OPC [12].

A typical heat of hydration curve is plotted in Fig.2.5. One can identify the initial reaction during the first minutes for which the water wets the cement surface and the dissolution of alkali sulfates, gypsum, alite and aluminate starts immediately. The high increase in K^+, Na^+, Ca^{2+} and SO_4^{2-} ions is contrary to the limited increase in silica and alumina ions. This results from the C-S-H and AFt formation, preventing further dissolution of their respective minerals as explained before, which leads to the induction period [12].

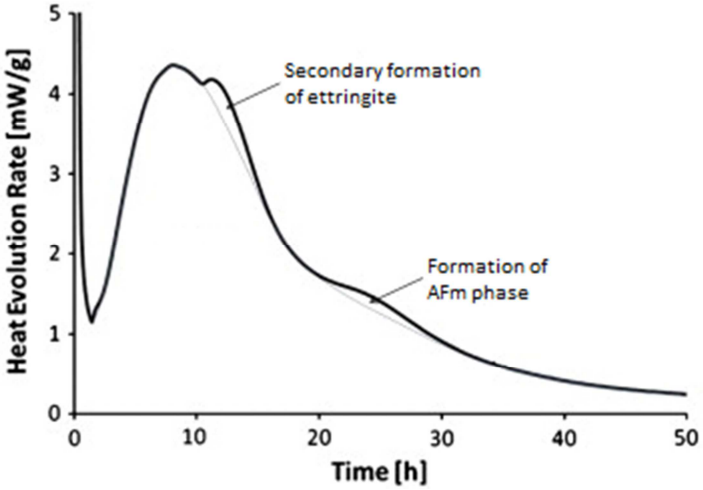

Fig.2.5 Calorimetry curve of modern Portland cement [13]

After about 2 hours, the hydration restarts and is controlled by nucleation rate and growth of the formed hydrates. The precipitation of CH is often related with the reinitiated formation of C-S-H, which is important in the stiffening of the cement paste. After the acceleration period, also (secondary) ettringite will be formed, due to an accelerated dissolution of the aluminate phase [12]. All solid gypsum is exhausted at this point and it is suggested that the sulfate, previously adsorbed on C-S-H is still used in the secondary AFt [13].

At a certain point in this stage of hydration, the paste is mechanically strong enough to support itself and even to resist some external loads. An arbitrary resistance has been defined in industry for which the paste is said

to *set*. The time for which this point is reached, is called the *initial setting time* and, after this point, it becomes hard to rehomogenize the paste by mixing. By the final setting time, one or few hours later, the paste becomes hard and totally unmixable.

After the maximum heat flow, the so-called deceleration period is started for which the remaining material keeps hydrating at a lower rate, controlled by diffusion of ions and slower local dissolution. The hydration of alite continues steadily but the hydration of belite increases. For the decreasing sulfate concentration in pore solution, the AFt is gradually converted into monosulfate (AFm). During the formation of the hydrated structures, the inter-particle spaces are filled with the hydration products which impede the transfer of dissolved ions. Therefore, the hydration becomes totally diffusion-controlled by the final stage of hydration. In this final stage, hydration will continue as long as water of any kind is available and the consolidation of hydrates determines the final strength of the material [12].

Despite some uncertainty concerning specific theories, visualization of the microstructural development has been very useful in constructing the sequence of mechanisms in particle growth. The most cited diagram of microstructural development stages is shown in Fig.2.6 [11, 21].

The early period of hydration, as seen in Fig.2.5 until about 3 hours after mixing, is corresponding with scheme (a) and (b) in Fig.2.6. The low concentration of silicates in solution causes the C-S-H to precipitate around the cement grains and an amorphous, colloidal “gel” layer, rich in alumina and silica, seals the cement grain surface. Moreover, some AFt rods are formed at the particle surface and within the pore solution. This configuration of these two main hydrate products (i.e. C-S-H and AFt) is also the microstructural state during the induction period [11].

In scheme (c) and (d), the hydration has restarted and about 30% of the cement reacts until 24h of hydration. A layer of C-S-H forms outward the cement particles by further dissolution from the particle and precipitation from pore solution. A hydrate shell is created which leaves a space between the remaining unhydrated particle and the outer product [11]. A recent study reports that the shells form only around the silicate part of the grain and are not empty but filled with a fragile fibrous C–S–H which appears to have a lower density than the other hydration products [22]. Next to the restarted C-S-H, also AFt starts to form from the continued dissolution of aluminate phases and the rods clearly grow outward to form

long needles [11]. During the late hydration period, the reduced sulfate concentration at the grain surface makes the remaining C_3A react with the AFt and forms AFm (scheme (e)). If the sulfate concentration drops also within the pore solution, the AFm crystals can form throughout the paste. Moreover, the C-S-H starts to depose inside the shell and forms inner C-S-H (scheme (f)) [11].

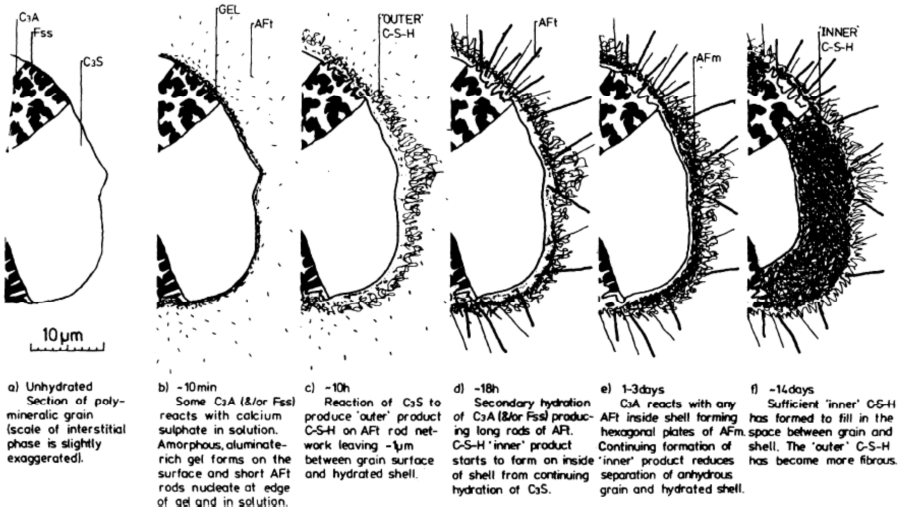

Fig.2. 6 Sequential microstructural stages during OPC hydration [21, 23]

Rheologically important ions and phases

In the light of the thesis scope, the attention is drawn to a few important ions and phases that show high relevance concerning cement paste rheology. On the one hand, there is the mineral morphology of certain phases that is capable of physical intervening the cement paste rheology. On the other hand there are ions and dissolution mechanisms that influence this morphology and that are quite vulnerable for superplasticizer addition. In the following, the importance of sulfates, alkalis, ettringite and syngenite will be illustrated.

Sulfates

The amount of available sulfate ions in pore solution is of utmost importance for transforming the hydrating aluminate phases into ettringite. For a too low initial concentration, the morphology of the ettringite changes to long calcium aluminate hydrate. This structure can bridge the inter-particle distance and influence the rheology of the cement

paste negatively. Therefore, the sulfate source needs to be tailor made for every batch of clinker [24, 25].

The sulfate in pore solution is generally originating from the dissolution of calcium sulfates and alkali sulfates. The latter are described under the alkalis section. For the calcium sulfate phases, there are three types encountered in nearly every cement and they are often referred to by their enclosed water molecules. During milling, gypsum ($CaSO_4 \cdot 2H_2O$ or dihydrate) and anhydrite ($CaSO_4$) are added to kiln feed. Due to the temperatures and potential water contact, a third phase can coexist with the gypsum and anhydrite, namely hemihydrate ($CaSO_4 \cdot 0{,}5H_2O$). The latter phase can evolve into secondary formed gypsum when water is added to the cement, resulting in poor rheology. However, this formation of secondary formed gypsum is rarely observed [24, 25]

More important for the rheology is the solubility of the different calcium sulfate phases. Besides the detectable amount of sulfate required for sufficient ettringite formation, also the balance between the three phases should be considered to provide a satisfying dissolution rate. The solubility of hemihydrate (6 g/l) is higher than for gypsum (2.4 g/l) and anhydrite (2.1 g/l) [25, 26].

Alkalis

The alkalis are embedded in the selected raw materials used to produce cement. During the melting process in the clinker oven, the alkali cations (i.e. Na^+ and K^+) are distributed over the different clinker liquids. Upon cooling, some redistribution of alkali cations and sulfate ions between the liquids may be expected to occur [11]. During the cooling process of the clinker, the alkali sulfates are crystallizing on the clinker surface, making them easily accessible for water. Besides some small variations in stoichiometry, the solubility of alkali sulfates in water is generally high compared to the other phases [11].

The rapid dissolution of alkali sulfates is of major importance because it has been shown to alter the C_3A/SO_4 balance [27]. Consequently, this influences the early formation of ettringite and gypsum which are important components of the hydration reactions. This influence has been reported to diminish the cement paste rheology or increase the water demand. It can however also been explained by the higher ionic strength, due to alkali dissolution, which favors coagulation of the particles [25, 27].

The amount of alkalis that dissolves in the first minutes of hydration also controls the fluidity and slump loss when superplasticizer is added [28]. In order to optimize the initial fluidity and the corresponding fluidity loss, the optimum amount of alkali was found to be on the order of 0.4%-0.5% Na_2O equivalent. This study based on polynaphtalene sulfonate superplasticizer and six different cements shows the role of alkalis in the cement/superplasticizer compatibility [25, 28].

Ettringite ($Ca_6Al_2(SO_4)_3(OH)_{12}•26(H_2O)$)

The aluminates react the fastest with water and only form ettringite during the hydration in the presence of gypsum. If no sulfates are present, thin and platy calcium aluminate hydrate crystals are formed, bridging the free space between the cement particles. In this case, the mix can stiffen directly, creating flash set. When sulfate is present, the ettringite normally shapes into rod-like crystals with a length from 100 to 400 nm and a thickness of 50 to 100 nm (Fig.2.7). The mineral is not solely present on the aluminate phase as it was also found on other clinker phases, though in smaller amounts [24].

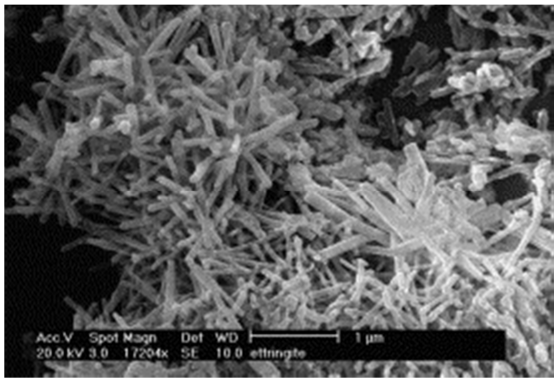

Fig.2.7 Scanning electron micrograph of fresh ettringite rods [29]

The addition of SP is capable of changing the initial morphology of ettringite to a “honeycomb” structure in the first half hour while without SP the radial growth of thin rods is expected. This is reported to occur specifically for the orthorhombic aluminate phase while for the cubic phase only very short fibers were detected upon addition of SP [30].

Syngenite ($K_2Ca(SO_4)_2•(H_2O)$)

The syngenite mineral appears as thin bars and needle shaped crystals with a length of more than 10 µm (see Fig.2.8). Because of their size, these crystals are expected to have a significant effect on the rheological properties of cement paste [25]. If too much syngenite is present, early stiffening can occur [31]. However, if the paste is stirred intensively after stiffening, the syngenite crystals are broken resulting in better rheology [24].

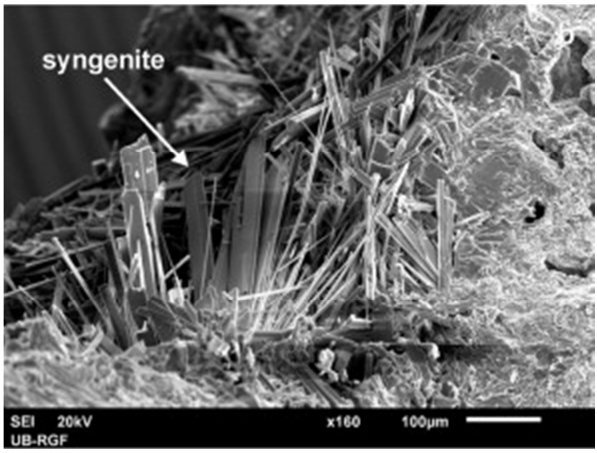

Fig.2.8 Needles and long prismatic crystals of syngenite [32]

The syngenite mineral is not part of the typical reaction products during OPC hydration. It differs from the other hydrate compositions through the presence of potassium ions in its structure. Therefore, it can only be formed if a sufficient amount of potassium is available in pore solution. The source of these potassium ions is related with the alkali sulfates in the cement, which are usually of the form of arcanite (K_2SO_4) and aphthitalite ($K_{4-X}N_XS_4$) [11].

2.2.2 Admixtures

In the following paragraphs the selected admixtures will be discussed in terms of material properties and their interactions with cement. The admixtures added to the cement paste in this project are – in chronological order – one superplasticizer, retarder and accelerator. While the first is particularly designed to enhance flow properties of the fresh paste, the latter two are used to affect the hydration reactions in order to alter the setting time of the paste.

Superplasticizer

Superplasticizers are chemical additives in concrete that are used to (1) reduce the water/cement ratio and (2) prevent particle agglomeration of cement particles. The first function is particularly useful for reducing the pore water volume and increasing the strength and durability of the hardened concrete. The second function enhances particle movement during the handling of the fresh concrete which results in improved concrete workability [27].

From a chemical point of view, superplasticizers are organic water-soluble polymers belonging to the family of polymeric dispersants. They act by adsorption at the solid-liquid interface between the cement particles and the pore solution. After adsorption, repulsive forces between the superplasticizer polymers lead to the dispersion of the cement grains. Another important effect is that the superplasticizer may delay the normal hydration reactions by its presence on the particle surface [33, 34].

Different kinds of superplasticizer families have been applied in the history of plasticized concrete. The following main groups of superplasticizers are often mentioned [27, 35]:

- polycondensates of sulfonated naphtalene formaldehyde (SNF)
- polycondensates of sulfonated melamine formaldehyde (SMF)
- modified lignosulfates (LS)
- polycarboxylate ethers (PCE)

All of these groups have in common that they adsorb on the charged cement grain surface through the charges embedded in their own molecular structure. The mechanism of particle repulsion, however, is expected to result from different origins. The first three families repel particles by the use of electrostatic forces, while the polycarboxylate polymer is supposed to repel by steric hindrance. These mechanisms are illustrated in respectively Fig.2.9 and Fig.2.10. The steric hindering is induced by the molecular side chains swirling into the liquid phase. Regardless the working mechanism, the PCE superplasticizers have become the most promising family because of its high adaptability, leading to nearly infinite product formulations that can be designed for specific applications. For that reason, the superplasticizer used in the experimental part of this thesis will be of the polycarboxylate kind.

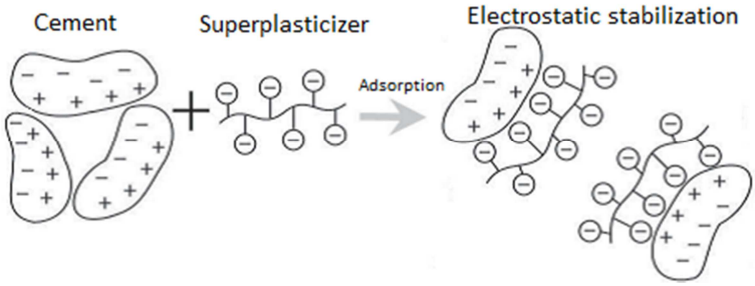

Fig.2.9 Dispersion through electrostatic repulsion [25]

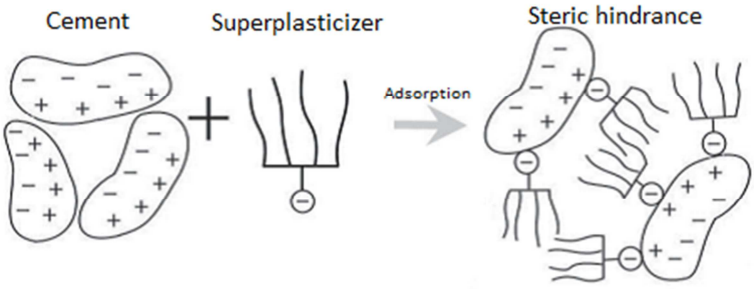

Fig.2.10 Dispersion through steric hindrance [25]

The customizable asset of the PCE family (see Fig.2.11) has led to a substantial amount of research focusing on different polymer structures. Several researchers have highlighted the influence of polymer architectures and their interaction with cementitious systems [36-44]. Different relations were found but overall it was conceived that polymers with short side chains and low side chain density – and consequently a high polymer charge - create strong adsorption especially on positively charged particle surfaces.

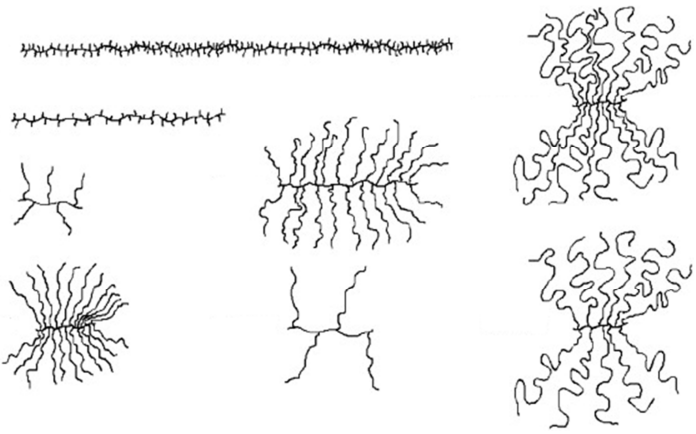

Fig.2.11 Schematic representation of different PCE architectures [45]

The adsorption of PCE superplasticizer has also gained a lot of attention in literature because it is closely related with the polymer effectivity. Only adsorbed polymer that is not intercalated by hydration products can function optimally as a dispersive agent in-between particles: If the polymer adsorbs too fast, it will be quickly covered with hydration products and too soon the concrete will lose its workability. If the polymer adsorbs too slowly, it is possible that it will be overdosed to obtain sufficient workability during the induction period, resulting in uneconomic practice. Further attention will be given to the adsorption phenomenon in section 2.3.

Generally, water reducing admixtures or superplasticizers also have a microstructural effect on the cement hydration. In systems without PCE, the early hydrates are instantaneously precipitating onto clinker surfaces and form agglomerates of a few microns in diameter [46]. In contrast, when PCE is added, more submicron particles can be observed in the interstitial pore space. Another study observed that, in the presence of water reducing admixtures and retarders, calcium silicate hydrates were found more frequently as fine, dense particles and the structure was said to resemble a compact gel kind of C-S-H [47]. Similarly, a more compact and interconnected foil-like C-S-H morphology was found for PCEs at the expense of the characteristic fibril formation [48].

Retarder

Retarders are used to postpone cement hydration and to keep a cementitious system workable. Their interference is useful when the available hydration time does not allow enough time for the concrete to be placed. For example, when the temperature of the concrete is above

standard conditions, the enhanced hydration reactions would cause the concrete to set before it is placed. So, for concrete under high temperatures conditions, the required amount of time to place the concrete is determining the retarder addition rate.

Retarders are defined as admixtures that extend the induction period of cement hydration [49]. Historically, two working mechanisms are considered to explain the retarding behavior of these admixtures. On the one hand, the retarder can reduce the solubility of the hydrating components in cement and, on the other hand, it can coprecipitate with a component to form a low-permeable coating on the cement surface [12].

Next to reducing the solubility, also the precipitation of certain phases might be hindered, for example, by calcium complexation in pore solution, the precipitation of portlandite could be prevented. However, this theory appeared unsuccessful for strong chelaters that acted as moderate retarders and vice versa [50]. This mechanism is rather considered as the poisoning of nucleation and growth of hydrates like portlandite. Please note that these two mechanisms should be mentioned separately as their impact on the hydration rate after the induction period is likely to differ.

As concerns the second mechanism, the low permeable coating should not be referred to as a layer of hydration products because SEM observations detected retarded C_3S surface free of hydration products [50]. This suggests that the retarder directly adsorbs at the mineral surface and prevents further hydration.

The result of the two mechanisms is that normal dissolution-precipitation reactions within the hydrating cement paste are hindered for as long as a sufficient amount of retarder is present in the pore solution. Eventually, the remaining admixture will be removed from the paste by alkaline hydrolysis or by intercalation and the normal hydration process will resume [50].

In the light of very recent developments, future retarder research would benefit from including the chelation ability and the dissolution potential of the retarder. For example, an admixture that solubilizes calcium ions and thereby increases the silica and sulfate concentrations can promote the formation of more C-S-H nuclei instead of preventing the CH precipitation [50].

In today's practice, the group of organic retarders is important because of their adaptability and wide applicability. Besides the doubtful calcium chelating properties, they are expected to operate through hindering the dissolution of calcium containing phases by coating especially on the mineral surface of the most rapidly hydrating cement phases like C_3A, C_4AF and C_3S [49].

The formation of a coating is enhanced by their molecular structure. Firstly, the feature of CHOH groups being present in their molecular structure enforces the chelating properties and the adsorption on the cement grain surface. One example of such a retarder, that will be applied in this thesis, is sodium gluconate $(CH_2OH)(CHOH)_4$-CO_2Na) (see Fig.2.12). It has been reported that gluconate ions are able to form aqueous complexes with calcium ions which can adsorb on the C_3A surface [51]. By hindering the aluminate hydration reactions, this adsorption can impede the ettringite formation [52]. The hindering is assumed to result from forming low soluble salts with calcium ions, sealing off the cement surface from the pore water. When the carbon chain would increase in length, the adsorption potential will raise and so does the retarding effect [49].

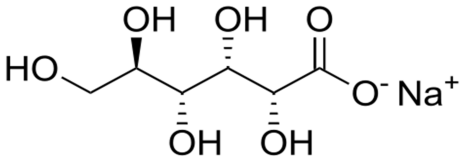

Fig.2.12 Molecular structure of sodium gluconate

Besides the effect on cement hydration, gluconates are also known to plasticize the cement paste [12] but only a relatively few studies remotely described this plasticizing effect of sodium gluconate [38, 53-55]. An interesting study on sodium gluconate investigates the retarding and plasticizing effect in function of the dosage. In this study, it was found that around 75% of the added retarder was adsorbed within five minutes for dosages up to 0.4%. This dosage is high enough to delay the setting for many days [50, 55].

For both cement and C_3S, Perez [55] found changes in the slopes of the function of the retardation and mortar flowability versus the sodium gluconate dosage. These changes were attributed to a saturation dosage beyond which the gluconate did not provide additional flowability but only a stronger retardation. If alite is the only adsorbing phase to be considered, a calculated layer thickness of 3 nm was believed to seal the hydrating surface [50].

Sodium gluconate has also been shown to interact with C_3A and a significant difference in degree of retardation has been observed for different crystal forms of C_3A [50, 56]. Their experiments on blended pastes with good sulfate supply showed that the total energy released during the first ten hours of hydration was around seven times higher for the orthorhombic-C_3A than for the cubic-C_3A blends. In contrast, for under-sulfated blends, the total energy released from the cubic system in the first four days was found to be about the half higher than that from the orthorhombic system. This example clearly demonstrates where small changes in kiln feed can lead to, especially when considering the cubic/orthorhombic balance of C_3A being influenced by the amount of sulfate in the raw mix.

Accelerator

Contrary to retarders, accelerators are used to accelerate the setting time of cementitious materials. This can be done to compensate extended setting behavior due to low environmental temperatures or to improve the construction process in function of a narrow planning. Typically, an accelerator will reduce the setting time and increase the early compressive strength. It is also possible that only one of these features is addressed by a particular accelerator.

A major distinction can be made between two types of accelerators based on the main mineral phase they affect. Generally, the accelerators working on the C_3A phase are considered to lead to fast setting. To that end, the dissolution of silica and alumina are promoted and interference with the C_3A-gypsum reaction is aimed for. Furthermore, the accelerators focusing more on the setting and hardening are working mainly on the C_3S phase to enhance early strength [49].

In this thesis, the focus is on the second group of setting and hardening accelerators because the first group knows only limited use in practice due to its tendency not to sustain high long-term strength. The second group of accelerators contains chemicals which focus on changing the hydration rate of alite, resulting in C-S-H gel formation at an early age. Most of them are soluble salts of alkali and alkaline earth metals incorporating both an anion and a cation that contribute to the acceleration [49].

Hewlett and Edmeades [49] mention anions which cause significant acceleration to be halide, nitrate, nitrite, formate, thiosulfate and thiocyanate although their activity appears to depend on the identity of

the associated counterion. Considering the cation, the divalent and trivalent cations such as calcium, magnesium, barium, ferric and aluminium appear to be more effective than monovalent ions such as sodium, potassium and ammonium [49]. In this thesis, the calcium nitrate (CN) accelerator is selected as it is a robust chloride-free admixture that is often used in recent scientific research (see Fig.2.13).

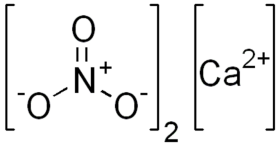

Fig.2.13 molecular structure of calcium nitrate salt

Despite its widely use, the working mechanism of calcium nitrate has been addressed by only few authors. Justnes and Nygaard [57] showed that the mechanism for accelerated setting of cement by calcium nitrate is two-fold: First, an increased calcium concentration leads to a faster supersaturation of the fluid with respect to calcium hydroxide, thereby shortening the time needed for initial crystallization and for the renewal of alite hydration. Secondly, a lower sulfate concentration will lead to slower/less formation of ettringite which shortens the onset of the aluminate hydration. Furthermore, the efficiency of CN as set accelerator was found to increase with the increasing belite content and decreasing alkali content of the cement [57]. Considering the plasticized cement pastes, it was suggested that calcium nitrate can partly counteract the retardation of lignosulphonate plasticizers [58].

It was often thought that calcium salt accelerate the hydration reactions by precipitation of Portlandite but it was found that the addition of Portlandite itself had no effect in this respect. Therefore, it is considered that calcium salts instead improve the homogeneous nucleation of C-S-H in the pore solution rather than nucleation and growth of C-S-H on a substrate [59]. This explains why recent developed accelerators, based on homogeneously dispersed nano-particles, are highly effective in improving C-S-H nucleation.

According to Cheung et al. [50], future studies incorporating the interaction of an accelerator with cement have to focus separately on the direct acceleration of the pitting of the bare silicate surfaces, the CH and C-S-H nucleation and the C-S-H growth. These mechanisms are important to estimate changes in the diffusion of ions through pore solution and through hydrate layers due to the influence of the accelerator [50].

2.2.3 Summary

In short, the cement hydration mechanism and the influence of admixtures can be summarized schematically as in Fig.2.14. The two main hydration products (CH and C-S-H) are important indicators of the hydration process and are formed by dissolution and precipitation of the required ions. In particular C-S-H has been shown to require the presence of coagulated nano-sized nuclei (called seeds) to allow further growth of this phase in-between particles. In this process, the admixtures intervene in their own way: (1) Calcium based accelerators are providing calcium ions close to nuclei and enhance the C-S-H formation. (2) Retarders can act through a supposed mechanism of shielding and poisoning the newly formed hydrates. It is only after its consumption that normal hydration reactions can fully restart. (3) For the superplasticizer, something similar happens in terms of hydration and consumption but its dispersing activity is the primary cause for homogeneously spreading of finer nuclei.

Due to or despite the admixture action, the C-S-H reaction product will eventually grow at the expense of the different oxides present in the cement particle. The location of growth might be right at the particle surface or more in the volume between particles, depending on the experienced admixture influence.

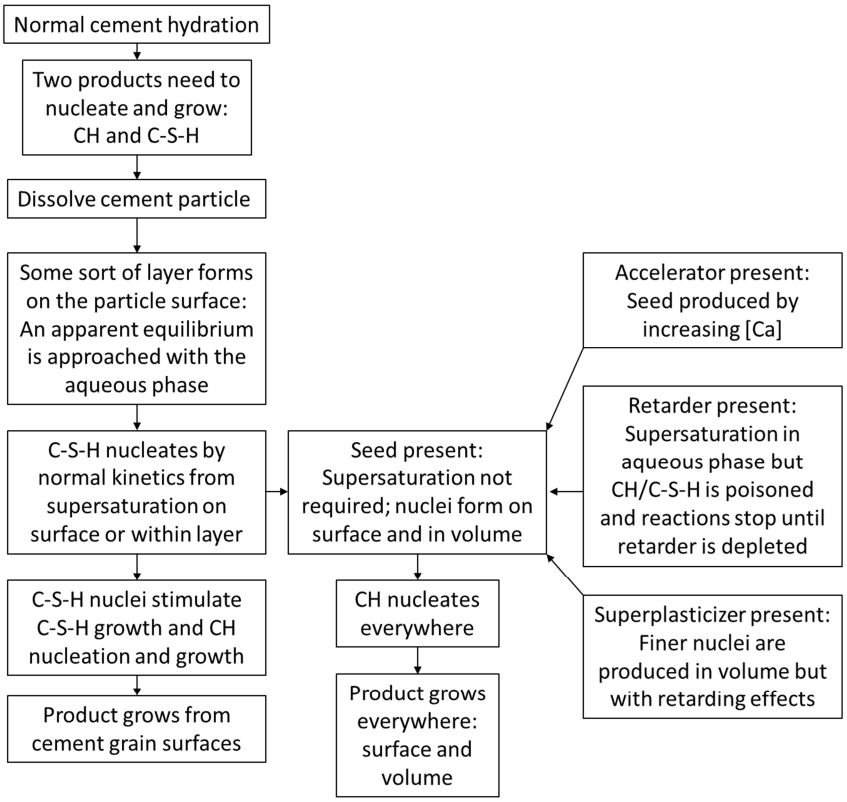

Fig.2.14 Schematic summary considering cement hydration in presence of admixtures (based on [13])

2.3 Cement paste rheology

From the previous section, it is clear how an aqueous solution of cement and admixtures gives rise to a complex chemical system with many parameters. In order to describe the rheology of this system, the influence of those parameters has to be incorporated as much as possible. In this way, the subsequent challenge is to retain the primary rheologically relevant parameters. To that end, the rheological problem of cementitious materials will now be approached from the rheological side and an overview of important forces and features is presented in the current section. Next to that, some important effects of admixtures will also be mentioned.

2.3.1 Forces within the cement/water/SP system

The flow of cement paste is the macroscopic response to the applied shear and it is in our interest to control this behavior by reliable prediction of the stress response. In that respect, several authors have addressed the prediction possibilities through rheology modelling and identified various input parameters [8, 60-63]. In order to describe the cement paste rheology accurately, several relevant forces need to be taken into account. A part of these forces will be purely physical but others will be of chemical as well as of physical nature. It is important to consider that the forces in-between suspended particles are active on different length scales and time scales. On the one hand, this consideration complicates a straightforward description of cement paste rheology, on the other hand it allows particular forces to be dominant in certain regimes which actually facilitates a comprehensive explanation during that regime.

The main reason for the complexity of the cement paste rheology is the comparable magnitude of the forces active in cement paste [8]. Incorporating the temporary dominance of few forces is far from trivial and depends on the different physico-chemical phenomena within the cement paste. Before getting into these phenomena, the relevant forces will be treated here first. The rightful description of the rheology problem involves a combination of all these forces.

Forces in-between particles

In his article, Flatt has addressed the prediction of superplasticized concrete rheology most thoroughly [8]. All the various mechanisms are listed that contribute to the rheological performance. This includes particle packing physics of granular media, hydration chemistry, colloidal science and polymer chemistry. These mechanisms are active in concrete as well as in cement paste but their relative importance depends on the mix composition. For both suspensions, these mechanisms give rise to several forces such as gravity, inertia, viscous drag, dispersion (van der Waals), electrostatics, steric forces and Brownian motion. Although the latter four forces are typically discussed for colloidal particles only, these kinds of forces are also influencing the rheology of the non-colloidal size range due to a relatively high share of surface activity in the interparticle interaction.

A few seconds after mixing, the dispersed particles will flocculate and form a network due to colloidal attractive forces [64]. The main force at this point is expected to be the van der Waals force, also called dispersion force. This is a confusing terminology as it results in attraction due to

dipole interaction and not in dispersion. The van der Waals force works most effectively on the fine colloidal fraction (< 1µm) of cement particles, which contains only around 10% (by weight) of the entire amount of particles. This fraction constitutes a major share of the specific surface area of the cement and it is most easily dispersed by superplasticizers due to its lower mass and volume [25].

When the cement paste flows, the colloidal attraction could be opposed by the Brownian motion, for the colloidal sized particles, but it has been reported that the Brownian forces appeared to be insignificant with respect to the viscous forces [65]. For larger particles, it is either shear forces or gravity that must be taken into account [8].

In the cement paste at rest, the network of interacting particles is already able to resist stress and will show an elastic modulus. As the hydration proceeds, divalent calcium ions will cause ion correlation forces[2] between negatively charged surfaces which enhances the connection in-between the increasing number of C-S-H contact points [8, 66].

Next to the van der Waals and ion correlation forces, another force acts on a larger length scale in the attraction and repulsion of cement particles. Electrostatic attraction results from the opposite surface charge of particles which might either result from the particles themselves or from the inhomogeneity in surface charge distribution. In an analogue way, the presence of similar charged opposing particle surfaces will contribute to particle repulsion.

As a measure for the electrostatic potential of suspended particles it is often referred to the zeta-potential. This potential is determined by the double layer model of Goüy-Chapman which distinguishes two zones around a particle surface (Fig.2.15). The first layer is called either the Stern layer or the compact layer and it defines the thickness of adsorbed ions which are closely linked to the surface in a way that they are unaffected by Brownian motion. The outer shell of this layer carries the net charge that is relevant for the next layer. The second layer is called the diffuse layer and it covers the region from the outer-bound of the Stern layer to the bulk solution, in which ions are affected both by Brownian motion and by the charged interface. The Stern layer and the diffuse layer together are called the double layer.

[2] Ion correlation force : attraction due to highly polarizable mobile ions in the double layer (< 4 nm)

The charge that will be sensed in-between particles is determined at a certain distance from the grain surface. Therefore, a conventionally introduced slipping plane is considered to separate mobile fluid from fluid that remains attached to the surface. In this slipping plane the electrostatic potential is called the zeta-potential.

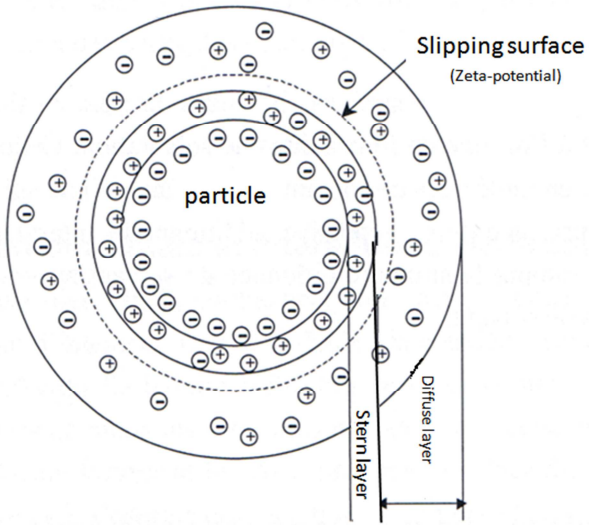

Fig.2.15 Schematic representation of the double layer theory

Similarly charged particles in a suspension will repel each other and the zeta potential indicates the degree of repulsion. For particles that are small enough, a high zeta potential will result in stability of the suspension, i.e. the particles will resist flocculation. When the potential is low, the colloidal attraction exceeds the repulsion and the particles will flocculate, reducing the workability of the suspension.

The high concentration of electrolytes within the cement paste pore solution reduces the electrostatic forces in-between cement particles. As a consequence, the electrostatic repulsion alone is generally insufficient to prevent agglomeration and other solutions are needed. In order to improve the inter-particles repulsion, different generations of superplasticizers have been developed and used. These admixtures are typically polyanionic organic polymers that adsorb on the particle surface and induce a negative electrostatic potential on the particles [8].

Admixtures based on electrostatic stabilization (lignosulfonate, naphthalene and melamine based) generally provide a good workability of

concrete during 30 to 60 minutes after water addition. The mechanism was illustrated in Fig.2.9. It is often reported that the increase in ionic strength of the pore solution causes a relatively fast loss of workability for these admixtures because the ionic strength compresses the polymer layers and reduces the electrostatic repulsion. As a result, the particles agglomerate again [25].

Only for the latest generation of polycarboxylate superplasticizers this mechanism of steric hindrance has become widely acknowledged (see Fig.2.10). It is based on the non-evident assumption that there is no type of attraction among the polymers. For example, it is possible in cement paste that calcium ions act as a bridging complexation agent in-between polymers and induce an attractive force. Similarly, the polymers could be connected through ion correlation forces in a similar way as for C-S-H cohesion [8, 67]. One study did report an attractive dispersion force among the polymer layers that is not negligible but the magnitude of this force remains small compared to the entropic tendency of the polymers to repel each other as much as energetically favorable [8, 68].

Suspension related forces

Above forces are acting in-between particles, ignoring the physical state of the suspension. When it concerns the rheology of cement pastes, the particles are also subjected to forces induced by the applied shear rate, stress or gravitation. This external load is transferred to the suspension by movement of the particles and the suspending liquid. The stress response of the suspension is then determined by the relative balance between all internal forces in the system. The forces resulting directly from the externally applied load are gravity, inertia and hydrodynamic forces:

- Gravitational forces originate in the mass of the particles subjected to the gravitational acceleration. For these forces to become dominant, the components of the suspension are lacking sufficient network forming capacity for a particular mass fraction. In a system at rest, for example, gravitational forces are best illustrated by the phenomenon of static segregation.
- The inertial forces are embedded in the kinetic energy of the flowing particles. Through the displacement of the suspending liquid and through particle collisions, the kinetic energy can be transferred in-between particles, even for a removed external force. The origin of the stress response can be visualized by assuming particles moving in an ideal fluid with zero viscosity.

- In suspensions, the interstitial fluid properties can cause important hydrodynamic forces which can change the velocity direction and magnitude of the moving particle. For example, the viscosity of the liquid can be sufficiently high to drag particles in its movement relative to the particles, which is referred to as viscous drag.

Recently a classification of a particle suspension was made that connects the state of the suspension with the dominant forces and consequent rheology. In Fig.2.16, Roussel et al. provided a rheo-physical diagram of cement suspensions in which the state of the suspension is determined in function of the particle volume fraction and the applied shear rate [5]. For increasing particle volume fraction, the boundary shear rates in-between the zones of different rheological mechanism evolve as indicated with the lines $\dot{\gamma}_C^F$ and $\dot{\gamma}_C^{Re}$. The volume fraction, written as φ_{perc}, is a critical volume fraction below which there are no direct contacts nor distance interactions between the particles and above which the suspension displays a yield stress. The critical volume fraction φ_{div} is found to be a limit above which the yield stress and the viscosity diverge. It is closely related with the flocculation degree and/or strength of the suspension. Finally, the transition volume fraction of the order of $0.85\ \varphi_{div}$ separates suspensions in which the yield stress is mainly due to a van der Waals interactions network and suspensions in which the yield stress is mainly due to a direct contacts network.

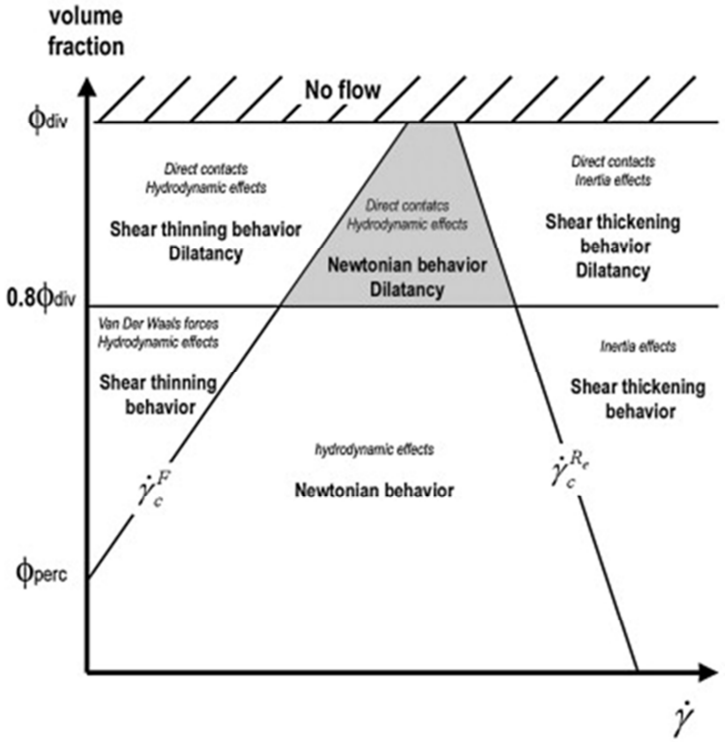

Fig.2.16 Rheo-physical classification of cement suspensions. The dominating physical phenomena (*italic*) are indicated above their macroscopic rheological behavior (**bold**) [5]

2.3.2 Rheological parameters

If one would like to move from cement paste to concrete rheology, one would need to include the broader grading of the particles for which the relevant forces are different, depending on the particle size. Besides this size, several other phenomena are relevant in describing the rheology of cementitious systems. The following parameters are crucial in determining specific regimes and forces within the cement paste in order to describe the rheology effectively:

- The chemical composition of the cement will determine the number and nature of the ions in pore solution and the surface chemistry. This will greatly affect electrostatic forces between particles.
- The particle size distribution, the specific gravity, the surface texture and geometrical shape of the cement are all relevant in terms of frictional forces between sliding particles and for particle packing.

- The volume fraction is the dominant factor in defining the nature of the interparticle interactions during shear and leads to different regimes of dominant forces that control the rheology as illustrated in Fig.2.16. It depends on the initial water/cement ratio and the evolution of this ratio throughout hydration.
- The dosage and properties of chemical admixtures influence the pore solution composition, the surface chemistry, the interparticle forces, the particle size distribution, the hydration rate, …
- As for any chemical reaction, the temperature and humidity of the environment are important. Also the mixing procedure and the energy added to the system are relevant.
- The rheological observations are also depending on the applied measuring procedure, the timing and the geometry. The applied energy determines the regime in which the cement paste response is measured.
- All above parameters are depending on the time because the cement particles are continuously hydrating. Therefore the hydration time is a last relevant parameter for the evolution of the pore solution composition, the particle size distribution, the surface chemistry, the consumption of suspending liquid (and the volume fraction), the admixture effectivity, etc.

Most of the above parameters can be coped with when only one particular cement is considered during testing and analyzing. For repetitive measurements of this one cement, the chemical composition, the particle size distribution, the volume fraction, the surface area, the testing conditions and procedure are more or less controllable in function of the hydration time. The remaining challenge is then to capture the SP influence on all of these parameters. Practically, its effects are limited to the induced changes in chemical composition and particle size distribution. The first has already been discussed in section 2.1 and showed particular relevance concerning the sulfate/aluminate balance. The effect on particle size distribution is also important and will be addressed shortly in the following paragraph.

Cement particle size distribution

Due to the formation of hydration product layers on the particle surface as well as to agglomeration, changes in the particle sizes of the hydrating Portland cement are occurring. Despite the importance of this parameter,

only few researchers have investigated the evolving particle size as such during hydration [69, 70]. They isolated the particle growth from agglomeration by strong mechanical dispersing of the cement particles before measurement. The obtained results are therefore interesting but not entirely representable for the particle volume in a real cement paste. The technical difficulties in these kinds of tests impede the desired result which explains the relatively poor scientific interest. In the field of particle agglomeration, slightly more research has been done, which will be discussed in section 4.

One very recent investigation has combined scanning electron microscopy and laser granulometry to characterize the dispersion states of cement pastes [71]. The different kinds of particles and their meso-structural organization were identified, along with transfers of particles that can occur between the different granulometric classes. The addition of polycarboxylate superplasticizer was found to cause a shift of the particle size distribution to the finer fractions, as shown in Fig.2.17. The researchers used the confined areas (A1-A4) under the curves to discuss the transfer between granulometric classes. The established method showed low accuracy to distinguish the effect of different polycarboxylates but this multi-scale approach seems promising in linking the mesoscopic state and rheological behavior of a cement paste.

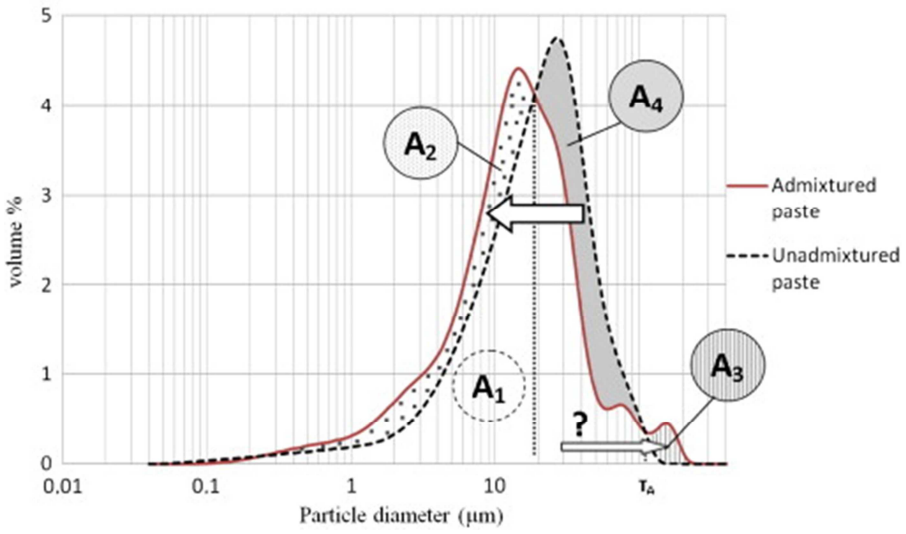

Fig.2.17 Identification of dispersion phenomena caused by the addition of 0.1% of polycarboxylate [71]

A more stable but also much more labor intensive method consists of high pressure freezing the cement paste for preserving the internal 3D structures [46, 72]. Combined with cryo- Focused-Ion-Beam sectioning and high resolution cryo-SEM, it was possible for the first time to investigate the spatial distribution of suspended cement particles and hydrates in function of hydration time. It was indeed found that the addition of PCE influences the volume of hydration phases and their spatial distribution. More exactly, the prevention of particle and hydrate flocculation was observed. This effect led to changes of the particle size distribution, specific surface area and numbers of particles and could be correlated with the rheology. Despite the promising results of this technique, its application is highly intensive in terms of labor and instruments.

At this point it is clear that a multitude of forces and factors is influencing the physical and chemical balance within a plasticized cement-water system. As can be deduced from above, the adsorption of the superplasticizer plays a crucial role in determining the size of the dispersion force, the ion composition at the particle surface, the intervention in hydration reactions, etc. Therefore, the following paragraph will focus specifically on the superplasticizer adsorption phenomenon.

Adsorption

In this section the adsorption of SP on cement particle surface will be discussed in terms of the basic and latest research on this topic. The current generation of SP is frequently incorporated in current research but has only been explicitly addressed since two decades.

SP adsorption parameters

As defined in section 2.1, the superplasticizer in this work is a polycarboxylate polymer which draws its adsorptive capacity from the COO^- group built in its structure. Upon immersion of the polymer in the suspending solution, the counter ion of the carboxyl group is partly released into solution. The remaining structure forms intermediates in water with various types of coordination for the polyacrylates shown in Fig.2.18 [73]. The adsorption of the intermediates or complexes results from four energy contributions [74, 75]:

- The attraction energy between the charged polyelectrolyte and the partially coordinated atoms of the mineral surface of the cement particle ($\Delta H < 0$)[3],
- an entropic gain from the large number of released counter ions into the pore solution upon adsorption ($\Delta S > 0$)[4],
- electrostatic repulsion from the other polymer backbones present at the cement surface and the hindering of their swirling side chains ($\Delta H > 0$),
- an entropic loss from the reduced conformational flexibility upon adsorption ($\Delta S < 0$).

The first two contributions favor adsorption while the last two work against it. Consequently, adsorption will only occur if the net contribution to the Gibbs free energy (Eq.2.8) is negative ($\Delta G<0$). The enthalpic and entropic contributions to the Gibbs free energy depend on the ionic composition of the pore solution, on the molecular architecture of the PCE molecule, its molecular weight and types of anchor groups and on the surface loading of the substrate with PCE [74].

$$\Delta G = \Delta H - T\,\Delta S \qquad (2.8)$$

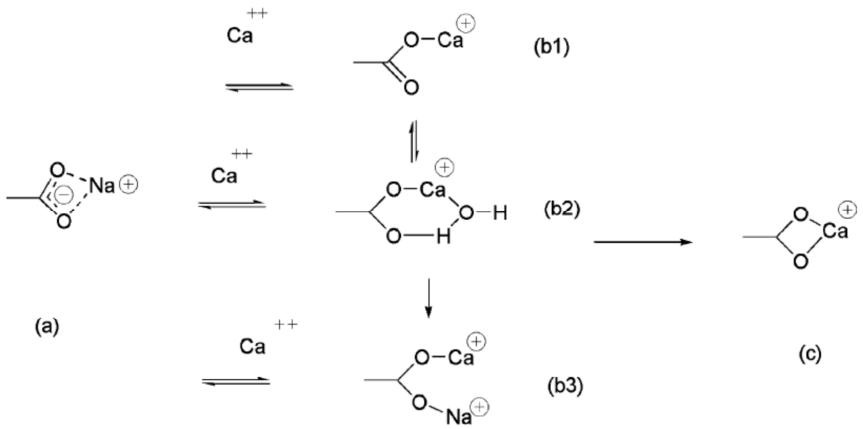

Fig.2.18 initial Na^+ complex (a); intermediate Ca^{2+} complexes (b1), pseudobridge with H_2O (b2), pseudobridge with Na^+ (b3); final Ca^{2+} complex (c) [73]

[3] ΔH: Change in enthalpy
[4] ΔS: Change in entropy

In a study on three different allylether-based PCE superplasticizers adsorbing to a $CaCO_3$ surface, the thermodynamic parameters Δ*H*, Δ*S* and Δ*G* were determined experimentally [74]. For all PCE molecules, negative ΔG-values were found which indicate that the adsorption of these polymers is a spontaneous process. In the presence of calcium ions, the adsorption was less favored because of the low net charge of the polymer due to calcium complexation of the carboxylate groups. The entropic gain of released calcium ions is too small to compensate this weakened attraction.

Considering the molecular architecture, a higher anionic charge density will lead to a higher negative enthalpic contribution to adsorption (ΔG<0). Similarly, a decreasing side chain length will reduce the entrotropic loss due to a relatively higher number of spatial conformations upon adsorption. It was found that, in the presence of Ca^{2+}, adsorption of allylether-based PCEs is almost exclusively driven by a gain in entropy, favoring more compact molecular conformations [74].

Furthermore, the presence of calcium is reducing the charge of the calcium complex more for polymers with high side chain density and long side chains than for low side chain density. In Fig.2.19, it can be seen at the right that the accessibility of the $–COO^-$ ligands is stereochemically restrained, which results in a higher amount of Ca^{2+} bound per $–COO^-$ group and the reduction of the anionic charge density is relatively stronger [76].

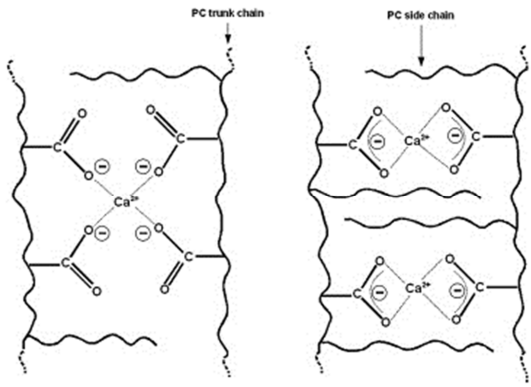

Fig.2.19 Schematic illustration of complexation of Ca^{2+} by two PC strains possessing low side chain density (left) and high side chain density (right) [76]

Superplasticizer consumption and adsorption conformation

After addition of the superplasticizer to the cement paste, the way of polymer consumption has been divided into three categories [77]. One part is adsorbed onto the cement particle surface where it is allowed to function as a dispersing agent, as illustrated at the right in Fig.2.20. A second part is consumed by intercalating in-between hydrate layers or coprecipitated with hydrate phases, as can be seen at the left in Fig.2.20. In this respect, the formed hydration product is called an organo-mineral phase (OMP). If the polymer adsorption and consumption comes to an end, a third part of the polymer is neither adsorbed nor consumed and remains in pore solution. This is shown in the top middle of Fig.2.20.

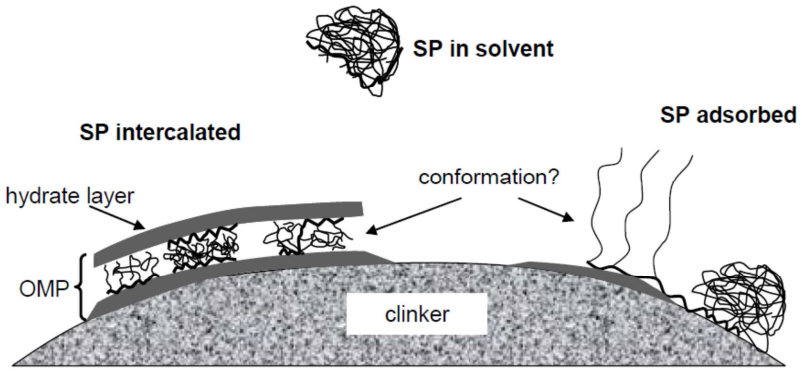

Fig.2.20 Three reservoirs of superplasticizers in cement-water system: intercalation of SP (left), adsorption of SP (right) or SP remaining in solution (top) (OMP = organomineral phase) [78]

The fundamental reactions leading to the intercalation of polycarboxylate superplasticizers into calcium aluminum hydrates were studied by hydration of pure C_3A [79]. It was found that, for higher sulfate to C_3A ratios, less SP was intercalated in OMP and more formation of monosulfoaluminate was promoted. The intercalated SP is no longer functional as a dispersing agent and therefore this process is unwanted. It was demonstrated that intercalation can be avoided by using PCs with long side chains or highly sulfated cements containing alkali or calcium sulfates which dissolve fast [80].

For the polymer that is adsorbed on the right in Fig.2.20 and that is functionally active, the conformation of the side chains can be coiled or stretched which are often referred to by respectively the mushroom and brush conformation, as originally mentioned by de Gennes [81]. Recent research with the AFM technique showed that, for comb-type

superplasticizers, the side chains are rather coiled than stretched [40, 82]. The coiled chains are predicted to become stretched when the average spacing between the chains is less than twice their hydrodynamic radius[5] [83].

Concerning the SP that remains in solvent, as sketched in the top of Fig.2.20, the functionality of the adsorbed SP cannot be provided but it has been suggested that it can still reduce friction between adjacent particles [39]. By filling the interstitial spaces between neighbor particles, direct contact is avoided and lubrication takes place. Furthermore, it is expected that the SP changes the liquid properties and improves the wettability of the particle surface. Finally, it is reported that the superplasticizer in solution also influences the nucleation, the growth and crystal shape of hydrate phases [17, 20, 78, 84, 85].

Besides polymer properties, the reactivity of the cement is also important concerning intercalation as higher reactivity leads to a higher consumption of polymer in hydration reactions and lower availability of the polymer for dispersion (see Fig.2.21). As a result, more polymer is required for equal performance. Similarly, Fig.2.21 can also be considered as the same cement at different hydration time. It illustrates how, in the case of direct SP addition with the mixing water, a considerable part of the polymer would be precipitated uselessly in the organo-mineral phase. On the other hand, if the SP is added around 10 minutes after the mixing water, more SP is available for dispersion [77].

[5] Hydrodynamic radius: $\frac{1}{R_{hyd}} = \frac{1}{N^2}\left\langle \sum_{i \neq j} \frac{1}{r_{ij}} \right\rangle$ where r_{ij} is the distance between subparticles i and j, and where the angular brackets represent an ensemble average.

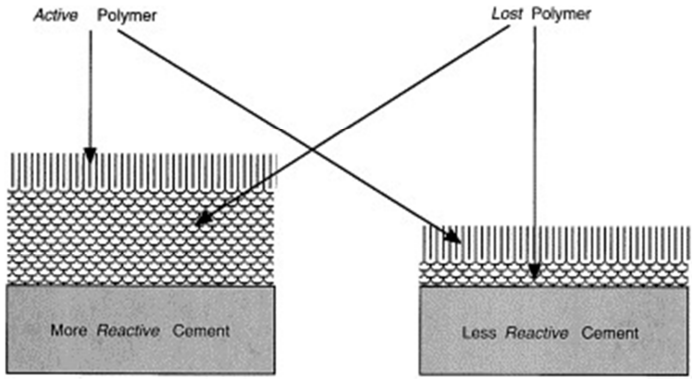

Fig.2.21 Schematic representation of the concept of reactivity of a cement towards a polymer. Higher reactivity leads to a higher consumption of polymer in side-reactions and lower availability of the polymer for dispersion [77]

The effect of adding the superplasticizer with the mixing water and after the mixing water has been compared for different kind of organic admixtures [86]. The flow properties were improved for cement pastes with delayed SP addition because the admixture consumption by the initiating hydration reactions is reduced.

In cement paste, several phases have been found to be positively charged and are adsorbing significantly more negatively charged polymer than other phases. For example, the intercalation of SP by the aluminate phase was reported to be higher than for the alite phase [86, 87]. It was even reported that admixtures show selective binding to their preferential crystal lattice directions of C_3S [50]. The alite and belite phase are negatively charged due to ionized SiO_2 groups present at the cement particle surface. However, the calcium ions in pore solution partly satisfy these sites and allow the local surface to transfer from a negative to a positive charge [88]. In this way, the calcium ions provide the possibility for the superplasticizer anion to adsorb at the originally negative phases.

Concerning the isolated hydration products, the SP mainly adsorbed on ettringite, monosulfate and C-S-H [89]. Without SP, separate pastes of C_3S and C_2S showed a negative zeta potential (around -5 mV) while for C_3A and C_4AF the zeta potential was positive (+5 to +10 mV) [87]. Therefore, it was suggested that the accelerated coagulation of cement particles might occur due to the electrostatic potentials that are opposite to each other. When SP is added, all mineralogical components showed a negative zeta potential due to the electrostatic charge of the SP. This corresponds with

the postponed coagulation observed in practice. Few phases are illustrated in Fig.2.22 in function of four different superplasticizers.

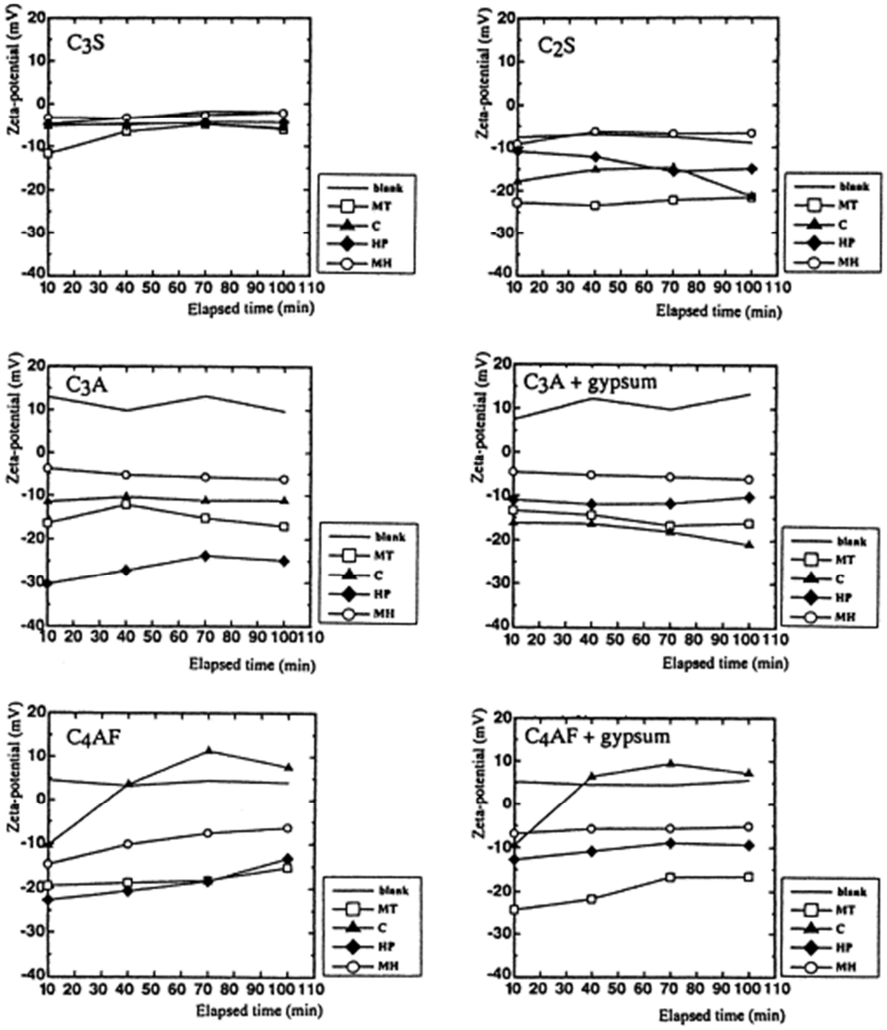

Fig.2.22 The zeta potentials of mineralogical cement phases in a solution with and without admixture (blank= reference;MT=Maleic acid derivative; C=Polysulfonic acid; HP=PC ether chain;MH=PC long ether chain) [87]

Other studies confirmed that ettringite is the cement phase which adsorbs most of the superplasticizer and therefore influences the rheology significantly in contrary way [39, 90]. On the one hand this hydration product negatively impacts the rheological properties, but on the other hand it provides a strong adsorption. Therefore, it has been reported that a

large amount of adsorbed PCE does not necessarily imply low apparent yield stresses when it concerns ettringite [39, 91].

Competitive adsorption

The fact that the superplasticizer adsorbs directly or indirectly through its negatively charged carboxylate group , makes it subject to competitive adsorption of negatively charged sulfate and hydroxyl ions [34, 92]. In literature, the focus has been on the SP/sulfate competition because of its relevance in AFt formation and SP consumption. Generally stated, the more superplasticizer adsorbs on the cement grain surface, the longer sulfate ions remain in the pore solution, the slower sulfate carriers will dissolve. Reversely, for higher initial sulfate concentration, there will be less SP adsorption and a lower repulsive effect will reduce the flow properties of the paste.

2.3.3 Combined admixtures

Next to the complex interactions between cement and SP, this thesis will also handle the combined addition of different admixture classes. As mentioned before, the focus will be on polycarboxylate ether (PCE) superplasticizer, sodium gluconate (SG) retarder and a calcium nitrate (CN) accelerator. In literature, the reports on the interaction between these kind of admixtures is limited to a few case studies. No reports were found on these particularly selected admixtures nor on the combined influence on rheology.

Concerning the combination of SP and retarder, a study has been done on a self-levelling mortar based on OPC, calcium aluminate cement and anhydrite. The polycarboxylate-based superplasticizer showed no plasticizing effect in combination with citrate retarder while good flowability was observed with tartrate retarder [38]. It was demonstrated that the citrate reduces the SP adsorption on the cement particle surface, making it less functional as a plasticizer.

In contrast, both retarders did not much affect the adsorption of a casein biopolymer in the same study which was attributed to the unchanged anionic charge density of the retarder complexes. It was found that molecules with lower anionic charge density will adsorb only if, after adsorption of the admixture with higher anionic charge, a cationic surface charge and enough adsorption area still exists. The incompatibility problem between the polycarboxylate based SP and citrate was solved by increasing the anionic charge density of the SP molecule [38].

Another study focused on aminosulfonic acid-based superplasticizer and studied the effect of the two retarders, sodium gluconate and citric acid, on the paste fluidity. At the same dosages, the citric acid did not improve fluidity. The effects of sodium gluconate on the competitive adsorption with the SP were weaker. It also had a smaller impact on the enhancement of ettringite formation than citric acid [54]. This can again be related with the charge density of the adsorbing complex: sodium gluconate has one carboxyl group while citric acid has three, which promotes its adsorption.

In addition, the same study showed that sodium gluconate seemed to enhance the distribution of that specific SP on C_3S and C_2S particle surfaces at low SP concentrations. Furthermore, it was found that sodium gluconate retarded the hydration of C_3S and that a 0.03–0.09% dosage should be used to effect higher fluidity and lower flow loss of the cement paste [54].

For the specific combination of PCE superplasticizer and sodium gluconate in this thesis, only little previous research was performed and even less on the rheological impact. One study demonstrated that sodium gluconate has the potential to fill the space in-between adsorbed polymeric superplasticizers [93]. They suggested a more densely packed organic layer on the cement surface when the SP is combined with SG but they did not include the effect on rheology. Others focused particularly on the effect on rheology but only for sodium gluconate and polynaphthalene sulfonate instead of PCE superplasticizers [54, 94, 95].

Concerning the combination of a superplasticizer with an accelerator, only one descriptive study has been found [58]. It utilized superplasticizers from the lignosulfonate and the polyacrylate type, combined with calcium nitrate in OPC pastes. The setting accelerator was used to counteract the retardation induced by the superplasticizers. It appeared that the polyacrylate SP retarded less than the others, but calcium nitrate was able to counteract both retardations. Increasing dosages of calcium nitrate lead to some increased flow resistance and static gel strength. However, the flow was still higher than for non-plasticized cement pastes.

No studies were found to address the triple combination of a superplasticizer, retarder and accelerator. However, its practical relevance appears from the commercial systems offered by admixture companies. For example, the DELVO system from BASF is said to contain a stabilizer and activator [96]. The stabilizer is added to freshly batched concrete and stops cement hydration by forming a protective barrier around

cementitious particles. Afterwards, the activator breaks down this barrier and allows cement hydration to proceed normally.

A similar system has been discussed in little more detail – but with commercial restrictions – by Kinney in 1989 [97]. The stabilizer seems to be composed of carboxylic acids and phosphorous organic acids and salts. Its function is clearly defined as retarding all clinker phases including calcium sulfate. It mainly affects the C_3S hydration but can also delay initial C_3A hydration or slow down the conversion of ettringite to monosulfate. It appears to retard by slowing the C-S-H nuclei formation and C-S-H and CH growth, causing finer CH and denser silicate hydrates. The activator is addressed as an accelerator without giving further details. Although these hydration controlling admixtures allow reactivation of the concrete, they were not specifically combined with superplasticizers nor was the effect on rheology studied.

By now, it is clear from the bibliographical research that, in case of a threefold admixture combination, the available parameters are numerous and highly correlated. It is conceivable that investigating one single combination will not be able to capture the performance of the wide variety of concrete admixtures. However, if ways are found to address the rheologically relevant parameters, it might become feasible to quantify the effect of this and other admixture combinations in terms of these parameters.

2.3.4 Incompatibility

Incompatibility, in a context of concrete admixtures, is the term that is often used to describe the phenomenon for which a superplasticizer does not perform as expected [98]. This could concern the plasticizing effect, slump retention or increased retardation of cement hydration. For unexpected performances, the superplasticizer is said to be incompatible with the used cement. The reality is that the superplasticizer has interfered in the cement hydration to such an extent that the typical timing and the normal hydration reactions become out of reach. This might be detected for several admixtures and it is related with its dosage and functionality but it is also always in relation to the used cement. The relation with the cement characteristics stems from the production process: Besides the chemical composition, the production criteria of cement manufacturing are rather empirical properties. It is reasoned that these properties are best related with the construction practice.

The production process is guided by i.a. the water demand, the initial and final setting time, stability, hydration rate, specific surface area and

compressive strength. Having empirical production boundaries allows for an economical optimization process of different operational parameters, which is embedded in the manufacturer's know-how. On the other hand, from a scientific point of view, the differences in product properties might seem quiet ungovernable and hard to control. The latter argument will be explained with specific examples below, where the focus is on rheological consequences of cement paste due to superplasticizer addition.

Let us consider one cement factory with a constant sequence of production operations. To simplify the control of the chemical composition of the kiln feed, several ratios are introduced in cement production [99]. The most important ratio is the lime saturation factor (LSF) for which the CaO content is divided by a combined amount of other major oxides. For example, according to German standards (Eq.2.9), the average value of LSF is regulated to be 96 during the production process with a maximum of 101 and a minimum of 90.

$$LSF = \frac{CaO}{2.8\ SiO_2 + 1.1\ Al_2O_3 + 0.7\ Fe_2O_3} \qquad (2.9)$$

It are these kind of ratios, rather than the exact calculated mineralogical composition of the clinker, which control the kiln feed and the eventual clinker composition. In this way, the operational practice allows small deviations in the clinker composition for which it can economically account for in the remaining production process. Although the manufactured cement will eventually meet the required performance criteria, the deviations in the raw mix composition are bound to affect the final cement properties, as will be demonstrated further in this section.

A direct consequence of the clinker composition is the grindability of the formed clinker nodules. For example, a low silica ratio of the raw mix results in efficient burning and a high melt content which causes a low clinker porosity and therefore hard clinker nodules to grind. After the initial breaking, the increase in fineness will mainly depend on the individual clinker phases in such a way that the lime saturation factor becomes now more relevant in terms of grindability [12].

In order to facilitate the grinding process and lower the grinding energy, chemical grinding aids are often added to the clinker nodules (e.g. triethanol amine acetate) in small amounts. Generally, it is agreed that they attach on the freshly broken clinker phase and, in this way, prevent the newly formed particle surfaces to reagglomerate again. However, the amount of grinding aid appeared to influence the adsorbed SP amount and

the rheological behavior of plasticized cement paste [77]. Nevertheless, its effect on SP adsorption is generally neglectable compared to SP-hydration interactions.

At the cement mill, the principal output criterion is based on the cement fineness or specific surface area. This is important in controlling the hydration rate of the finalized cement. In closed-circuit systems a part of the poorly-grinded granules can be returned to make a correction. A traditional Portland cement is usually ground to a surface area in the range of 300-350 m^2/kg. A complementary criterion at this point is the optimum sulfate content which is important to regulate the set of the cement. The required sulfate level can be achieved by the addition of gypsum to the milling process [12].

As mentioned before, the sulfate concentration in cement paste is constituted by sulfate ions from different sources. Any K_2O or Na_2O in the kiln feed combines preferentially with sulfur to alkali-sulfates. Any excess of sulfur over that required to combine with available alkalis combines with calcium [12]. So, in the raw mix there are already different calcium salts present. It is important to note that each type of sulfate carrier in the cement has his own solubility product and the balance in dissolution speeds will eventually determine the sulfate level where cement manufacturers are aiming for.

When superplasticizer is added to a water-cement system, it will change the ionic strength of the paste by introduction of (counter) ions in pore solution. This may already affect the solubility of the sulfate carrying phases and induce changes in the sulfate concentration in pore solution. Another example is the effect of the SP on the supersaturation requirements of CH [65, 100]. These kind of effects are usually referred to as chemical effects opposed to the physical effect that is related to modifying the interparticle force [101].

Both the dissolution and precipitation in the cement system will depend on the amount of superplasticizer that is able to adsorb on the cement grain surface, which is also related with the specific surface area available for adsorption. So, although the cement specific surface area and the required sulfate level are part of the production criteria, they do not account for the complex effect of superplasticizer addition on the rheological behavior.

At this point it is clear that a commercial cement is a tailor made product defined mainly by the raw input materials. Although the finalized cement falls within one specific product category (e.g. CEM I), the small cement

differences within one category can still result in inconsistent rheological performance when certain SPs are involved [102]. From a practical point of view, compatibility parameters are most desirable in order to facilitate the discussion on incompatibility issues. One step in this direction is the sulfate sensitivity parameter (SSP) for admixtures, that takes into account the impact of both the ester ratio and side chain length on the competitive adsorption with sulfate ions [103].

2.4 Modelling cement paste rheology

Rheology prediction models for cement paste are essential to comprehend the macroscopic flow behavior of concrete. The cement paste has a major contribution to the concrete flow because it constitutes the suspending medium of the small and large aggregates in the concrete. However, all factors described in previous sections clearly demonstrated that a complete description of the cement paste rheology is particularly challenging. The current section will discuss different kinds of models from literature that distinguish themselves in their selection of physico-chemical parameters and their purpose.

On the one hand, one could try to correlate the applied shear rate ($\dot{\gamma}$) with the measured shear stress (τ) and fit a mathematical law through the experimental data, like in Eq.(2.1-2.3). Considering an appropriate range of shear rate, this method allows iterative adaptation of the mix components to reach the desired stress level. Several of these models have proved to be useful in describing differences between rheological behaviors but this is only with respect to the macroscopic flow behavior. The disadvantage is that the flow behavior cannot be readily predicted with these models when mix components are new. Indeed, the model does not allow the input of physico-chemical parameters related with these components.

On the other hand, it is possible to write a rheological parameter, like the yield stress, in function of physical parameters, like the ones mentioned in the previous sections. The number of these models is less abundant but widely studied as they would allow concrete predictions based on measurable properties of the mix components. Recent progress has come from studies of the yield stress of metal oxide suspensions as a function of particle size, volume fractions and pH [83]. The basic expression is written as (Eq.2.10):

$$\tau_0 \cong \frac{A_0 a^*}{d^2 H^2} f_\sigma^* \frac{\varphi^2(\varphi-\varphi_{perc})}{\varphi_m(\varphi_m-\varphi)} \qquad (2.10)$$

where 'd' is the median cement particle diameter [nm], $f_\sigma^*$is an explicit function of particle size distribution, a* is the radius of curvature [nm] of the contact points between grains, H is the surface to surface separation distance [nm] at contact points and A_0 is the Hamaker constant [J]. The particle volume fraction is represented by φ and the percolation volume fraction below which the suspension does not display any yield stress is φ_{perc}. Its values are around 0.20-0.40 and vary according to the physico-chemical properties of the cement powder and to the nature and amount of the additives used in the mixture. φ_m is the dense packing fraction for which identical spherical particles form a closed network with maximal density (±0.64) [5].

Substantial attention has been given to this recent model as it seems to allow incorporation of the polymer adsorption effect to some extent [5]. It was reported that this relation captures the fact that the yield stress decreases with increasing adsorbed layer thickness [88]. Furthermore, for the case of steric stabilization and at full surface coverage of the particles, the yield stress would scale with the −6/5 power of the side chain length of polycarboxylate superplasticizers [43]. Relations of this nature are particularly helpful in the bottom-up description of the concrete rheology as they relate component properties with rheological behavior. The use of this model is limited to pastes including water reducing admixtures because for ordinary water/cement mixes the flocculation is too high to guarantee the modeled divergence of the yield stress at the dense particle fraction φ_m.

Similarly to the yield stress, the apparent viscosity (μ) has been expressed by various empirical equations, with the most famous one being the Krieger–Dougherty equation (Eq.2.11). The general form of this equation is the following:

$$\mu = \mu_0 \left(1 - \frac{\varphi}{\varphi_{div}}\right)^{-q} \qquad (2.11)$$

Where μ_0 is the suspending liquid viscosity and q is likely to equal the value two, for spheres, but might also depend on particle shape. The volume fraction for which the yield stress diverges is φ_{div} but its value is still matter of debate [5]. Because of the deviating properties of real cement paste, this model requires careful adaptation while it is more easily accepted for simpler materials.

Predicting the yield stress and viscosity has been and still is of great practical relevance. However, it is only a first step for the more advanced concrete modelling. Knowing the cement paste component properties does not automatically tell how the corresponding concrete will behave. There are still different aggregate properties to incorporate. To that extent, one frequently used method to predict the concrete rheology is the homogenization approach. For this method, it is assumed that the properties of a matrix of scale n can be predicted by the properties of the matrix of scale n-1 along with those of the particles at the same scale [8]. The principal is schematically illustrated in Fig.2.23 where one can imagine a matrix of water and particles of cement at the scale n-1. In this way, at scale n, one could have a cement paste matrix and sand particles to become a mortar at scale n+1.

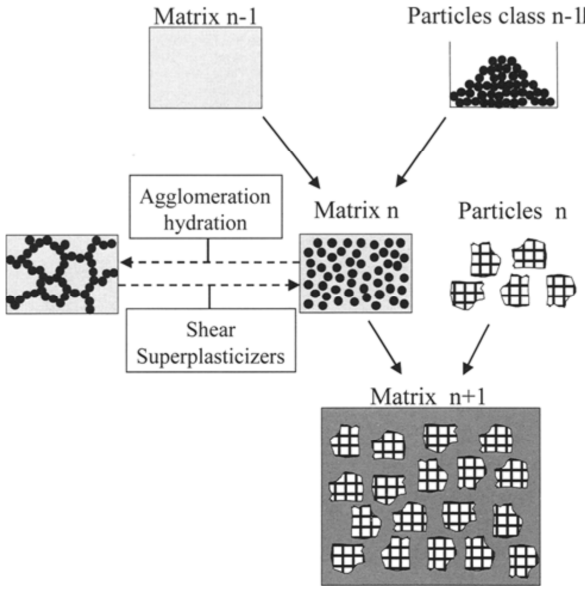

Fig.2.23 Schematic representation the homogenization approach [8]

Furthermore, once the material is flowing, the yield stress is no longer that useful and the viscosity is likely to change for the evolving shear rate and hydration time. For this reason, more extensive models are needed to include the varying parameters during flow. As illustrated in Fig.2.23, agglomerates can be formed due to agglomeration and hydration and these may be larger than the particles of size n-1. In this way, the rheological performance of the matrix of size n (mortar) is no longer independent of the particles of size n [8]. For this and other prediction

methods, the major problem concerns the many length scales that agglomerates can span. This disability to incorporate agglomeration is due to the lack of time dependent parameters that relate to the agglomerate growth. Therefore, this thesis will focus on the relation between agglomeration kinetics and the physico-chemical properties of cement paste.

Agglomeration kinetics

Adding water to cement in typical proportions results in cement pastes with a high solid volume fraction and in these pastes particles will agglomerate due to the high number of particle collisions and inter-particle forces [104]. The agglomeration of particles is described as the tendency of particles to cluster in floccules (or flocs) which are also tended to unite in one continuous large floc [105-107].

At the origin of agglomeration are interparticle forces resulting from surface charges, ionic species and concentrations and the mechanical strength of a floc is higher for high particle concentrations or for small interparticle distances. In a suspension at rest, the latter distances are relatively fixed but they may change when shear is applied (see Fig.2.24 after [64] and [108] in [109]). For example, during mixing the interparticle attraction is subjected to mechanical dispersion forces and the floc may lose its coherence called *structural break-down*. If the floc strength (or stability) is sufficiently high to resist a designated stress level, the particle cluster will be called a *coagulated structure* or an *agglomerate* under that stress level. For increasing shear rate, the particle collisions increase and consequently, agglomerates are broken down into smaller flow units.

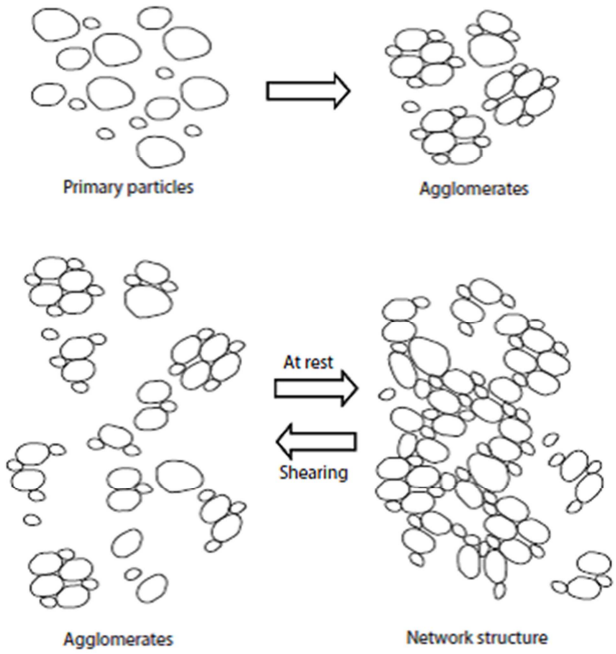

Fig.2.24 Schematic relation between agglomerates and network structure

For rheological purposes, it is desirable to have information about the flocculated state of the suspension. However, obtaining this kind of information in cement pastes is technically challenging due to the required combination of relevant volume fractions, application of shear and a monitoring technique with sufficient resolution. Several studies are dedicated to estimate the degree of flocculation (e.g. [110, 111]) and provide useful information but they face limitations such as too much dilution or lack of particle flow. Only recently, new methods were investigated to study the floc stability incorporating these limitations [112, 113]. With the Focused Beam Reflectance Measurement (FBRM), the influence of shear-induced forces on the microstructure was studied for the first time on fresh cement pastes [112].

Besides direct probing methods, it is also possible to make indirect estimations of the floc size or stability through quantification of the paste structure. The strength of this structure is usually measured by the elastic response to an external stress or deformation, like the storage modulus. When strain is applied to a high strength structure (highly elastic), the structure will break up into high strength agglomerates with corresponding size and stability or will not break up at all [109, 114]. In the latter case, the cement paste is definitely set. The resistance to deagglomeration will

ultimately define the stress response to the applied strain. At rest, the disaggregated particles will reagglomerate and build up the network structure again. Similarly, during macroscopic flow of the paste, the shear stress response is influenced by the evolving agglomerate size and, when the external force is reduced, reagglomeration will occur. In this context, several characteristic flow behaviors can be distinguished in the following paragraphs.

Shaughnessy and Clark [105] made a schematic overview (Fig.2.25) of the possible flow curves reported by Banfill [115]. The obtained shapes of the hysteresis loops are directly related to the duration of the measurement cycle. They change from thixotropic (type 1 in Fig.2.25) to anti-thixotropic (type 3) under the influence of balancing deagglomeration and reagglomeration processes. For the complex shapes of type 2 these two processes are in equilibrium, and their effect on the flow curve is irregularly balanced.

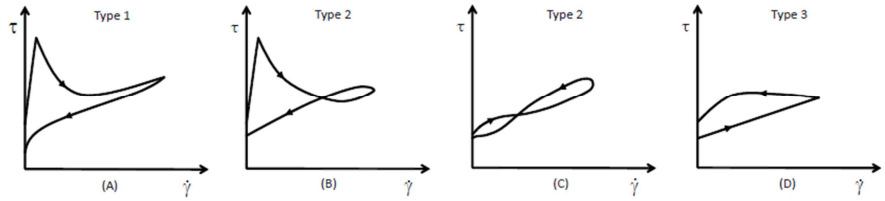

Fig.2.25 Hysteresis cycles of different durations, increasing from type 1 to 3 [105]

The shear induced deagglomeration process is most likely due to the rupture of the links in-between the individual cement particles, as originally suggested by Tattersall (as referred to by Banfill [115]). The mechanical dispersion forces could break the links or force links to loose contact with one of the particles. The longer a shear force is applied, the more links will be ruptured and the smaller the eventual agglomerate size will become. This is what we see in the left scheme of Fig.2.25 once the paste is made to flow (i.e. after the yield stress is reached). The applied shear rate causes the average agglomerate size to decrease which in turn facilitates further flow. As a consequence, a decreasing shear stress is observed for increasing shear rates. The first part of the loop is often referred to as the *accelerating ramp* because of the increasing shear rate. Therefore, it has an arrow in the direction of the *x*-axis.

When the agglomerate size has reached a minimum value and no further deagglomeration is possible, any increase in shear rate will lead to an

increase in shear stress in the remaining of the acceleration ramp of scheme A. This should not be confused with some kind of reagglomeration. Afterwards, during the *deceleration ramp*, the minimum agglomerate size is exposed again to previous forces but now the smaller agglomerates cause lower stresses. This is only possible when the reagglomeration forces remain small and the rebuilding of the agglomerates occurs slower than the dispersing. This behavior is often called *thixotropic* because the viscosity of the paste decreases in function of the time for which a shear stress is applied and it starts rebuilding when the shear stress is removed [116]. However, thixotropy can also be found for a constant shear rate as it is related to time. The evolution from scheme A to scheme D can be seen as the increasing dominance of these reagglomeration forces. They will cause the deceleration ramp to appear gradually above the acceleration ramp which means that the agglomerate size grows faster than it can be mechanically dispersed. In order to enhance reagglomeration, Banfill observed that the reagglomeration process should be given the time to dominate by longer cycle durations [115]. This is a first indication that the reagglomeration forces are induced by time dependent chemical reactions.

Parallel to structural break-down the reagglomeration process is called *structural build-up,* whose dominance during flow is also referred to as *anti-thixotropic* behavior [109, 117, 118]. At lower shear rates during the deceleration curve, the attractive interparticle forces can become again predominant over the dispersive ones which will enhance the floc formation.

Previously, several mechanisms have been proposed to be at the origin of the structural build-up or reagglomeration. One possibility can be the removal of water due to chemical reaction with cement, which would physically hinder the particles moving aside each other and lead to higher interparticle friction. Consequently, a higher stress is obtained for pastes with higher degree of hydration [115]. However, the water consumption during one hysteresis cycle is limited. Another possible mechanism, previously considered, is the physical immobilization of water in the spaces between developing outgrowths from the surface [115] [119]. Of course, the increased contact area between particles as a result of outgrowth formation could also increase the particle interlocking and as a consequence, also the macroscopic stress response of the paste [115]. Because of the high relevance of the particular mechanism for today's concrete rheology, some recent research has focused on this matter. In the

next section, the way agglomerates connect to each other during shear is thoroughly discussed by means of the most recent progress.

Agglomerate connectivity

A recent work by Garrault has studied the rheology of cement paste during setting and incorporated the function of the hydration product C-S-H [120]. In this work it is mentioned how the cohesion of cement paste is due to the formation of a dense network of C-S-H nanoparticles. These nanoparticles are highly 'linked' together through short range ion correlation forces and depend on the composition of the pore solution and the C-S-H surface [120]. Furthermore, the C-S-H surface is reported to be characterized by a high density of electric charge resulting from the oxygen atoms on the ends of silicate tetrahedra. This charge originates from the ionization of silanol groups at the surface, which are formed by protonating the oxygen atoms that are not connecting two tetrahedra nor coordinating a calcium ion. The ionization is favored by the high pH in cement paste and is illustrated as follows:

$$Si\text{-}OH + OH^- \rightarrow SiO^- + H_2O \qquad (2.12)$$

A recent study by Roussel et al. [64] has described the bridging potential of C-S-H in a mechanical way after collecting considerable number of arguments to verify that indeed C-S-H is at the origin of the structure development within the paste. Although these bridges were treated as solids, it was also noted here that, at nano-scale, they can also be seen as dense suspensions of particles. Furthermore, this study distinguishes between colloidal percolation and further rigidification of the bridge forming. It is shown that the network of interacting cement particles evolves as shown in Fig.2.26 [64].

In Fig.2.26(a) the cement particles are shown in dispersed state, which can be found at the end of the mixing phase. Particles are wetted and the pH of the pore solution is raised due to continuing dissolution of metal oxides. The ionization of the cement surface induces charge differences over the heterogeneous cement grain surface which allows colloidal interactions (i.a. van der Waals forces) in-between particles. After a couple of seconds of rest, cement particles are flocculated forming a percolated network of colloidal interactions in Fig.2.26(b). A percolation path is constituted by the darker particles and at the pseudo contact points in-between them the nucleation of C-S-H (black and white dots) starts immediately. This turns the locally soft colloidal interaction between cement particles into a far more rigid interaction that can still be disrupted if sufficient mixing energy is applied. After tens of seconds, it is observed in Fig.2.26(c) that all the

particles within the percolation path (black particles) are linked together by C-S-H bridges forming a percolated rigid network. Finally, it was demonstrated by means of the elastic modulus that, parallel with the increasing size of the C-S-H bridges (black and white dots in Fig.2.26(d)), the strength of the network structure increases. Ultimately, the rigidified structure becomes mechanically more and more irreversible, leading to setting of the cement paste [121].

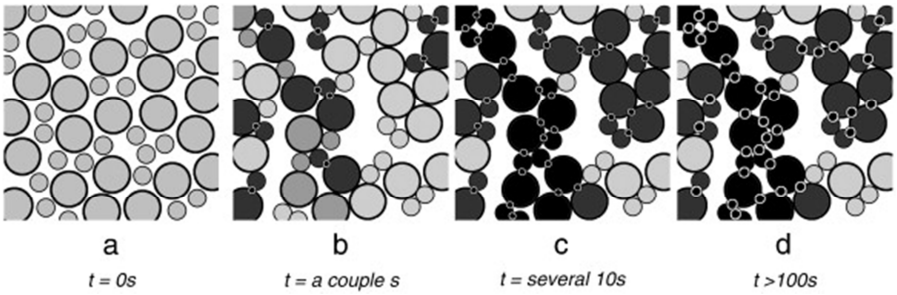

Fig.2.26 Network of interacting cement particles in the dormant period [64].

Roussel et al. [64] isolate the contribution to the elastic modulus of the colloidal network by increasing the frequency of the applied strain oscillation so that the influence of C-S-H nucleation is eliminated when the system reaches a zero strain rate configuration. To that end, they found that the applied frequency is best taken equal to 10Hz or higher [64]. This high frequency demonstrates that the initial formation of C-S-H bridges occurs almost immediately for particles that are adjacent for only a fraction of a second. Therefore, it can be expected that this mechanism is also at the basis of the connectivity in-between particles during flow. This is possible because of local cluster formation, due to colloidal attractive forces in-between particles, where the shear rate is locally very small. The longer the particles remain clustered during flow, the more C-S-H nucleation and reinforcing of the hydrate bridge occur. This will be enhanced by a lower applied shear rate which induces a lower disrupture frequency.

It has been shown by Garrault and Nonat that germination of C-S-H takes place at the surface of the anhydrous grain [64]. Moreover, the probability of germination is greater for water films on cement grains with higher supersaturation of the C-S-H components. For two adjacent particles the proximity of the neighboring surfaces is creating at least one local pseudo

contact zone with high supersaturation conditions and therefore high C-S-H formation opportunities.

In case of disruption of the pseudo contact point due to flow, the weak C-S-H that germinated on one particle is expected to remain available at the surface and is then transferred into a next pseudo contact with another flowing particle. It is clear that for immediate disrupture, the inter-particle bridge will have reached only limited strength but the nucleated material still improves the supersaturation conditions in future potential pseudo contacts. It can be noted that also single C-S-H nuclei from the pore solution can be intercalated in these pseudo contact zones during flow.

From the above it is clear that the C-S-H production rate must be related with the strength of inter-particle bridges and the structural-build up rate of cement pastes. A similar relation is expected to hold between the C-S-H production rate and the agglomerate stability. Therefore, it is particularly interesting to investigate the connectivity potential of C-S-H for different aspects of the cement paste pore solution.

This connectivity potential has been addressed by Garrault as the mechanical efficiency, defined as $R = \delta G'/\delta Q$ [120]. It contains the increase in elastic modulus $\delta G'$ corresponding to the formation of a certain amount of C-S-H in the resting paste, estimated by the released hydration heat δQ. Because this ratio is calculated in the 'strengthening' regime of G' versus time, it can be associated with the precipitation of C-S-H [64]. This concept will be redefined within this thesis and extended for use in cement pastes that truly flow instead of rest. This will allow the chemical activity of the C-S-H to be linked with the agglomeration in a quantifiable way. The obtained information should then facilitate future model development that can incorporate agglomeration.

At the time of writing, no studies have been found that explicitly relate the true chemical activity of cement to the corresponding flow behavior. Different studies did experimentally relate cement properties with flow behavior but not in the micromechanical way [122-124]. For example, a mathematical correlation was found between the flow behavior and a model incorporating modified cement fineness and clinker composition, taking into account the reactivity of C_3A and C_3S [124]. Based on six cements, a linear or exponential function could relate the cement characteristics and the shear resistance, depending on the plasticizer type and dosage. The observed relation was partly explained through the potential activity of the observed mineral phases but does not include the true chemical activity like it was measured by Garrault. Nevertheless, the

existence of the obtained relation strongly indicates that a relation is also apparent between the hydrate formation energy and the flow behavior. The existence of this relation will be explored in this thesis and will be discussed in terms of hydrate/admixture interferences.

Chapter 3 - Materials and methods

In this chapter the material properties, mixing procedures and analytical techniques are introduced. First, the cement and admixture characteristics will be investigated after which the cement paste production will be explained. In a second part, the rheometrical set-up and measuring procedures will be given together with the analytical techniques that have been applied for the different cement pastes.

3.1 Material properties and mixing procedures

In the experimental part of this thesis, cement pastes with admixtures were tested and analyzed in fresh state. To allow meaningful interpretation, the material characteristics are investigated as much as possible and the analytical methods are performed with great care.

3.1.1 Cement

The selected cements in this research are both ordinary Portland cement (CEM I 52.5 N), named C1 and C2. Their production method is the same but they belong to different batches. There was one month in-between their production date. In the remaining of this research, the following abbreviations will be used:

- ‘C1’ refers specifically to the dry cement powder
- ‘C1REF’ refers to a paste of water and C1 without superplasticizer
- ‘C1SP’ refers to a paste of water, C1 and SP
- ‘C1SPSG’ refers to the C1SP paste with additional retarder (SG)

- ‘C1SPSGCN’ refers to the C1SPSG paste with additional accelerator (CN)

Cement properties

The characteristics of C1 and C2 that have been determined in this section are the Blaine fineness, the BET specific surface area, the particle size distribution, the chemical composition and the mineralogical composition. The Blaine fineness was measured through the standard NEN-EN 196-6:2010 and the BET specific surface by the use of nitrogen isotherms with the TriStar 3000 V6.04 A. Both areas are represented in Table 3.1 and show a significantly higher surface area for C1.

Table 3.1 Specific surface are of C1 and C2

	Blaine [cm²/g]	BET [cm²/g]
C1	4343	13788
C2	3536	9975

The particle size distribution of the cements was measured in isopropanol by laser granulometry with the Malvern Mastersizer Micro. In Fig.3.1, the absolute and cumulative volume fraction of the different particle sizes are plotted. For the particle size smaller than 10 µm, C1 shows to have the highest volume of small particles. This particle fraction has a relatively high specific surface area which is confirmed by Table 3.1.

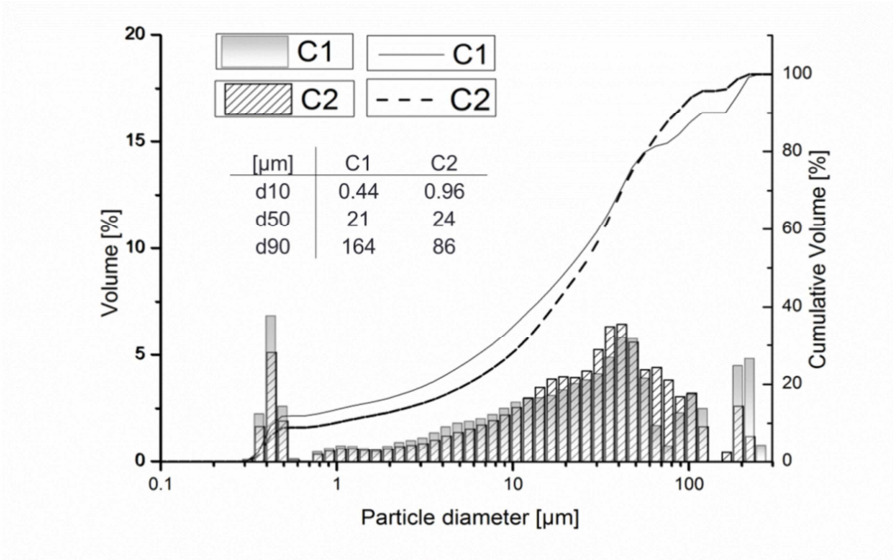

Fig.3.1 Absolute (left) and cumulative (right) volume percentage for cements C1 and C2

The chemical composition of the cements was determined with the X-ray fluorescence (XRF) technique, using the Philips PW 2400 and the result is presented in Table 3.2. In order to achieve more information about the clinker phase distribution and properties in both cements, quantitative X-Ray diffraction (QXRD) measurements were performed on the dry cements with 10 wt% ZnO powder as reference material. For this, a powder X-ray diffractometer (XRD; Philips Analytical) was used with CuKα radiation generated at 45kV and 30mA, 10 and 70 º2θ measuring range, 0.02 º2θ step size and 1.25 s/step counting time. The results for both cements are shown in Table 3.3.

For QXRD measurements on cement pastes, the hydration of those pastes was stopped by quenching the paste in liquid nitrogen, prior to crushing and to introducing this sample in the freeze dryer (-62°C; 0,03mbar for 2 hours).

Table 3.2 Cement chemical composition determined by XRF [weight %]

	CaO	SiO_2	Al_2O_3	SO_3	Fe_2O_3	K_2O+Na_2O	MgO	TiO_2	SrO	ZnO	MnO	Cl
C1	63.27	18.97	5.58	5.01	4.42	1.09	0.866	0.335	0.212	0.0985	0.0981	0.068
C2	63.01	18.86	5.59	5.31	4.28	1.29	0.932	0.342	0.18	0.0999	0.087	0.117

Table 3.3 Cement mineral composition determined by QXRD [weight%]

	C_3S	C_2S	C_4AF	C_3A_{cub}	C_3A_{orth}	Gypsum	Hemihydrate	Anhydrite
C1	39.6	15.9	10.5	4.4	1.7	0.7	2.7	0.0
C2	44.4	17.0	10.1	6.0	1.3	1.1	2.3	0.1

Cement storage

Prior to the experiments, the consistency in hydration performance of the cements was verified with isothermal calorimetric measurements for several weeks. It was observed for the long-term stored cement how the heat of hydration was slightly decreased and postponed. It was suspected that the irregular results were due to the changes in the cement reactivity caused by repeated, prolonged exposure to humidity: While the cement was stored in closed, air-tight barrels, these were opened few times a week, exposing the cement to a fresh batch of humid air. Therefore, the storing conditions and its effect on the hydration behavior were investigated.

As a result of this investigation, it was decided to pack new batches of cement under vacuum in airtight, heat sealed bags. This packaging method showed major improvement compared to barrel packed cement. The final vacuum packaging method required large vacuum bags, a vacuum pump and a household sealing apparatus with vacuum option, as can be seen in Fig.3.2. Satisfying results were obtained for cement portions of 500g that were wrapped and sealed twice under vacuum. The use of silica gel pouches to absorb residual humidity was also applied but was not found to improve the result.

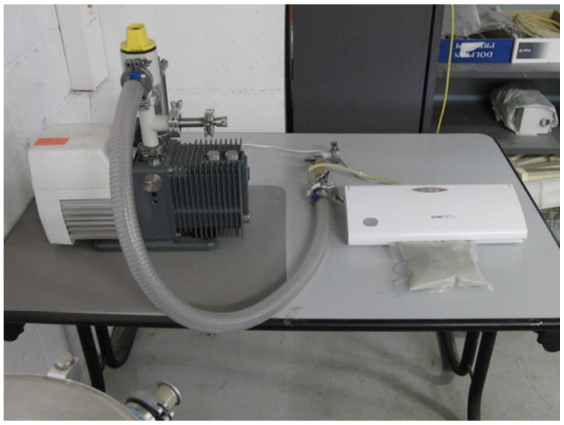

Fig.3.2 The vacuum conservation device (right) in line with the vacuum pump (left)

3.1.2 Admixtures

The admixtures used in this thesis are one type of superplasticizer (SP), one type of retarder (sodium gluconate (SG)) and one type of accelerator (calcium nitrate (CN)). For the superplasticizer, it is important to know some particular product properties which are hard to obtain from commercial products. Therefore, it was chosen to synthesize a comb-type copolymer in the category of the polycarboxylate ether (PCE) superplasticizers. The retarder and accelerators are selected as granular salts from commercial suppliers.

Superplasticizer

The superplasticizer was synthesized as a copolymer of (methoxy polyethylene glycol)-methacrylate (M_n~1100) and methacrylic acid. The chemical structure is presented in Fig.3.3. The statistical side chain density “m:n” is equal to 1:3 and the length of the ethylene oxide chain “p” is equal to 23. Following the description in [37], it was chosen to polymerize pre-formed polyethylene glycol methyl ether methacrylate units and methacrylic acid units through radical copolymerization. The solid content amounts 45 wt% referring to the liquid content. Afterwards a fatty alcohol alkoxylate defoaming agent was added with a dosage of 0.1 wt% of the liquid content.

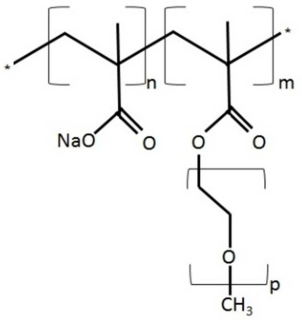

Fig.3.3 Statistical representation of the superplasticizer

Retarder

The sodium gluconate retarder was obtained as a granular salt from VWR and it was added to cement paste with a dosage of 0.03% of the cement weight. In section 5.2, the dosage was exceptionally varied from 0.03% to 0.08 % of the cement weight. The molecular structure is shown in Fig.2.12. It should be noted that this product on its own also shows some plasticizing capacity.

Accelerator

The calcium nitrate accelerator was also obtained as a granular salt from VWR and it was always added to cement paste with a dosage of 2% of the cement weight. The molecular structure is given in Fig.2.13

3.1.3 Mixing procedure

Cement pastes were prepared with a water to cement ratio equal to 0.36, including the water contained in the superplasticizer, using a mechanical mixer. Admixtures were added by mixing them in the cement paste for one minute. The liquid superplasticizer (0.065% or 0.13% of the cement weight) was added 8 minutes after water addition to the cement paste. If the retarder or accelerator were used, then they were added at respectively 38 and 50 minutes after the water addition. For the retarder, the extra half hour towards the addition is adopted to have the aluminate reacting with the gypsum to some extent and thereby it would consume less retarder [23]. In this way, also the delayed addition in practice is simulated. The timing of the accelerator is chosen to have the retarder adsorb first to a reasonable extent.

3.2 Analytical techniques

3.2.1 Rheometry

Two rheometers are used in this thesis. One is the Brookfield Viscometer for which viscosity measurements were performed by means of the smallest T-bar spindle at the rotation speed of 10 rpm. The obtained parameter (i.e. apparent viscosity) was merely used as a reproducible measure for the shear resistance which will be a subject of discussion in this thesis.

A second rheometer is the stress controlled MCR Anton Paar rheometer. For this system, the paste is contained in a steel cup at 20°C, as can be seen in Fig.3.4. The used vane geometry is a six-bladed paddle with a diameter of 22 mm (Fig.3.5). The outer cup diameter is 27.6 mm and its depth is 75 mm. This geometry was calibrated for a shear thinning thixotropic material and the narrow gap in the cylinder proved to be highly efficient in reducing stress deviations.

The vane tool was chosen to overcome difficulties concerning slip between cement paste and metal surfaces of considered plate and cylindrical geometries. Because surface roughening was hard to establish and proved unreliable, the vane geometry was selected while showing consistent results. When submerged, the space in-between the vane blades is filled with paste where it is expected to remain during rotation. This creates a hexagonal shear plane that will be analytically treated as a cylindrical bob. The difference with a cylindrical metal bob is that the cement particles in the shear plane are contained by “soft paste walls”, which prohibits slipping.

Recently, Ovarlez et al. demonstrated with magnetic resonance imaging that the vane geometry is also vulnerable for ‘wall’ slip [125]. More specific, particle depletion near the blades causes a layer of suspending liquid around the fictitious cylinder. In this way, one would be monitoring the viscosity of a non-representative fluid. However, the artifact was demonstrated for yield stress fluids with non-colloidal particles and large particles like in mortar or concrete. Considering the ratio of the current vane size to the small particle sizes in this research, the results are considered reliable and at least comparable within the research program.

The vane is totally submerged in the cement paste for which a snap shot during introduction can be seen in Fig.3.4. The final position of the vane is fixed at 1 cm above the bottom plate of the steel cup. To assure that all samples were in the same conditions before the tests, each sample was pre-sheared at 500 s^{-1} for 200 s followed by a strain sweep exceeding the critical strain of the material.

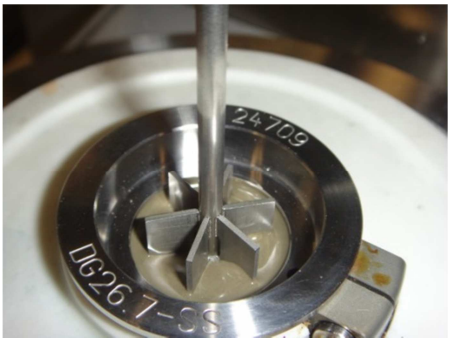

Fig.3.4 Vane during introduction in paste

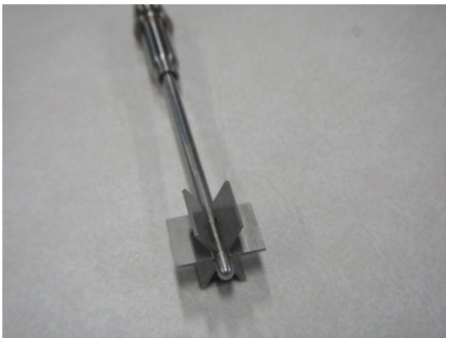

Fig.3.5 Vane geometry

Two kinds of rheological test procedures were performed, each time on different samples. The first is known as a *hysteresis loop* and describes the flow curve for an accelerating and consecutive decelerating shear rate sweep, as in Fig.2.25. The second rheological test is in essence a small amplitude oscillatory measurement alternated with short strain sweeps.

Hysteresis loop

The use of flow curves for studying the flow properties of cement paste has been a returning practice in viscometric studies [115]. It has been criticized that no rheological model should be deduced from the flow curves [126]. However, it is found to be an experimental procedure that provides comparative data, for example, to investigate the effect of admixtures within one paste [127]. Furthermore, it always remains necessary to specify the rheometer geometry and the shear procedure. When one secures these test conditions to be constant for a paste, the differences in shape of the hysteresis loops over time allow comparative judgments through a qualitative model. This model is based on the simultaneous processes like structural breakdown and structural build-up.

By varying the shear procedure (i.e. cycle time and maximum shear rate) several types of hysteresis loops can be obtained like in Fig.2.25. Actually, this variation shifts the balance between the two simultaneous structuring

processes. For example, it is often recommended to minimize the cycle time below 2 minutes for ordinary Portland cements in order to keep the deceleration curve below the acceleration curve. However, in this research, one specific shear procedure was pursued in order to obtain a transition in-between the structuring processes. This must permit a satisfactory description of the hysteresis evolution per cement but still allow sufficient comparison in-between the cements.

The selected shear procedure is schematically shown in Fig.3.6 and involves an increase and a consecutive decrease in the shear rate while measuring the resulting shear stress. The shear rate was first ramped from 15 to 100 s^{-1} in 14 discrete steps and decelerated back to 15 s^{-1} in the same way, in approximately 16 minutes. For each measuring point the shear stress was allowed to stabilize or the average value was taken after 50 seconds of measuring at constant shear rate. The first test started 25 minutes after water addition.

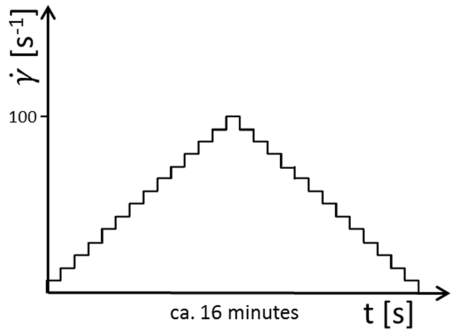

Fig.3.6 Applied shear rate sweep during hysteresis loop

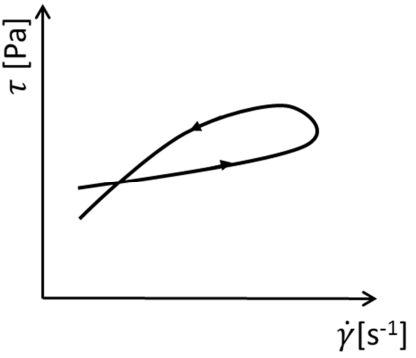

Fig.3.7 Scheme of the targeted hysteresis loop

The targeted type of hysteresis loop is sketched in Fig.3.7. It can be seen that there is an intersection point before which the decelerating curve is under the accelerating curve and after which the situation is vice versa. The time for which this intersection occurs will be called the *intersection time* further in the text.

When the intersection is reached and the decelerating curve dives below the accelerating curve, the structure is broken down to parts that are smaller than the original parts. This suggests that the structural build-up mechanism is reversible and potentially prone to long shearing. It is the

time of intersection and the area enclosed by the loop that will be in our interest.

The position of the decelerating curve above the accelerating curve is a sign of dominant structural build-up during the shear rate sweep. The type of flow curve can be recognized in Fig.2.25 as a type 2 hysteresis curve with a low yield stress (scheme B), due to the presence of the superplasticizer. The applied shear rate did not allow to visualize the very beginning and end of the scheme in Fig.2.25. However, it did allow to visualize the transition over time from type 1 to type 2 hysteresis loops in Fig.2.25 with a fixed shear procedure.

Oscillatory rheometry

For oscillatory measurements, the vane is in the same position in the paste as for the hysteresis loops but it does not rotate. In contrast, the vane only describes an almost invisible vibration over a very small angle. This method is frequently used to evaluate the structural properties of fresh cement pastes, from mixing to setting, because it allows monitoring structural properties without rupturing the paste [66, 128-131]. To this end, the so-called time sweep needs to be performed in the linear viscoelastic domain of the paste, where the storage modulus[6] does not depend on the applied deformation. This region is limited by the critical strain and the deformation amplitude was fixed at 0.0077% to remain within this region.

The oscillatory test was alternated with a strain sweep that consists of an oscillation at fixed frequency with an amplitude increasing from 10^{-5} to 10^{-1}. This assures that the strain exceeds the critical strain of the paste and destroys its structure. The frequency for both tests was fixed at 1 Hz.

In order to guarantee that all samples were in the same conditions before the tests, a strain sweep was performed first, followed by 20 minutes of time sweep. This sequence was repeated about seven times, as illustrated in Fig.3.8, and was similar to that performed by Betioli et al. and Nachbaur et al. [66, 114]. The timing of the strain sweep corresponds with the timing of the hysteresis cycles. It was preserved that each strain sweep occurred half way a hysteresis loop at the maximum shear rate. In this way, the first time sweep started at 30 minutes after water addition.

[6] Storage modulus (G') : the real number of the complex shear modulus $G^* = G' + iG''$

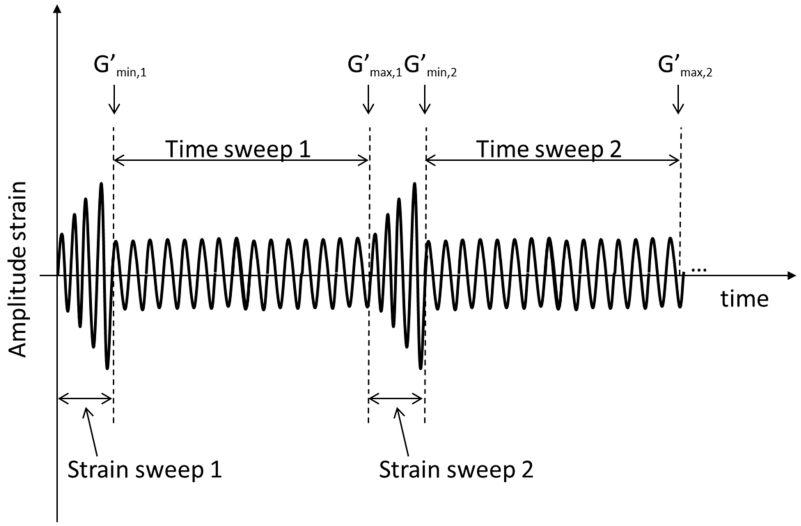

Fig.3.8 Schematic representation of the applied strain amplitude, after [114]. The timing of G'_{min} and G'_{max} registration is indicated.

In Fig.3.9, a monitored storage modulus evolution is shown to clarify different notations that are used in this text. One can see that the time sweep is limited by the initial value G'_{min} and the final value G'_{max}. After each cycle, the time sweep is alternated with the strain sweep. One arbitrary cycle number is indicated with the letter *i*.

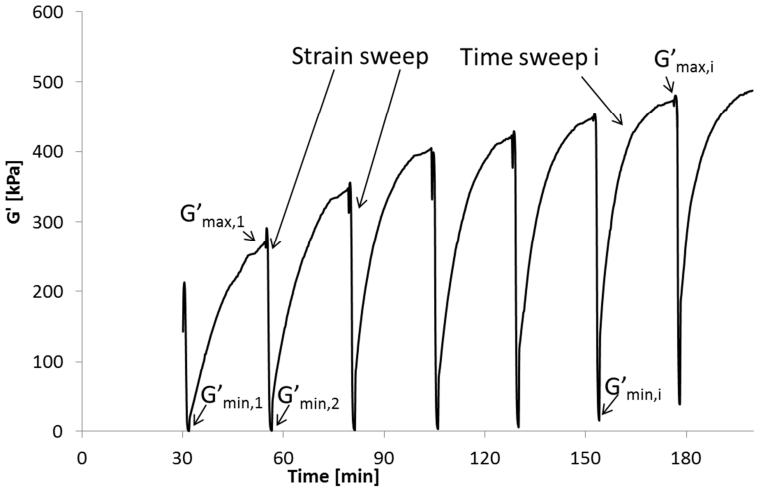

Fig.3.9 Monitored storage modulus example for cement paste. The values of G'_{min} and G'_{max} are indicated.

The above rheometrical tools provide only a snapshot of the rheological evolution and its progress is strongly influenced by hydration reactions. To that end, it is preferred in this thesis to elongate the monitoring time frame through the use of a superplasticizer in a slightly retarding dosage. The induced delay in hydration reactions stretched the different rheological stages over time and the improved flow properties facilitated smoother stress registration.

3.2.2 Cement physico-chemistry

In this section, all technical aspects are described concerning the analytical techniques used to investigate some of the (physico-)chemical aspects of cement. The chemical aspect of cement is often estimated with isothermal calorimetry, the ion composition of the pore solution and thermodynamic modelling. The zeta-potential concerns a physical attraction between particles but is highly sensitive for the cement chemistry. The mineral characteristics are studied by scanning electron microscopy.

Isothermal calorimetry

To study the early-stage hydration reaction kinetics, the heat of hydration was monitored with isothermal conduction calorimetry at 20 °C using the TAM Air device from TA Instruments. Cement pastes were prepared using a mechanical mixer before inserting in the measuring unit. The sample mass was 7 ± 0.5 g. The data were recorded as heat (q) in Watt as a function of the time in seconds. The heat evolution was expressed in Joule per gram of cement per minute for comparison of the data.

Ion concentrations

Ion concentrations in the pore solution were determined after the cement paste was filtrated with the Buchner funnel for 1 minute. The filtrate was immediately acidified with 2% nitric acid (65 % p.a.) to prevent salt precipitation. The ion concentrations in the extracted pore solutions were determined with inductively coupled plasma optical emission spectrometry.

Total organic content (TOC)

The total organic content in the pore solution was determined after the cement paste was filtrated with the Buchner funnel for 1 minute. The filtrate was immediately acidified with 2% nitric acid (65% p.a.) to remove any inorganic carbon.

Zeta-potential

The zeta-potential was studied using the ESA-9800 system from Matec that works on the basis of the electroacoustic method and has an upper limit solid volume fraction of 50 %. Therefore, the cement pastes in these measurements had an initial solid volume fraction of 37 %. During measurements, the pH, temperature and conductivity were monitored simultaneously and the paste was stirred constantly.

Environmental Scanning electron microscopy (ESEM)

Microstructure of the cement suspensions was investigated by Environmental Scanning Electron microscopy with Field Emission Cathode (ESEM-FEG, XL 30, Philips/Fei). Sample preparation occurred similar to the rheological tests and the cement paste was stored in closed containers at room temperature. For the analysis, the fragments of the cement paste were taken from the container and analyzed right away on the Peltier cooling stage. Images were recorded at 10 mbar and a temperature of 12 °C. This corresponds with relative humidity of approximately 85 %. The beam voltage was adapted to the desired resolution and varied between 5 and 20 kV at a working distance of about 8 mm. An elemental distribution map was obtained by energy dispersive X-ray spectrometry (EDX) throughout the sample surface with the EDX system from EDAX. The accelerating voltage was 12 kV and the take-off angle 35.15 degree.

Thermodynamic modelling

It is very difficult to identify the formed hydrates chemically in wet cement paste at young age due to the low resolution of X-Ray techniques in aqueous environment and the physical nature of the hydration products. Therefore, an indirect method was also applied to elaborate on the hydration products that should be formed. The use of thermodynamic modelling in cement chemistry relies on a series of equations that describe the relationship between the pore solution composition and the mineral phase formation in the paste. By modelling the saturation levels of the different phases, information is obtained on the type and formation rate of the hydration products that form.

The use of thermodynamic modeling in cement hydration is often doubted and sometimes considered as a “non-equilibrium” process. Nevertheless, a considerable number of studies have shown the usefulness of this method in cement chemistry [132-139]. They confirm that the cement hydration follows the basic principles of physical chemistry by minimization of the free energy of an isochemical system [132]. However, the success and the

accuracy of these predictions are strongly linked to a reliable thermodynamic database. Furthermore, during the modelling, a local chemical equilibrium is assumed so that mineral solubilities control the chemistry of the aqueous phase. To this end, the rate of dissolution/precipitation is supposed to be locally much faster than rates of ionic transport.

A first step toward modeling saturation levels is determining the thermodynamic activity of the aqueous species for the relevant equilibria in the system. With this activity, the deviations from ideal behavior in a mixture of chemical species are taken into account. The activity of each species (a_i) is expressed by Eq.3.1 [140]:

$$a_i = m_i \gamma_i \qquad (3.1)$$

where γ_i is the activity coefficient [-] and m_i is the molality [mol/kg] of each species, i. The activity coefficient is calculated using the Debye–Hückel equation based on the calculated ionic strength and ion characteristic parameters. The molality can be deduced from the measured ion concentrations. The relation between the true activity of the ionic species and the theoretical solubility is then implemented in the saturation index to determine the saturation point of a certain solid. The definition of the saturation index (SI) is given in Eq.3.2:

$$SI = \log \frac{IAP}{K_{sp}} \qquad (3.2)$$

where IAP is the ion activity product, calculated from the relevant activities derived from the measured concentrations in the solution and K_{sp} is the theoretical solubility product of the ionic species and solid phases considered in the calculations. The form of Eq.3.2 dictates that SI = 0 indicates saturation, SI > 0 indicates supersaturation, and SI < 0 indicates undersaturation.

Determining the activities of all the ionic species in solution requires iterative calculations and for that the GEMS V 3.2 geochemical software was used based on the cement-specific up-to-date CEMDATA database [136, 141, 142]. As the use of saturation indexes can be misleading when comparing phases which dissociate into a different number of ions, “effective” saturation indexes are calculated by dividing the saturation indexes by the number of ions participating in the reactions [137, 138].

Chapter summary

In this chapter, all material properties and measuring methods were fully described to allow meaningful interpretation of experimental results in the following chapters. Moreover, the theoretical concepts touched upon throughout this chapter form a specific answer to the experimental challenges mentioned in the state of the art and also provide a technical basis for the experimental results in the following chapters.

This chapter started with introducing the cement and admixture characteristics, followed by the mix procedures and the rheometrical methods. First, it was shown in what aspect the two selected cements differ and how both cements are stored in vacuum wrapped double bags to prevent pre-hydration. The type and origin of the three selected admixtures was provided together with the mixing procedure of all cement pastes. In a second part, analytical techniques were presented concerning the rheometry and the cement chemistry. The benefits and concerns of the chosen vane geometry were critically evaluated. The vane will be used for shearing the cement paste and measuring hysteresis flow curves as well as for dynamic oscillations to monitor the structure development. For both methods, the measuring procedure and precautions are explained. Finally, the tools for analysis of cement characteristics related with physical and chemical performance were listed accompanied by practical and theoretical considerations on the measurement technique.

Chapter 4 - The influence of superplasticizer on cement paste rheology

The cement paste rheology is determined by many factors, as explained in the state of the art. In order to cover some of the important differences in-between cement batches, two commercial cements, C1 and C2, were investigated. They are described in Chapter 3. When it comes down to rheology, these cements are expected to perform in a very similar way, but it is unsure how they will respond to superplasticizer interactions. Therefore, a rheological study was conducted for the cement pastes with and without superplasticizer. After that, the observed differences were further investigated and explained in the second section. Finally, the relation in-between the experimental observations from the first section was examined and quantified in the third section.

4.1 Experimental observations of the superplasticizer influence

The influence of the superplasticizer in cement paste can be detected on many levels but it will always originate in the altered hydration chemistry. It is possible for the superplasticizer to intervene with the hydrate formation in physical and chemical ways as could be read in the state of the art. For example, the physical presence on the grain surface might prevent phase precipitation which postpones the setting of the cement paste. On the other hand, the SP can also chemically interact with clinker phases to enhance their dissolution speed which can change the phase morphology and subsequently the rheology. Although physical, the first example will show changes in the chemical kinetics and, although chemical, the second example will be manifested in the physical performance of the

paste. In that respect, it is opted in the current paragraph to cover the hydration kinetics, the structure development and the flow behavior for both cement pastes. In this way, a considerable number of microscopic parameters are obtained to use in further comparison and discussion on the cement-rheology relation.

4.1.1 Hydration kinetics

The two selected cements in this research have been discussed in Chapter 3. The hydration rate of these two cements is measured by isothermal calorimetric measurements. The heat of hydration can be observed in Fig.4.1 and 4.2 for both cements, with and without superplasticizer. The cement paste without superplasticizer is abbreviated with the suffix 'REF' and the paste with superplasticizer with 'SP'.

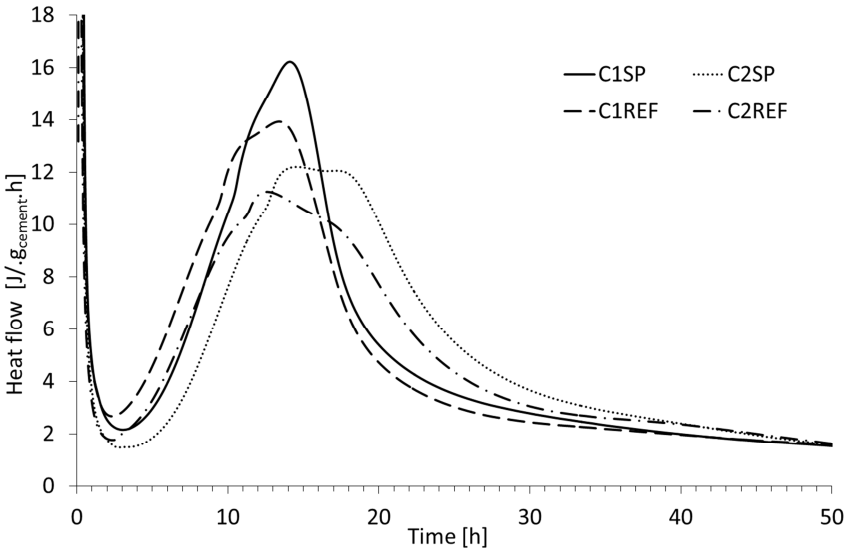

Fig. 4.1 : Heat flow for C1 and C2

Without superplasticizer, C1REF clearly shows a higher heat release in Fig.4.1 than for C2REF and a small delay in hydration stages is observed for C2REF. The higher hydration rate of C1REF is due to the higher fineness of this cement (see Table 3.1).

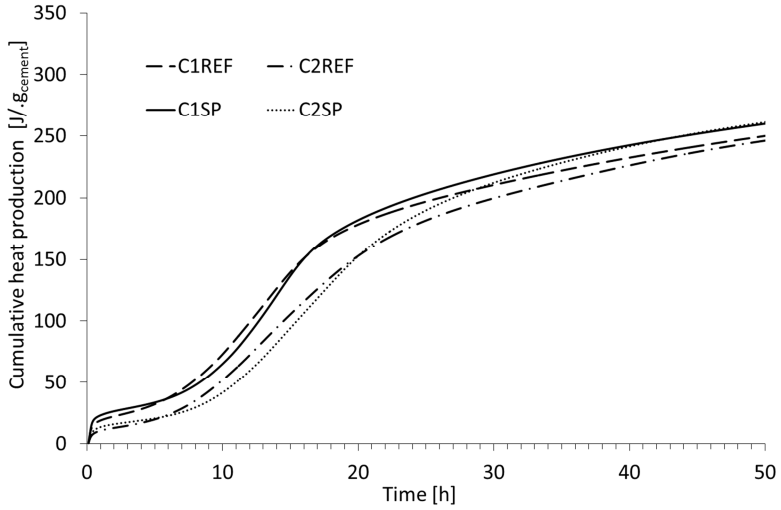

Fig.4.2. Cumulative heat production for C1 and C2

In case superplasticizer is added, both cements show significant retardation of the hydration reactions. The difference in delay was investigated by measuring the total organic carbon (TOC) content in pore solution to verify the differences in adsorption of SP. It was found that at the age of 20 minutes the pore solution contained 123 mg/l carbon for C1SP and 133 mg/l carbon for C2SP. In absolute values, this means that C1 adsorbs more superplasticizer than C2 and more SP molecules can be expected on its grain surface. However, if we divide the adsorbed amount by the respective cement specific surface area, it shows that the adsorption density is 0.23 mg/cm² for C1 and 0.33 mg/cm² for C2. This means that C2 has a denser layer of adsorbed superplasticizer polymer. Therefore, it can be expected that the hydration kinetics will be delayed relatively more for C2SP than for C1SP.

Fig.4.3 shows the adsorption isotherms for both cements where the adsorbed amount of PCE is determined by measuring the TOC in filtrated pore solution for the increasing addition of SP. It can be observed that C1 continuously adsorbs most of the SP and that for the highest dosage the adsorbed amount seems to decrease. The latter can be explained by a SP depletion of the pore solution for which the filtration became ineffective.

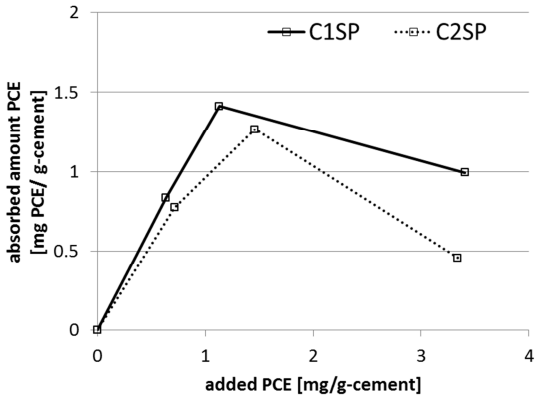

Fig.4.3 Adsorption isotherms C1 and C2 for gradual addition of SP

Due to the different surface coverage, also different flow behavior of the plasticized cement pastes can be expected. In the following sections these differences are quantified and the origin is examined into more depth.

4.1.2 Structure development

To monitor the structure development of the cement pastes, the storage modulus was measured for all setting pastes. For all cements the prescribed oscillatory procedure (see section 3.2.1) was performed and the minimal and maximal storage moduli were collected. The evolution of the minimal storage modulus (G'_{min}) in function of time is given in Fig.4.4 at the left and the maximal storage modulus (G'_{max}) at the right. Each curve shows the average of three repeated measurement series and the range of the values corresponds well with the work of Betioli et. al. [114] considering cement paste with hydroxymethyl ethyl cellulose.

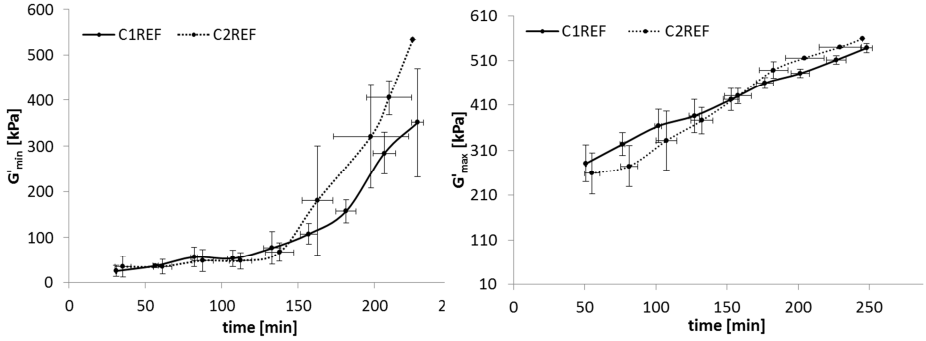

Fig.4.4 Evolution of G'_{min} (left) and G'_{max} (right) in function of time for the reference cement pastes

For both cements it can be observed in Fig.4.4 that the minimal and maximal storage modulus evolves in a similar way. The minimal modulus shows a joined slope increase around 150 minutes which indicates that for both cements a network structure develops which can be only partly destroyed by the intervening shear rate sweeps from section 3.2.1. For the maximal modulus, a constant slope is observed for both cements, which indicates the growing setting rate during each time sweep.

In Fig.4.5 the evolution of G'_{min} and G'_{max} for the plasticized cement pastes is added to the figure of the references. It is observed that the storage modulus for the reference pastes increases faster than for the plasticized pastes. Moreover, the two cements show a quite close correlation for the reference paste compared to the plasticized pastes. The difference between the plasticized pastes is much more pronounced and its significance was confirmed by the standard deviation intervals for each data point, based on the three repetitions for each plasticized paste.

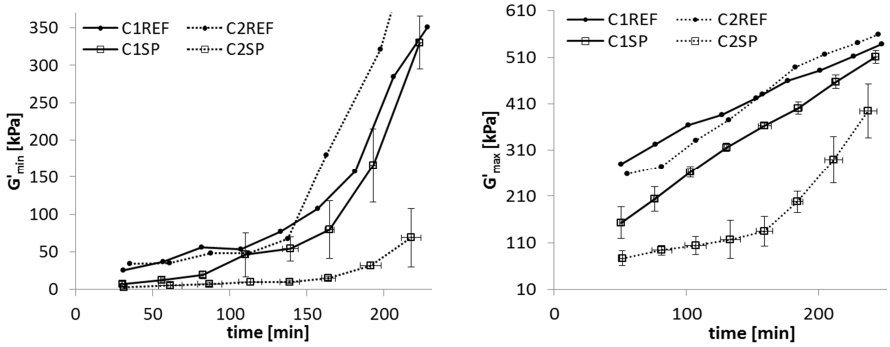

Fig.4.5 Evolution of G'_{min} (left) and G'_{max} (right) in function of time for the plasticized cement pastes

For G'_{min} and for G'_{max} in Fig.4.5, it can be observed that C2 has the slowest structure development, despite the similar cement characteristics. A significant slope increase is detected for C2 at about 160 minutes for both G'_{min} and G'_{max}. Regarding C1, a modest slope is observed for G'_{min} until about 140 minutes, after which the slope increases significantly. In contrast, G'_{max} shows an approximately constant slope for C1.

4.1.3 Flow behavior

In order to investigate the flow behavior, a series of hysteresis cycles was only performed on C1SP and C2SP as the reference pastes were too stiff to permit a relevant shear procedure. The resulting stress in function of shear rate is useful in describing the distinction between C1 and C2 and is

presented in Fig.4.6 and 4.6. The number of cycles is constant for both pastes but due to the different hydration rates only a limited number of cycles remain representative for the fluid pastes. In the case of C1SP, one can see in Fig.4.6 five cycles above each other for increasing stress levels and increasing hydration time. The sixth and following cycles are omitted because they showed no longer a stress increase nor a reliable shape of the curve. The number of the cycle corresponds to the hydration time, given in Table 4.1, for which the maximum shear rate is applied during that cycle. The length of one entire hysteresis interval is about 16 minutes and it is followed by a period of rest towards the next cycle.

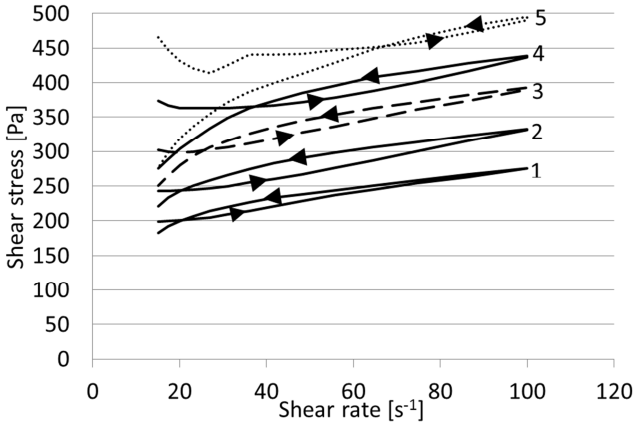

Fig.4.6 Hysteresis loops C1SP with cycle numbers indicated in Table 4.1

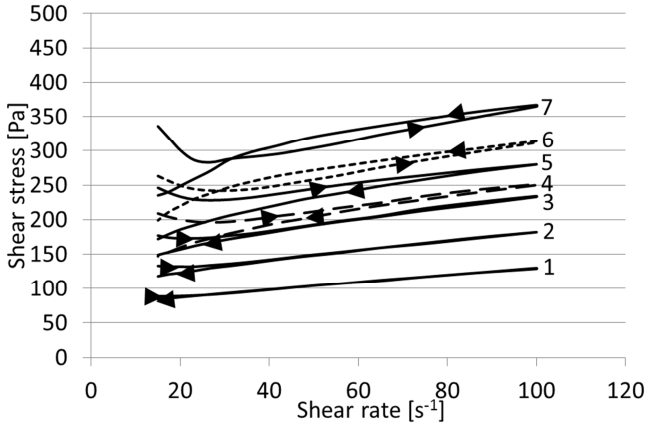

Fig.4.7 Hysteresis loops C2SP with cycle numbers indicated in Table 4.1

Table 4.1 Cycle number with the corresponding time of the maximum shear rate, for both cements

Cycle number	1	2	3	4	5	6	7	8
Time after water addition [min]	30	56	84	110	137	164	191	218

In Fig.4.6, it is observed for C1SP that all cycles show an anti-thixotropic loop while for C2SP in Fig.4.7 it is only from the sixth cycle onwards that the curves become anti-thixotropic. Below this sixth cycle, the curves are thixotropic and the area between the accelerating and decelerating ramp is increasing for higher hydration times. In the anti-thixotropic curves the intersection of these ramps occurs at time t_i during the hysteresis interval and this time interval is referred to as the intersection time. So, this particular time interval starts with the beginning of the acceleration ramp and closes when the deceleration ramp crosses the acceleration ramp.

It is noticed for both cements, but particularly for C1SP, that a series of cycles can be found for which the intersection of the ramps occurs earlier in the hysteresis loop for higher cycle numbers. This means that, in these series, the hysteresis area between the anti-thixotropic ramps is decreasing for higher cycle numbers and consecutively t_i decreases. This behavior of the intersection time will appear to be a returning feature in all cement pastes in this thesis.

4.2 At the origin of different rheological performance induced by superplasticizer

While both cements in the previous section have the same product name and production process, there is a significant difference in rheological performance as soon as the superplasticizer is added (i.e. Fig.4.5). Some important reasons for poor consistence of cement-superplasticizer systems have been explained earlier in the state of the art. In the current section we go deeper into the origin of this inconsistency for the two cements C1 and C2.

As indicated in the state of the art, the sulfate ions play a crucial role in the adsorption effectiveness of the superplasticizer. Therefore, the SP adsorption and the ion concentration of the pore solution will be the first to be investigated over time, considering the main ions composing the pore solution. The adsorption of the superplasticizer was determined in section 4.1.1 by measuring the carbon content in the pore solution. From the specific surface in Table 3.1 it was deduced that this results in an adsorption density of 0.23 mg/cm² for C1 and 0.33 mg/cm² for C2 which means that C2 has a denser layer of adsorbed superplasticizer polymer.

For four kinds of pastes, the ion concentration was determined with ICP-OES on the extracted pore solution. In order to create a concentration evolution, this measurement was performed as function of time, each time for a new subpart of the same paste. For example, the sulfur ion concentration evolution can be seen in Fig.4.8 for the pastes without SP (C1REF and C2REF) and with SP (C1SP and C2SP). The sulfur ion (S^{6+}) is only present in the pore solution as a part of the sulfate ion (SO_4^{2-}), so Fig.4.8 will be discussed directly in terms of sulfate. It is observed how the reference pastes show an equal initial amount and how C2REF shows a faster increase in the sulfate content than C1REF. The subsequent evolution is somewhat oscillating for both pastes but it is clear that the average sulfate concentration is significantly higher for C2REF.

The peak behavior of the reference C2 in Fig.4.8 can be attributed to fast-dissolving sulfate phases causing the steep rise. Indeed, besides the small difference in sulfate content (0,3% more in C2) in Table 3.2, there is also a difference in alkali oxide (0.2% more in C2). Generally, these alkalis are introduced into the cement through alkali sulfate salts, like Na_2SO_4 and K_2SO_4, which are the fastest dissolving sulfate phases in OPC [135]. In this way, the extra alkali sulfates can explain the steep rise of the sulfate content for C2REF.

When SP is added, it is observed in Fig.4.8 that for both cements the sulfate concentration increases significantly, compared to the reference. This indicates a higher sulfate dissolution or a longer retention of the initial sulfate content, due to the prevented sulfate adsorption by the SP. Subsequent to the high initial value, the concentration decreases sharply to a quiet continuous value that remains higher than the respective reference concentrations. The smooth continuity suggests that the concentration gradient towards the pore solution reached a maximum level which is less prone to other changes in the pore solution than in the reference cases.

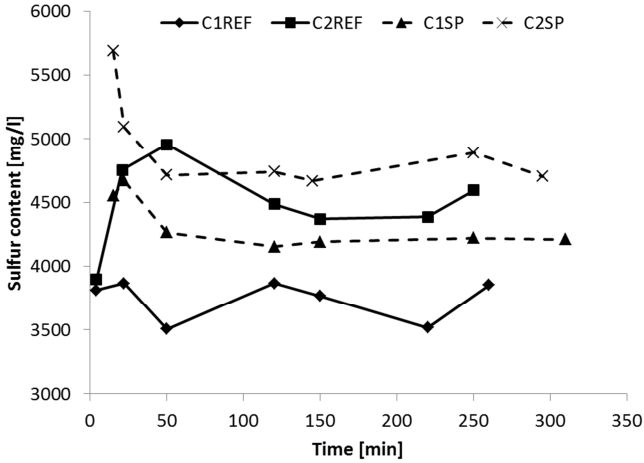

Fig.4.8 Sulfate concentration in pore solution

Thus, after 50 minutes, the sulfate supply for the plasticized pastes becomes limited and the concentration evolves towards an asymptotic value balanced by the remaining sulfate carrying phases. It can be noted that the sulfate concentration at 50 minutes is temporarily very similar for C2SP and C2REF. This is possible, for example, when abundant sulfate ions in C2SP are buffered into an amorphous phase which dissolves again later in the hydration process. However, based only on ion concentration evolutions, this possibility remains questionable.

Based on these results, for both systems, the exact sulfate concentration is determined by the precarious balance between dissolution and precipitation of all phases. Knowing this, the use of a more sophisticated instrument is recommended to describe the relevant processes. Therefore, the thermodynamic state of the system will be used to identify and capture the influence of the important cement phases.

Thermodynamics and mineralogy

The experimental pore solution analysis (Appendix A) provides the concentration of the required ions to simulate the phase behavior in geochemical software. It has been reported that the cement suspensions attempt simultaneously to reach equilibrium between aqueous species and reactive minerals, as well as to reach the equilibria between aqueous species [65]. Before equilibrium is reached for the reactants, the system

becomes supersaturated with respect to the products. This means that precipitation becomes possible but it will only occur for some critical supersaturation values [65]. In order to precipitate rapidly, the concentrations needed for critical supersaturation have to be smaller than those obtained once the reactants are in equilibrium with the solution.

In order to discuss the phase dissolution and precipitation, saturation indexes can be used. However, the saturation indexes as described in Section 3.2.2, can be misleading when comparing phases which dissociate into a different number of ions. Instead, the saturation index will be divided by the number of ions participating in the reactions and this will be called an 'effective saturation index' (further abbreviated as 'SI') according to Lothenbach et al. [137, 139]. Hydrates in equilibrium with the pore solution are able to precipitate and are represented by SI = 0 ± 0.2 SI-units. When the pore solution is undersaturated with respect to a certain solid (SI < 0), it is not formed or it will be dissolved when it is present. If it is supersaturated (SI > 0), the solid might form unless this is kinetically hindered.

Reference pastes

In Fig.4.9, the effective saturation indexes of the sulfate containing phases are shown for the reference pastes (i.e. C1REF and C2REF). It is observed that all saturation indexes are quite continuous, except for monosulfate, and that C2REF contains generally slightly higher SI values compared to C1REF. Additionally, the effective saturation indexes of non-sulfate phases are presented in Appendix B. It was found that the portlandite and C-S-H, represented by the minerals jelenite and tobermorite, are in equilibrium with the pore solution for all pastes during the first 4 hours.

As stated before, the primary difference between C1 and C2 is the higher alkali sulfate content for C2 and therefore this might contribute to the observed SI behavior. For example, Clark and Brown showed how alkalis can slightly retard the kinetics of ettringite formation [143, 144]. With the ions being hindered to precipitate, this would explain the higher saturation degree for ettringite in C2REF compared to C1REF. Moreover, the retarded formation of ettringite may in return affect the saturation degree of the other sulfate containing phases and therefore it could be explanatory for all slightly higher SI values of C2REF compared to C1REF.

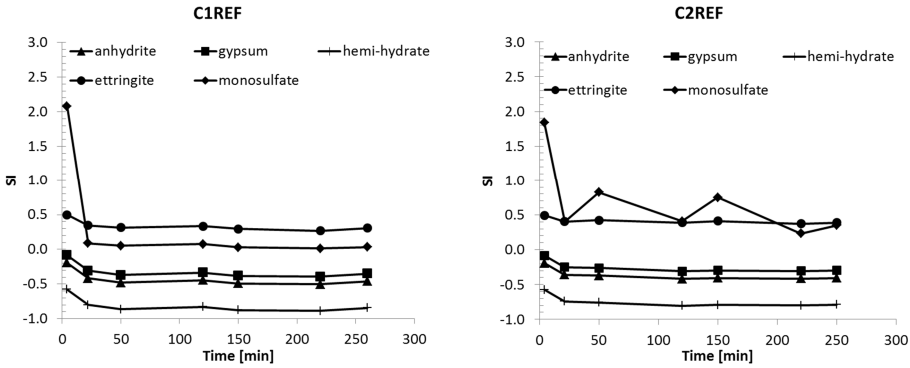

Fig.4.9 Effective saturation index for the sulfate phases in the reference pastes

It can also be observed in Fig.4.9 that, for C1 and C2, the sulfate supplying phases are continuously undersaturated or close to equilibrium. This means that – if gypsum, hemihydrate and anhydrite are present - these phases are dissolving and are delivering sulfate ions to the pore solution. For all three phases a small initial decrease of the curve indicates a dissolution of those phases which is most likely due to a proceeding wetting of the entire grain size distribution in the paste. After half an hour, the dissolution continues unchanged which is confirmed by the subsequent stabilization of the SI.

For C1REF in Fig.4.9 (left), ettringite is supersaturated and monosulfate is in equilibrium with the pore solution. As ettringite is most likely to be formed, this makes ettringite the more stable aluminate containing phase and it will form before monosulfate. For C2REF (Fig.4.9 right), something similar is observed, although it is not clear which aluminate phase is dominant. Monosulfate is also supersaturated in this pore solution which indicates a different sulfate supply mechanism for C2REF compared to C1REF. Both ettringite and monosulfate start high and decrease during the first half hour which coincides with the consumption of sulfate resulting from the gypsum/hemihydrate dissolution. While the remaining SI evolution of ettringite is more continuous, the behavior for monosulfate is significantly different. Actually, after the sharp decrease, the monosulfate curve remains oscillating compared to the other phase behaviors.

At the origin of this difference between C1REF and C2REF could be time-depending kinetic restraints changing the dissolution rates [145]. For example, a sudden increase in SI could be due to a sudden increased ion dissolution caused by hydrate gel penetration exposing new mineral

surface to the pore solution. A changing sulfate supply might therefore be related with an incongruent clinker dissolution, changing ionic strength, physical restraints, etc.

To obtain more information about the dissolution or precipitation of the sulfate carrying phases, QXRD was used to determine the content of gypsum, hemihydrate, anhydrite and ettringite in all pastes. In Table 4.2, this composition is given for all reference pastes, at the age of 0, 120 and 220 minutes (e.g. resp. C1 REF, C1 120, C1 220). It can be observed that for both reference cements the amount of hemihydrate is higher than of gypsum and that no anhydrite could be detected during hydration.

From Table 4.2 it can also be observed that the gypsum quantity is likely to increase in the early stage of the hydration reactions (< 120 min.). This can result from the immediate dissolution of hemihydrate which will first form secondary gypsum before dissolving into pore solution [12]. The amount of gypsum is then quickly accumulated after water addition and it is estimated to reach a peak value around 30 minutes based on Fig.4.9. After that, both gypsum and the remaining hemihydrate will dissolve through the rest of the induction period, which is also compatible with the determined saturation indexes.

Table 4.2 Mineral composition powdered pastes by QXRD [wt.%] at start and at 120 and 220 min of hydration

wt. %	gypsum	hemihydrate	anhydrite	portlandite	Ettringite
C1 REF	0.6	2.5	0.0	/	/
C1 120	2.0	1.0	0.0	0.0	0.0
C1 220	0.9	1.0	0.0	1.0	0.5
C2 REF	0.9	2.2	0.0	/	/
C2 120	1.8	1.4	0.0	0.0	0.0
C2 220	1.6	1.0	0.0	0.2	0.5

It is also found in Table 4.2 that C1REF contains slightly more hemihydrate and slightly less gypsum than C2REF. The dissolution speed of the hemihydrate is higher than for the di-hydrate phase, which explains - apart from the grain fineness - how more sulfate could have been available in C1. However, this virtual shortage of early sulfate in C2REF seems to be compensated by extra alkali-sulfates in the production process. This small amount of alkali sulfate is too small to be detected by XRD but was quantified before with XRF (Table 3.2). Its addition might have been a conscious decision of the cement manufacturer or the result of natural

impurities in the calcium sulfate rock. Either way, this kind of highly solvable sulfate source is increasing the initial pore solution concentration of sulfate but is less long lasting than the effect of calcium sulfate phases [12]. As a consequence for C2, relatively less hemihydrate will dissolve and will be available as sulfate source at later age. Similarly, the higher amount of gypsum can maintain the longer term sulfate supply. This is confirmed by the QXRD results showing a slower dissolution of the formed gypsum and a slower dissolution of the initial amount of hemihydrate for C2REF compared to C1REF. These mechanisms are also compatible with the slightly higher saturation indexes for the dissolving sulfate phases of C2REF.

It is clear now how the higher alkali sulfate level in C2REF is contributing to the averagely higher sulfate concentration evolution as seen in Fig.4.8. The small overlap with the sulfate evolution of C2SP will be discussed further in this section. Another observation is that the alkali sulfate is able to suppress the fast dissolution of hemihydrate. As a consequence, the sulfate counter ion (Ca^{2+}) supply might also be postponed. This is also in line with the earlier reported decrease in calcium solubility in presence of alkali ions [146]. In this way, progressive consequences in the further hydration kinetics can be expected. All together, these unknown effects are suggested to result in the delayed heat of hydration evolution for C2 compared to C1, as observed in Fig.4.1, and in the lower stability of the monosulfate SI evolution in Fig.4.9.

In the above analysis, it is demonstrated that slight differences in cement composition cause important changes in the reaction kinetics. Generally, for each commercial cement, the amount of reagents will differ to some extent but the cement performance will still be retained between empirical limits. However, this is no longer the case for cement pastes combined with certain PCE superplasticizers. As the superplasticizer compatibility is no design criterion for the cement manufacturer, the cement-superplasticizer performance might exceed the empirical limits required in construction practice. Therefore, the effect of PCE superplasticizer is elaborated for the cement pastes above in the remainder of this section.

Plasticized pastes

Adding a fixed amount of SP to the above systems is bound to result in different SP influences as the surface interaction is prone to the different reaction kinetics on the surfaces and in the pore solution. It should be noted that the superplasticizer addition is not correspondingly

incorporated in the thermodynamic simulations: The measured sodium ion concentration is now influenced by the partly dissolved polymer salt. In contrast, the remaining organic anion is excluded from the thermodynamic input because the precipitating phase is unknown. More specifically, the exact amount of polymer involved in the (reversible) coprecipitation with sulfate phases is hard to determine. However, all related small changes in measured ion concentrations are considered as indirect evidence for the true phase formations. Therefore, the following simulations can only function as indicative evidence.

When superplasticizer is added, the same order of saturation indexes for C1SP as for C1REF are obtained in Fig.4.10 (left), but not for C2SP (right). It can be seen that the monosulfate saturation level of C2SP is now no longer in the range of ettringite but much more supersaturated, especially around 120 minutes where it reaches a value of 6.33 SI units. Only the hemihydrate dissolution seems to correspond with this change and stabilizes around that time.

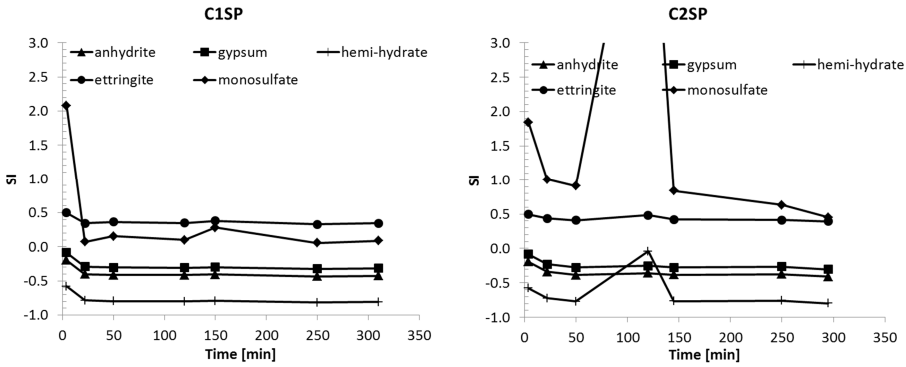

Fig.4.10 Effective saturation index for the hydrate phases in all pastes

In the case of C2, we know that the hemihydrate dissolution speed is limited compared to C1, due to the presence of more alkali sulfates. Nevertheless, from the SI evolution of C2SP, it seems that around 120 minutes the sulfate consumption is temporarily stopped as no hemihydrate is dissolving anymore. If we compare this with the amount of crystalline hemihydrate in Table 4.3, we see at 120 minutes that this is practically at the level of 220 minutes. This implies that more hemihydrate has dissolved than in the reference case and even faster. In this way, the stopped dissolution implied in Fig.4.10 (right) might mark the depletion of available hemihydrate. On the contrary, the change in gypsum dissolution remains very small in Fig.4.10 and in Table 4.3 compared to Table 4.2. As the increased amount of dissolved sulfate ions does not lead to a higher

gypsum or ettringite precipitation, it is expected that the precipitation of these phases is prevented due to another SP effect.

Table 4.3 Mineral composition powdered pastes by QXRD [wt. %]

Amount [wt.%]	gypsum	hemihydrate	anhydrite	ettringite
C1 SP 120	1.7	1	0	0
C1 SP 220	1.2	1	0	0.2
C2 SP 120	1.8	0.5	0	0
C2 SP 220	1.3	0.6	0	0.2

The contradictory observation of a faster dissolving hemihydrate and a prevented precipitation of ettringite for C2 is hard to explain based on the current state of literature. Especially for PCE's, little research has been conducted to the sensitivity of the separate mineral phases to the superplasticizer. Generally, it is accepted that superplasticizer molecules on hydrated cement grains can slow down the dissolution rates of the constituents and modify the nature of the compounds formed [147]. For example , superplasticizers have shown to interfere with the sulfate dissolution and the value of the SO_4^{2-}/AlO_2^- ratio. It was also found that a naphthalene superplasticizer strongly interacted with hemihydrate, delaying in some cases the precipitation of gypsum ([148] in [149]p. 131). This could also have been the case for C2SP.

In a recent study performed by Plank et al. [79] the fundamental mechanisms for polycarboxylate intercalation into C_3A hydrate phases have been investigated. This was done in an aqueous sulfate-C_3A system and it allowed clear determination of the sulfate to C_3A ratio. However, it is clear that some of the experimental conditions such as the reaction temperature and time, the absence of other phases and surplus ions are different from the usual conditions in cement paste. Nevertheless, this fundamental study illustrated potential mechanisms that have not been under consideration for cement paste elsewhere. In this respect, it is remarkable that from a certain threshold dosage of sulfate, the SP was found not able to intercalate in the organo-mineral phases anymore. On the contrary, sulfate filled in the interlayer space and formed monosulfate with different water contents. Also Prince et al. detected monosulfate at the early beginning of hydration when superplasticizer was added [147]. It should be considered that this monosulfate can be initially formed and afterwards be transformed into ettringite, when the local availability of sulfate ions

reaches a sufficient level [150]. There is no doubt that at locally high sulfate concentrations ettringite is the thermodynamically more stable phase in comparison to monosulfate ([151] in [79]).

Plank et al. mentioned that, even at high sulfate concentrations, no ettringite could be detected due to the superplasticizer and that this can be possibly explained by the SP causing ettringite to form in an amorphous form [79]. They also reported on other authors having established that SP generally reduces the size of ettringite crystals or that amorphous ettringite needles can be formed, possessing only a very thin crystalline shell. These small or amorphous phases cannot be detected by XRD.

If we consider the possibility of temporarily monosulfate and amorphous ettringite in case of C2SP, it is possible to explain the faster dissolution of hemihydrate as the virtual surplus sulfate ions in solution are still removed from the pore solution through undetectable phases. The absence of crystalline ettringite precipitation causes the hemihydrate to dissolve further than in the reference of C2.

Sensitivity factors of cement

Besides the reaction mechanism, it is also important to consider the reason for the C2 sensitivity to the superplasticizer. To this end, the sulfate to C_3A ratio could have been used to probe the sensitivity according to the isolated systems of Plank et al. [79]. However, it is not possible to determine the exact amount of C_3A that is in contact with the pore solution. Alternatively, the sulfur to aluminum ratio is plotted in Fig.4.11 and it can be observed that this ratio is continuously smaller for C2SP than for C1SP. Intuitively, this corresponds with the higher monosulfate supersaturation for C2SP as less sulfate is available for the aluminum present in C2SP than in C1SP. However, as the sulfate concentrations in pore solution are similarly increased by the SP for both pastes (see Fig.4.8), the origin of the lower concentration ratio should be found in an increasing aluminum content for C2. This is indeed confirmed in Fig.4.12 where the aluminum content is plotted in function of time. It can be observed how this content is not differing much for the reference pastes during the first 50 minutes. However, the addition of SP makes the aluminum increase for C2SP and decrease for C1SP.

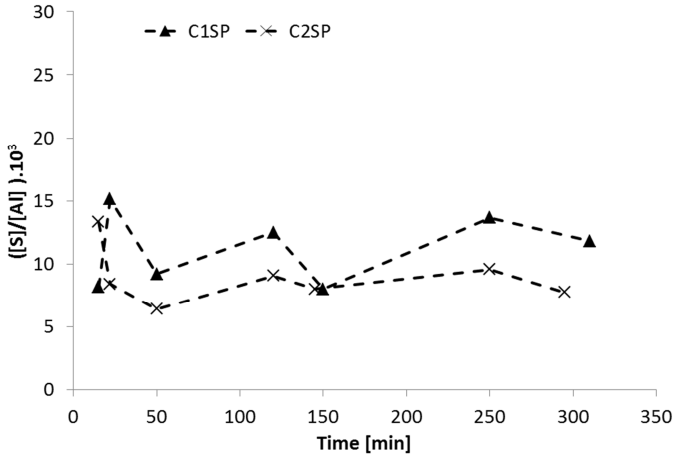

Fig.4.11 Sulfur to aluminum ratio in pore solution

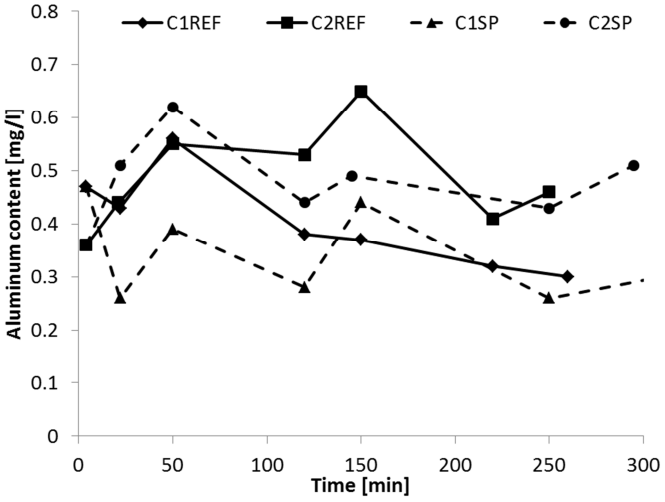

Fig.4.12 Aluminum content in pore solution

In order to change the Al dissolution rate, the SP would be required to interact with the aluminum supplying mineral phases which are C_3A and C_4AF for which C_3A has the highest reactivity in the beginning of cement hydration. It is worth mentioning that, if the C_3A is cubic, it reacts rapidly with sulfate ions to form an almost impervious ettringite shell around C_3A which prevents its further hydration [149]. In such case sulfate ions must be available very rapidly. If the C_3A is orthorhombic, it reacts less rapidly

but forms a loose network of long ettringite needles which keep growing without creating the same kind of tight barrier as when C_3A is cubic [149]. In such case it is important that a steady release of sulfate ions occurs in order to control the rheology (p. 120 in [149]). In this respect, the higher alkali sulfate content of C2, compared to C1, already suggests that C2 contains a relatively larger area of cubic C_3A in the cement grain surface for which the rapidly available sulfate ions had to be provided to prevent flash set. The higher amount of cubic C_3A for C2 is indeed confirmed by the QXRD measurement (Table 3.3).

It has been reported before that the adsorption of SP on the surfaces of cement particles depends on the surface charge [87, 89]. Hence, the superplasticizer preferentially adsorbs on the surface of minerals displaying opposite charge in solution, such as C_3A and ettringite. The phase that is most attractive for the SP can be expected to be cubic C_3A, as it is also attracting most of the sulfate ions. However, this has not been investigated thoroughly yet. One author mentions a close correlation between the amount of cubic aluminate and the setting time of cement and no correlation for the orthorhombic phase [124, 152]. This was investigated for SNF and lignosulphonate plasticizers and also for polyacrylates which are more closely related with the SP in this thesis.

From the QXRD measurement, it could be deduced that C2 contains slightly more cubic C_3A than C1. Assuming that this phase shows the highest affinity to the PCE superplasticizer, it is reasonable to conclude that the hydration reactions in C2 will be most affected by the SP dosage. Moreover, if the thickness of the SP adsorption layer is included (section 4.1.1), it becomes clear how the high amount of sulfate ions is repelled from the C_3A surface into pore solution. This mechanism is also favorable for the formation of amorphous ettringite as a lot of SP is present to intercalate in the hydrates. In this way, the lack of crystalline ettringite covering the aluminate phase leads to an increased aluminum dissolution and a different rheological effect. Locally, the sulfate concentration can then be low enough to enhance monosulfate formation neighboring the amorphous ettringite, analogous to Plank et al. [79].

Summary

In summary of this section, the difference in rheological behavior of C1 and C2 due to the SP is explained by the changes in hydrates formation. In both cements, the SP hinders gypsum dissolution and ettringite precipitation, which extends the induction period and keeps the pastes from stiffening. Only for C2, the SP causes also the hemihydrate to dissolve faster, probably

because part of the sulfate ions is buffered in temporarily monosulfate and amorphous ettringite. The latter phase formations are favored by the lower sulfate to aluminum ratio for C2 which originates in the increased aluminum concentration after SP addition. This increase is due to an enlarged exposure of the aluminate phase to the pore solution. More specifically, the SP rich cubic aluminate phase seems to remain 'uncovered' by the postponed ettringite formation. As C2 has a significantly higher share of cubic aluminate in its clinker composition, its hydrates formation is controlled at a lower rate than for C1. As a consequence, the resulting phase formations for each cement contribute differently to the rheological behavior, resulting in the different performances in section 4.1.2.

Ultimately, we can conclude on how the different performance of the plasticized cement pastes can be related with the SP-cement interaction: The SP changes the dissolution behavior of the sulfate carrying phases and can change the morphology of certain hydration products. The amount of adsorbed SP is related with the nature of the aluminate phase and therefore the clinker composition is of primary importance in SP interactions.

The precarious balance between all these facets makes it almost impossible to foresee the exact paste performance, during cement production. Therefore, current and future research is focusing on the SP compatibility with the different mineralogical phases of cement clinker. Puzzling this future knowledge into a workable *phase model* for predicting the rheological performance of real cement pastes (e.g. as aimed for in the rheograph of Fig.2.2) will be certainly arduous and time consuming. Therefore, as a preparatory step, it could also be considered to relate more macroscopic properties of the cement pastes to the rheological performance. These relations could then be combined in a *microscopic model* as a counterpart to the nanoscopic scale of the phase formation. Although the microscopic model would neglect the exact physico-chemistry, it could also allow new tools for directing the future mineralogical research or deliver advanced instruments for practical applications. Therefore, the development of such microscopic model has been addressed in the following section based on the cement pastes investigated above.

4.3 Relating rheology and hydration kinetics through an agglomeration model

In search for a better understanding of the basic principles that govern the fresh state properties of cementitious materials, a quantitative relation between the chemical kinetics and macroscopic flow behavior of cement paste will be investigated here. Describing this micromechanical relation, at the microscopic scale of fresh concrete, contributes to a bottom-up understanding of the concrete flow behavior.

The investigation starts by trying to characterize the rheological and chemical behavior of the cement paste. As described in the previous section, it is not intended to include the separate phase formations in this description. It will, however, be investigated how the hydration kinetics can be related with the rheological differences observed in section 4.1. For these rheological differences an appropriate measure should be developed.

Anti-thixotropic histogram

In order to quantify the thixotropic tendency of each hysteresis cycle in Fig.4.6 and 4.6 three histograms are assembled per cycle in Fig.4.13 and 4.13, respectively for C1 and C2. The thixotropic part is the area in the Fig.4.6 and 4.6 that is enclosed by the accelerating ramp on top and by the decelerating ramp below, as illustrated in Fig.4.15. Vice versa for the anti-thixotropic histogram. For each cycle, a third bar indicated by 'time' is given in Fig.4.13 and 4.13 to show the evolution in the intersection time t_i, as explained in section 4.1.3. This time interval, with length t_i, starts with the beginning of the acceleration ramp and closes when the deceleration ramp crosses the acceleration ramp.

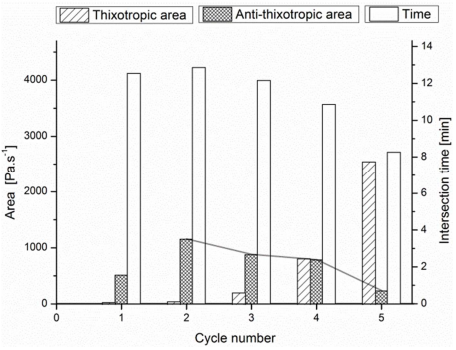

Fig.4.13 Hysteresis properties for C1SP

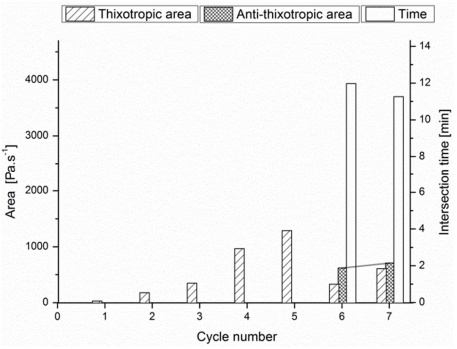

Fig.4.14 Hysteresis properties for C2SP

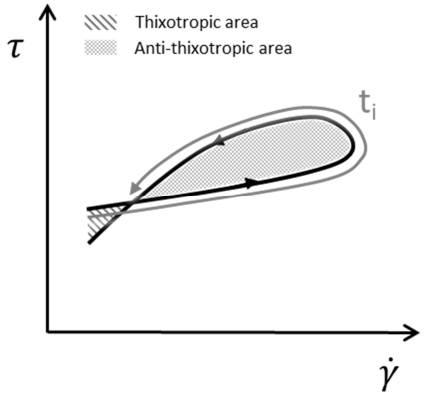

Fig.4.15 Schematic representation of the hysteresis areas and intersection time

In Fig.4.13 and 4.13, a series can be detected for which t_i decreases for higher cycle numbers. This can be visualized for C1 in cycles 2-5 where the anti-thixotropic area descends from 1153 to 233 Pa.s^{-1}, as indicated by the grey line. For C2, t_i can be observed to decrease as well but the corresponding anti-thixotropic area slightly increases from cycle 6 to cycle 7. For both cements, these particular series incorporate the continuous presence of an anti-thixotropic area, an increasing thixotropic area and a monotonous decreasing t_i. All these characteristics together represent a steadily descending acceleration ramp over the anti-thixotropic cycles in Fig.4.6 and 4.6. Series according to all these characteristics will be further called *anti-thixotropic series*.

Please note that cycle 1 of C1 is not included in the anti-thixotropic series, although it shows anti-thixotropic behavior. Actually, t_2 is higher than t_1 which does not conform to the monotonous decrease requirement. Only the decrease will appear to be a returning feature in all tested cement pastes in this thesis.

Concerning the above observations for similar cements, there are two prior questions raised: First, what determines the start time of these series for which t_i steadily decreases? For C1, t_i starts decreasing from cycle 2 and for C2 this starts only from cycle 6. Second, what defines the nature of this selected hysteresis evolution? For C1, the anti-thixotropic area decreases but oppositely for C2 we observe a slight increase even while t_i remains decreasing.

In order to answer the above questions, the structural build-up due to cement hydration should be addressed. As could be read in the state of the art, the hydration reactions in cement paste influence the floc stability in the agglomerate formation which is directly related to the shear response of the paste. A hysteresis dependence on the chemical composition of the cement has been assumed previously by several authors but a quantitative consideration was never proposed [115, 117]. The chemical activity of the two cements in this research is quantified by isothermal calorimetric measurements. The heat of hydration can be observed in Fig.4.1 and 4.2 for both cements, with and without superplasticizer. In case superplasticizer is added, both cements show significant retardation of the hydration reactions. It was also shown that C2 has a denser layer of adsorbed superplasticizer polymer and therefore the hydration kinetics will be delayed relatively more for C2 than for C1.

The postponed start of the anti-thixotropic series in Fig.4.7 for C2 could indeed result from the delayed hydration reactions of C2 compared to C1. However, no good correlation was found neither between the hysteresis behavior and the absolute value - nor for the derivative - of the heat of hydration. Therefore, it is assumed that more physical information on the particle agglomeration is needed to interpret the flow properties correctly.

The oscillatory measurement of the storage modulus provides information on the structure development during the initial hydration and induction period. Its evolution depends on the agglomerate stability and the chemical activity of the cement. The initial value of a monitored modulus mainly depends on the stability of the agglomerates as no new chemical activity has taken place yet [114]. Therefore, the evolution of G'_{min} can be considered representative for the average agglomerate stability evolution.

As shown in Fig.4.5, the network structure increases faster for C1SP than for C2SP. However, at the time of starting the anti-thixotropic series (at 56 and 164 min., respectively) the G'_{min} shows almost the same value. This suggests that a minimum agglomerate stability is a prerequisite to start the anti-thixotropic series for both cements.

Above observation does not necessarily mean that the minimum agglomerate size is the same for both cements. Fine particles with more particle bridges will induce lower stress in the bridges than large particles with less contact bridges. Therefore, as the initial particle size distribution of the cements is different, the measured stress might result from differently sized agglomerates. On the other hand, to perform a hysteresis loop, a finite (yield) stress is applied to break down the flocculated

structure into smaller flocs or individual particles. Although the yield stress is not registered in Fig.4.6 and 4.6, it is observed that the minimal stress of the acceleration ramp is the same for the beginning of the anti-thixotropic series (±240kPa). The latter suggests that both cement pastes are broken down in similarly sized agglomerates at the beginning of the anti-thixotropic series.

Internal and external hydrates concept

Now the G'_{min} evolution is associated with the start of the anti-thixotropic series, it may also correlate to the hysteresis evolution mechanism. During the strain sweep in the oscillatory measurement procedure, the agglomerated structure is reduced to a minimal agglomerate size. It is assumed that this minimal agglomerate is sufficiently strong to resist all future strain sweeps in the oscillatory procedure because the strain sweep remains the same during the rest of the procedure. As a consequence, the stability of these minimal agglomerates can only be reinforced by the internal interparticle bridging of hydration products. This reinforcing could be held responsible for the further increase in G'_{min} without considering a further agglomerate size increase. However, the same agglomerates are subjected to the hysteresis loops and the shear stress in the flow curves is much more sensitive to agglomerate size than to agglomerate inner stress. Thus, the agglomerates need to grow as well over the different strain sweeps. Therefore, it is concluded that the evolution of G'_{min} during the anti-thixotropic series is caused by both the inner reinforcement of the initial agglomerates and the agglomerate growth. The share of hydration products responsible for the latter mechanisms will be called the *internal* hydration products. This concept is further clarified in Fig.4.16, Fig.4.17 and Fig.4.18.

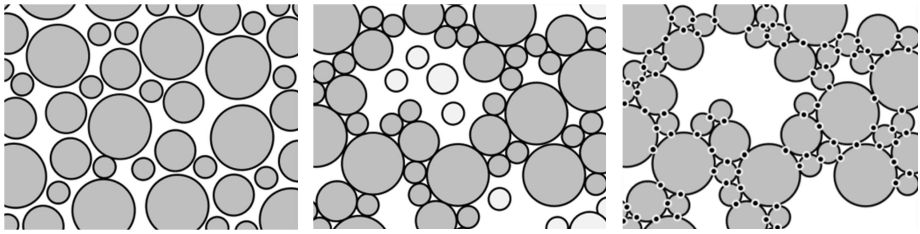

(a) Dispersed cement particles (b) Percolated network of dark grey particles (c) nucleation at the pseudo-contact points

Fig.4.16 Initial evolution of the cement particle network structure

Initially, the cement particles are dispersed during mixing, as is shown in Fig.4.16a, similar to Fig.2.26a [64]. This state of the suspension

corresponds approximately with the state during the first strain sweep in Fig.3.9 at 30 minutes. A couple of seconds after the strain sweep, cement particles will flocculate to form a percolated network of colloidal interactions. A part of the particles does not belong to a percolation path. They are colored light grey in Fig.4.16b. Within a minute, at the pseudo contact points between particles in Fig.4.16c, nucleation of C-S-H (black dots) starts immediately to turn the soft local colloidal interaction between cement particles into a far more rigid interaction, called a hydrate bridge [64].

At the end of the first time sweep in Fig.3.9 the paste has been resting approximately 20 minutes. The network strength is then given by the value of the storage modulus. When shear is applied to the percolated rigid network of Fig.4.16c during the second strain sweep (at 55 minutes), part of the network bridges does not disrupt and holds the particles together in an agglomerate. This can be seen in Fig.4.17a. Because these bridges remain within the agglomerate, they are called *internal hydrates* (black dots with white borders). At the agglomerate surface, the former hydrate bridges are now exposed to the pore solution and are therefore called *external hydrates* (white dot with black border).

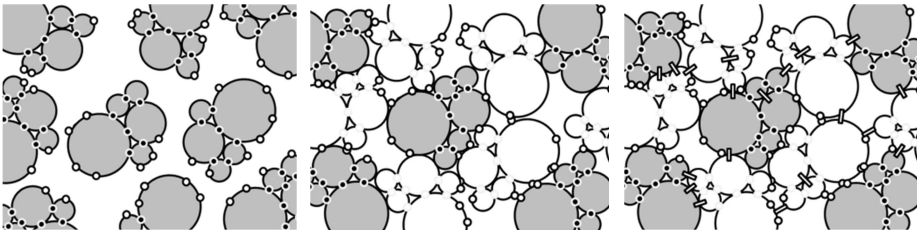

(a) First stage agglomerates with internal hydrates (black dots with white line) and external hydrates (white dots with black line)

(b) Network structure of first stage agglomerates

(c) Nucleation in-between the first stage agglomerates

Fig.4.17 Evolution of the agglomerate network structure during time sweep

During the second time sweep in Fig.3.9, the first stage agglomerates consolidate again in a new network structure. This is drawn in Fig.4.17b and in order to distinguish the original agglomerate shape, six of the agglomerates are drawn in white for visual clarity. As a result of the spatial reorganization during shear, a part of the external hydrates is still exposed to pore solution and another part is now again in-between neighboring particles. During rest, these former external hydrate bridges are likely to have a catalytic effect on renewed bridge formation in-between the neighboring agglomerates. So, on the one hand, existing hydrate bridges

will be reinforced (all black and white dots in-between neighboring particles). On the other hand, new inter-particle bridges will be formed as in Fig.4.17c (white rectangles).

Considering the second time sweep, all of the bridge reinforcement and formation energy is contained in the heat $Q_{tot,2}$ during that time interval. It is only after the third strain sweep, when again new agglomerates are formed, that it becomes clear which part of this hydration energy was due to internal resp. external hydrates. To visualize the relation between the internal and external hydrates on the one hand and the agglomeration rate on the other hand, the proposed agglomeration mechanism from Fig.4.17 is developed a little further in Fig.4.18.

During the third strain sweep, shear is applied to the new network structure from Fig.4.17c and a part of the reinforced and new network bridges does not disrupt and holds the particles together in second-stage agglomerates. This will occur at the expense of weaker agglomerates which will lose (part of) their coherence. In Fig.4.18a, four arbitrarily white agglomerates will lose their coherence. The subtracted agglomerate parts are colored in dark grey and will be incorporated in the neighboring light grey agglomerates. The network structure will be again disrupted and the new agglomerates are brought in suspension, as shown slightly dispersed in Fig.4.18b. In principal, the weaker agglomerates will show further decrease of their average size and eventually will be totally incorporated in other agglomerates. The averagely larger second stage agglomerates are drawn in black in Fig.4.18c.

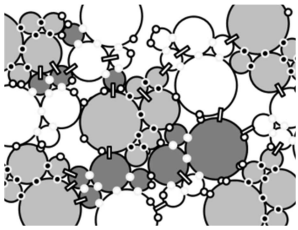

(a) Disruption of weakly connected agglomerate parts (dark grey)

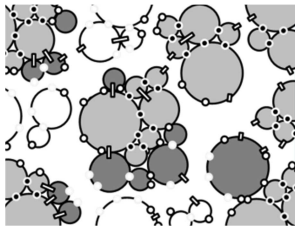

(b) Growth of first stage agglomerates (light grey) by addition of other agglomerate parts (dark grey)

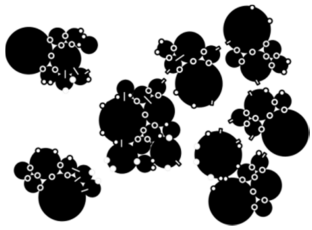

(c) Second stage agglomerates in suspension

Fig.4.18 micromechanical relation between the different hydrates and the agglomeration rate

It is clear now how the spatial distribution of the first stage agglomerates is a determining factor for disruption of weaker agglomerates. Although this

is merely a random process, surface active concrete admixtures could limit the number of favorable connection sites on the agglomerate surface.

It is observed in Fig.4.18c that the different kinds of hydrate bridges (resp. internal and external) could have been initiated at any time sweep interval. More specific, within most of the agglomerates one can find some initial internal hydrate bridges (black dots), some initial external hydrate bridges (white dots) and some recent internal hydrate bridges (white rectangles). However, the exact appearance of these hydrate bridges is irrelevant. More important is their chemical activity in the time sweep interval and therefore the hydrate bridges should be quantified by their produced heat of hydration in that interval.

In this way, at the current agglomerate surface, all kinds of former bridges can be found and they are all catalytic for new C-S-H nucleation. It is clear from Fig.4.18c that the surface of the agglomerates will be covered increasingly by former hydration bridges over time. On the one hand, this will favor further bridge formation in-between agglomerates. On the other hand, the increasing volume and weight of the agglomerates will burden these potential connections more and more. Based on the surface/volume ratio, the number of additional external hydration bridges is expected to decrease compared to the number of internal hydration bridges, for increasing agglomerate size.

Quantifying agglomeration parameters

During one cycle of the dynamic oscillation, the increase in storage modulus ($G'_{max,i}$-$G'_{min,i}$ in Fig.3.9) is caused by all the hydration products formed during that cycle, producing the total heat of hydration $Q_{tot,i}$. A part of this increase in storage modulus is due to the reinforcement of the initial agglomerates and the agglomerate growth. This share of the increase can be measured by the difference between $G'_{min,i}$ and $G'_{min,i+1}$ and it is due to the internal hydration products, producing the heat $Q_{int,i}$. Because the formation of hydration products occurs over the entire structure of the paste (i.e. inside and outside agglomerates) and everywhere a similar strength reinforcement can be expected during the induction period, it is reasonable to assume the following proportionality within one cycle *i* (Eq.4.1):

$$\frac{Q_{int,i}}{Q_{tot,i}} \sim \frac{G'_{min,i+1} - G'_{min,i}}{G'_{max,i} - G'_{min,i}} \qquad (4.1)$$

During the pre-induction period, the formed hydrates consist mainly out of C-S-H and ettringite (AFt) [12]. Hereafter, during the induction period, all phases hydrate steadily producing the total heat $Q_{tot,i}$ during the oscillatory measurement. Still, C-S-H and AFt have the biggest share in the heat production. It should be noted that all the hydration products could have macroscopic consequences on the rheological behavior but a considerable number of arguments has been collected in literature to assume that the nucleating product at the origin of the storage modulus evolution is C-S-H [64].

It is hard to address the exact share of $Q_{tot,i}$, that is produced solely by C-S-H formation because of experimental limitations. On the other hand, the hydrate formation percentage of C-S-H and AFt evolves in a similar way during the first 4 hours of hydration (p.267 in [12]). Therefore, it is assumed that during the anti-thixotropic series in these experiments the heat production ratio of C-S-H to AFt ($Q_{C\text{-}S\text{-}H,i}$ /$Q_{AFt,i}$) remains constant. As these products are the main constituents of $Q_{tot,i}$, it is reasonable to assume that $Q_{tot,i}$ is proportional to $Q_{C\text{-}S\text{-}H,i}$.

If it is assumed that $Q_{tot,i}$ is totally produced by C-S-H formation or even that $Q_{tot,i}$ is the heat production of all mineral phases that are contributing to the storage modulus evolution, it is possible to rewrite the proportionality in Eq.4.1, keeping in mind that a constant factor is contained in $Q_{tot,i}$, in Eq.4.2:

$$Q_{int,i} = Q_{tot,i} \cdot \frac{G'_{min,i+1} - G'_{min,i}}{G'_{max,i} - G'_{min,i}} \qquad (4.2)$$

Equation 4.2 defines the internal hydrate activity without knowing anything on the physical appearance of the hydrate bridges. It is possible to calculate the value of $Q_{int,i}$ for both cements from the measured heat of hydration in Fig.4.1. The heat production during a time sweep is plotted in Fig.4.19 and the cumulative heat $\sum Q_{int,i}$ is plotted in Fig.4.20.

It is noted that the used isothermal heat evolution is not entirely representative for the true heat disposal that occurs in the rheometer. Although both set-ups are maintained at exactly 20°C, the mechanical stirring by the rheometer will create additional hydration activity in its paste. This additional heat of hydration is not registered in the separate calorimetric tests. However, excluding the dissipation energy of the rheometer, the share of this additional hydration energy in the total heat

of hydration is neglectable. Moreover, if the total heat of hydration during the consecutive time sweep would be noticeably higher, no change in rate of hydration during the sweep is expected.

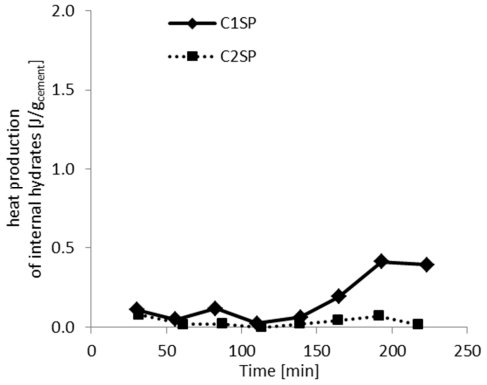

Fig.4.19 Heat production of internal hydrates

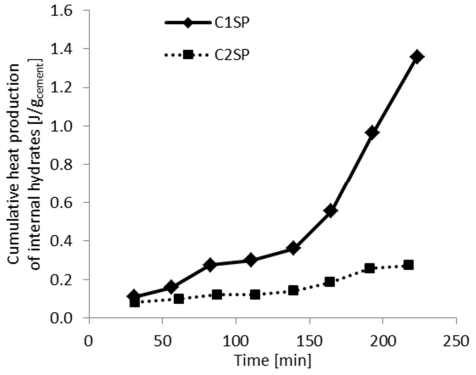

Fig.4.20 Cumulative heat production of internal hydration products

The information obtained from Fig.4.20 is, by definition, related to the evolution in the storage modulus and to the chemical activity of the cements. In this way, it is not surprising that C1SP at 56 minutes and C2SP at 164 minutes show approximately the same value. This suggests that a certain amount of hydration energy is required to have the anti-thixotropic series started. In the case of the coarser cement (C2), the slightly higher value at 164 minutes can be explained by the lower C-S-H effectivity and therefore more interparticle bridges were needed to resist the same amount of stress as for C1 at 56 minutes. In contrast to the storage evolution modulus, both points are now preceding a similar slope increase of their curve, suggesting that these hydration energies indicate the start of a similar mechanism (i.e. anti-thixotropic series).

At this point it has become clear what determines the start time of the anti-thixotropic series: The hydration reactions control the stability of cement particle agglomerates and for delayed hydration reactions, the agglomerate growth will be delayed as well. From a threshold agglomerate size, the shear stress during flow in Fig.4.6 and 4.6 increases towards a level for which the structural build-up mechanism is dominant over the structural break-down. Therefore, it is in our interest to find out more about the nature of the build-up mechanism.

It seems that for the onset of anti-thixotropic behavior a certain agglomerate size needs to be obtained in order to enhance the reconnecting of sheared agglomerates. For this agglomerate size, it could be argued that the inter-agglomerate stress has increased to a level favorable for reconnecting. From this purely physical point of view it remains hard to explain the difference between cycle 1 of C1SP and cycle 5 of C2SP. Both cycles are close to the mentioned stress level in Fig.4.6 and 4.6 but they show significantly different behavior. Therefore the chemical component of the hydration reactions should also be included in the nature of the reconnection mechanism. It is in this respect that the chemical activity of the agglomerate surface will be considered.

We defined the internal hydration products as the share of hydration products that is responsible for agglomerate reinforcement and growth. The remaining share of hydration products is also formed during one cycle of the oscillatory measurement but does not succeed in resisting the mechanical dispersion forces during the strain sweep. Therefore, these former bridging hydrates are located at the surface of the irreversible agglomerates and their presence is likely to improve the surface connectivity in a physical or chemical way as demonstrated for C-S-H in section 2.4.

Similarly, for freshly broken agglomerates at the maximum shear rate during the hysteresis procedure, the newly created agglomerate surface might show unexploited connectivity potential. All these surface hydrates are included in the external hydration products. It is expected that the inter-agglomerate connectivity potential is strongly correlated with the amount of external hydration products at the agglomerate surface.

The amount of external hydration products can be represented by the heat of hydration $Q_{ext,i}$, defined in Eq.4.3 as the difference between the total and the internal heat of hydration.

$$Q_{ext,i} = Q_{tot,i} - Q_{int,i} \quad (4.3)$$

The value of $Q_{ext,i}$ is plotted in Fig.4.21 and it can be observed that the calculated heat production for C1SP is again higher than for C2SP. It seems that $Q_{ext,i}$ follows approximately the measured heat of hydration evolution in Fig.4.1, respecting the cement differences. Remarkably, for C1SP, the amount of additional external hydration bridges decreases compared to the slightly increasing amount of internal hydration bridges in Fig.4.19. This is completely in line with the conceptual expectations considering the volume/surface ratio of the agglomerates.

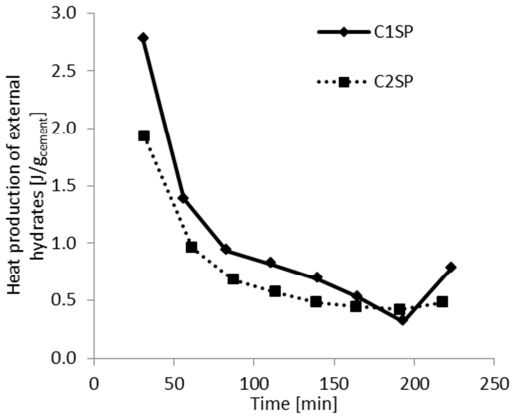

Fig.4.21 Heat production of external hydrates

In the cumulative value of $Q_{ext,i}$ for both cements in Fig.4.22, no particular characteristics are observed related with the start of the anti-thixotropic series. Of course, the effect of the external hydration products on the reagglomeration amount is most pronounced at the maximum shear rate during the hysteresis loop. Therefore, it is the hydrate formation at that particular time that is supposed to have an influence on the connectivity potential. In this way, it is more logical to consider the absolute value of $Q_{ext,i}$ instead of the cumulative value like for $\sum Q_{int,i}$.

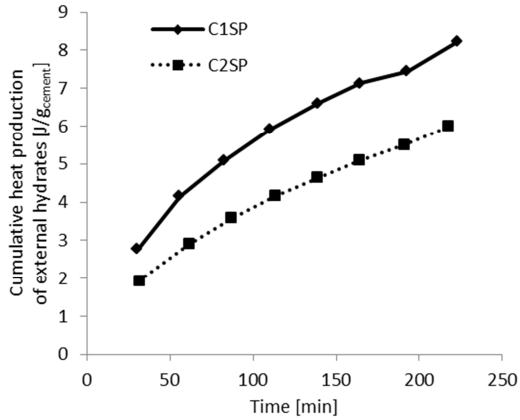

Fig.4.22 Cumulative heat production of external hydrates

At the start of the anti-thixotropic series (at 56 and 164 min.) the value for $Q_{ext,i}$ is 1,5 times higher for C1SP than for C2SP as seen in Fig.4.21. It would be incorrect to associate this parameter directly with the anti-thixotropic area from Fig.4.13 and 4.13 because this area is also function of the agglomerate size. For example, from a certain agglomerate size, the inter-agglomerate shear stress might reach a level which favors the interconnecting potential and causes the growth of the hysteresis area. Therefore, it is proposed to include the effect of the agglomerate size by making the sum of the cumulated heat of the internal hydration products ($\sum Q_{int,i}$) and the absolute heat of the external hydrates ($Q_{ext,i}$). These values are plotted in Fig.4.23 and show a similar global evolution for both cements.

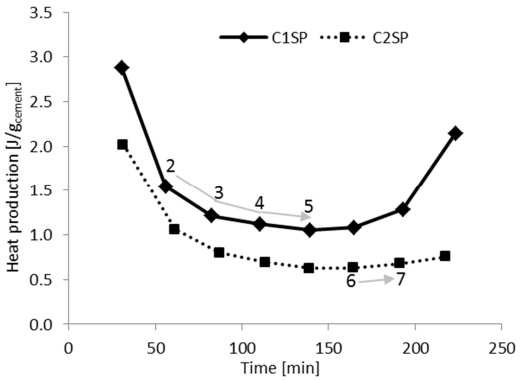

Fig.4.23 Sum of cumulative heat production for internal hydrates ($\sum Q_{int}$) and heat production of external hydrates ($Q_{ext,i}$)

To relate the agglomeration with Fig.4.23, the values of ($\sum Q_{int,i}+Q_{ext,i}$) have been isolated for the anti-thixotropic series in Fig.4.24 and are compared with the hysteresis area from Fig.4.13 and 4.14. It can be observed that there is a good qualitative correlation between these two parameters. For the steady decrease of the anti-thixotropic area in C1SP, the plotted heat also decreases in a similar way. For the small increase in anti-thixotropic area of C2SP, the heat follows as well.

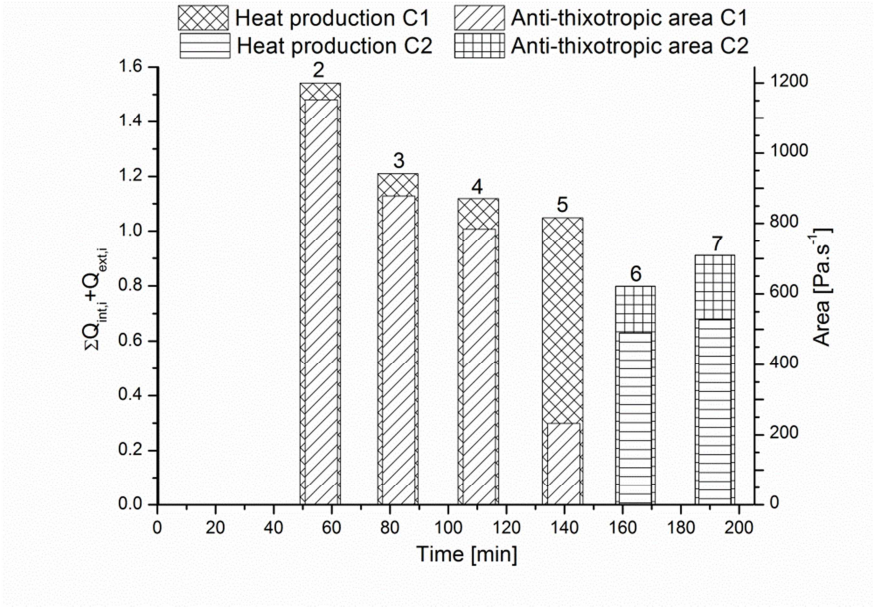

Fig.4.24 Comparison between the anti-thixotropic area and hydrate production

In order to quantify the correlation, we take the difference between the initial value of the area (A_1) and others (A_i) in Fig.4.24 and we divide those differences by A_1 (Eq.4.4). In this way, the absolute change of hysteresis area during the anti-thixotropic series is made relative. This also creates perspectives for other shear rate ranges for which an anti-thixotropic series could be visualized but that will not be treated here. The heat production can be made relative (Eq.4.5) and the couples of relative area change (ΔA_i) and relative heat change ($\Delta(\sum Q_{int,i} + Q_{ext,i})$) can be plotted in Fig.4.25. The closer the couples are to the bisector, the more correlated is a change in heat production and the corresponding change in anti-thixotropic area over the different cycles.

$$\Delta A_i = \frac{A_1 - A_i}{A_1} \qquad (4.4)$$

$$\Delta(\sum Q_{int,i} + Q_{ext,i}) = \frac{(\sum Q_{int,1} + Q_{ext,1}) - (\sum Q_{int,i} + Q_{ext,i})}{(\sum Q_{int,1} + Q_{ext,1})} \quad (4.5)$$

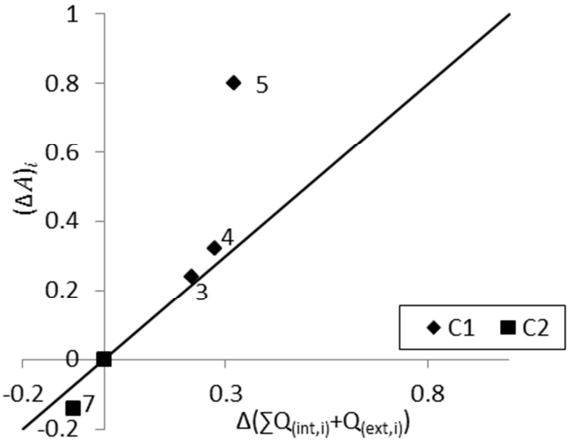

Fig.4.25 Comparison between the relative change in anti-thixotropic area (ΔA_i) and hydrate production ($\Delta(\sum Q_{int,i} + Q_{ext,i})$)

For both cements, most cycles in Fig.4.25 show a reasonably good correlation between the agglomeration and the chemical activity defined by ($\sum Q_{int,i}+Q_{ext,i}$). The low correlation for cycle 5 of C1 is expected to be due to a low accuracy of the hysteresis area. It is possible that for long hydration times and large agglomerates a disturbance of the stress response occurs. It can be observed that a smooth hysteresis curve for cycle 5 and 7 was indeed hard to obtain in resp. Fig.4.6 and 4.6. When the paste is close to setting, the tendency might exist for the major part of the structure to form larger irregular flocs that incorporate some less hydrated flocs leading to a low correlation.

Although the correlation does not hold for all cycles, it is clear that the transformation of the storage modulus and the heat of hydration into a combined internal and external hydration energy allows a more founded discussion on the rheological mechanisms. The fact that these hydration energies are - by definition - merely proportional to the true amount of interconnecting hydration bridges is handled by using only relative differences in Fig.4.25.

In order to reduce the impact of the large agglomerate sizes, the stress level of each hysteresis cycle should be neutralized. For example, the

hysteresis area (A_i) can be divided by the corresponding minimum stress of each acceleration ramp ($\tau_{min,i}$). This adaptation of the reagglomeration amount does imply that the combined heat term ($\sum Q_{int,i}+Q_{ext,i}$) should no longer contain any parameter considering the internal hydrates. In this way, only the external hydration energy ($Q_{ext,i}$) remains.

Furthermore, it is also noted in Fig.4.6 and 4.6 that the acceleration ramp becomes more curved for higher stress levels which might also be an effect of the growing agglomerate stability. As the structural build-up does not dominate long enough at these high stress levels, the curved acceleration ramp is not taken into account properly. This underlines the importance of the time interval in which the full reagglomeration occurs. To this end, it is suggested to divide the neutralized hysteresis area by the time during which this area could originate $\Delta t_{A,i}$. In this way, more value is attached to the speed of reagglomeration and an agglomeration rate (R_i) is obtained (Eq.4.6):

$$R_i = \frac{A_i}{\tau_{min,i} \cdot \Delta t_{A,i}} \qquad (4.6)$$

This rate could be more closely related with the connectivity potential of the external hydration products than the amount of reagglomeration itself. To describe the evolution of R_i the following relative difference is considered (Eq.4.7):

$$\Delta R_i = \frac{R_1 - R_i}{R_1} \qquad (4.7)$$

In Fig.4.26, the relative changes in reagglomeration rate (ΔR_i) are plotted in function of the relative changes in $Q_{ext,i}$ (Eq.4.8) and the bisector clearly shows a good proportional correlation for all cycles. This means that a change in the amount of external hydrates results in a comparable change in reagglomeration rate during flow.

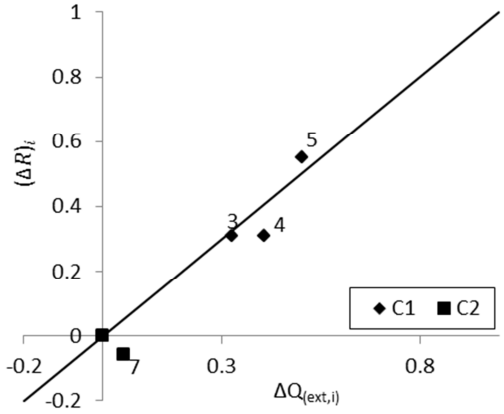

Fig.4.26 Comparison between the relative change in reagglomeration rate and hydrate production

$$\Delta Q_{ext,i} = \frac{Q_{ext,1} - Q_{ext,i}}{Q_{ext,1}} \qquad (4.8)$$

For C2, a slight increase in agglomeration rate is observed for a small decrease in external hydration energy. The increase in agglomeration rate is indeed confirmed by the increasing hysteresis area in Fig.4.14 but it seems to contradict with the slightly lower amount of external hydration products. On the other hand, it is clear from Fig.4.21 that after cycle 7 (at 191 min) the amount of external hydration products starts to increase. Perhaps a small difference between the calorimetric results and the actual heat of hydration in the rheometer caused this incongruence. In that case, no great value should be attached to the sign of the number as the difference in external hydration energy is close to zero. This is different for Fig.4.25 where $\sum Q_{int,i}$ is included. Another possible explanation will be addressed in the next chapter.

At this point it is clear that for both cements the hydrate formation at coagulating surfaces, deduced from an oscillatory measurement, is closely related with the reagglomeration rate during flow. This means that, when the rheological evolution is sufficiently stretched over time and only the heat production during the first anti-thixotropic interval is known, these relations virtually allow to determine the further heat evolution of the cement solely from the rheological behavior. Furthermore, the above

analysis has not shown any compatibility conflict with the interconnecting potential attributed to C-S-H. All this information and especially the association between chemical and physical behavior of cement paste might help future mechanistic models to capture the true performance of fresh cementitious materials and in particular of fresh concrete.

Summary

To summarize, a conceptual model based on agglomerate formation has been described to capture the relation between the heat of hydration and the rheological behavior of cement paste. The designated oscillatory procedure appeared to be viable for probing the agglomerate stability and for addressing the hydrate production inside and outside the agglomerates. The conceptual distinction in-between hydration products allowed relating the interparticle connecting potential with the C-S-H production during the induction period.

In short, this is how the hydration reactions control the stability of cement particle agglomerates and how these agglomerates control the flow behavior of the paste:

- From a threshold agglomerate size, the shear stress during flow of all tested cements increases towards a level for which the structural build-up mechanism is dominant over the structural break-down.
- During that anti-thixotropic period, the amount of reagglomeration changes in a quite similar way as the amount of internal and external hydrates.
- The cumulative amount of internal C-S-H influences the agglomerate stability and the amount of external C-S-H determines the reagglomeration rate.
- Close to setting, the impact of the hydrates is somewhat obscured by a low flow curve resolution.

Knowing only the heat production during the first anti-thixotropic interval, the described relations are able to predict the further heat evolution of the cement solely from the rheological behavior.

Chapter summary

Two cements of the same type, but from different batches with separate fineness, showed unexpected different rheological behavior upon addition

of a PCE superplasticizer. Partly determined by the physical properties of the cement powder, the SP adsorption particularly affected the chemical nature of the hydration products. For the cement with a higher share of cubic aluminate phase, it was indicated that the SP changed the morphology of ettringite, which interfered with the dissolution behavior of the sulfate carrying phases and with the dissolution rate of C_3A. The thermodynamic modelling indicated the presence of temporarily monosulfate due to the higher availability of aluminate ions. As a consequence, the resulting phase formations for each cement contribute differently to the rheological behavior.

The precarious balance between all these facets is representative for the modelling difficulties due to the unpredictable coherence between different cement properties and the limited amount of experimental techniques at that nanoscale. Therefore, it was decided to scale up the chemical activity of the cement to the level of the heat of hydration, which was further implemented in a microscopic agglomeration model. The model parameters were obtained from the experiments in the first section and provided a measure for the amount of agglomeration and the agglomeration rate during flow. Through the definition of internal and external hydrates, a concept was founded to describe the connection mechanism between flowing agglomerates in function of the heat of hydration. A consistent proportional relation was found between changes in the chemical activity of the agglomerate surface and the changes in reagglomeration rate of those agglomerates under shear. This demonstrates that, for one particular cement, a rheometrical procedure can be found that relates the rheological behavior with the underlying micromechanical mechanism. This is of particular interest in order to quantify the rheological implications of additional admixtures in that cement paste.

Chapter 5 - The influence of retarder on the plasticized cement paste rheology

In the previous chapter, it was learned how the superplasticizer influenced the rheology of cement pastes. Furthermore, the model was founded to describe the different performances of similar cements in a more adequate manner. However, it is not sure how the addition of a retarder to these plasticized systems would affect the agglomeration model. Therefore, the influence of a specific retarder/superplasticizer combination on the cement paste rheology will be investigated in this chapter.

Parallel to the fourth chapter, the influence of the retarder will be first determined by similar experiments as for C1SP. In the second paragraph the origin of the retarder influence is investigated by different experiments, allowing a more comprehensive view on the retarder action mechanism. After that, in the third paragraph, all findings are implemented in the agglomeration model that was initiated in the previous chapter. By completing this model, an instrument is developed for understanding and describing the combined effect of the current admixture combination.

5.1 Experimental observations of the retarder influence

The influence of the retarder on the plasticized cement paste is expected to be detected on many levels. As described in the State of art, this particular retarder (sodium gluconate) also acts as a plasticizer. So, besides the induced changes in the cement chemistry, an unknown physical effect may be expected as well. The retarder performance will be investigated by

the same type of experiments as for C1SP to permit the same parameters in the model discussion. These experiments describe the hydration kinetics, the structure development and the flow behavior of the retarded cement paste.

In these experiments, one cement paste (C1SP) and one retarder are selected. The retarder is sodium gluconate, abbreviated with 'SG', and will be added to the C1SP paste upon production. Pastes are prepared according to the mixing procedure in section 3.1.3 and they contain 0.13% SP and 0.03% SG. The final paste will be referred to as C1SPSG.

5.1.1 Hydration kinetics

The hydration kinetics of the reference, the plasticized and the retarded cement paste is represented by isothermal calorimetric measurements. The absolute heat of hydration can be observed in Fig.5.1 and the cumulative amount in Fig. 5.2 for all three pastes. It is clear that the retarder induces significant delay in the hydration kinetics as the heat flow in the induction period is lowered far below C1SP. Furthermore, the hydration acceleration of C1SPSG is postponed by approximately 5 hours and reaches a higher peak value than for the other pastes. It can be seen in Fig.5.2 that it takes 50 hours for the total heat production to draw even for all pastes.

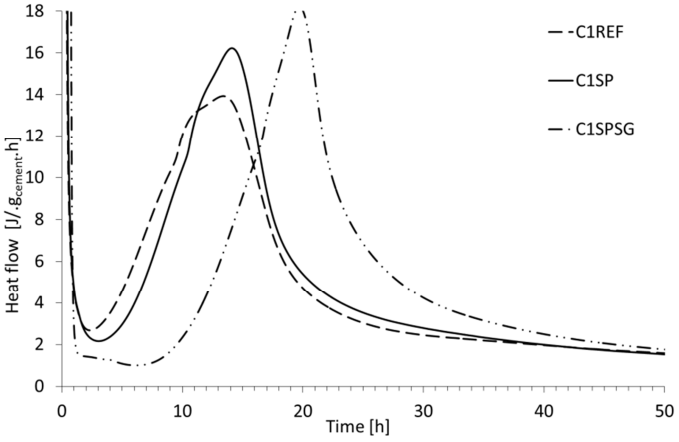

Fig.5.1 Heat flow for C1, C1SP and C1SPSG

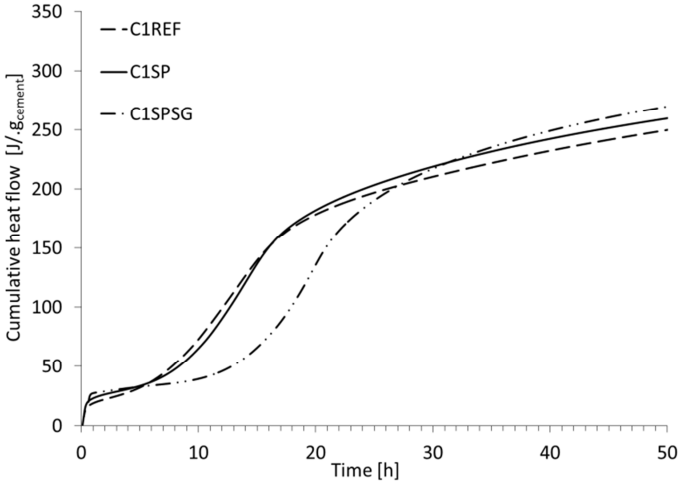

Fig.5.2 Cumulative heat production for C1, C1SP and C1SPSG

5.1.2 Structure development

The storage modulus was measured for all setting pastes according to the prescribed oscillatory procedure (see section 3.2.1). The minimal and maximal storage moduli were collected for the plasticized paste with and without retarder. The evolution of the minimal storage modulus (G'_{min}) in function of time is given in Fig.5.3 at the left and the maximal storage modulus (G'_{max}) at the right.

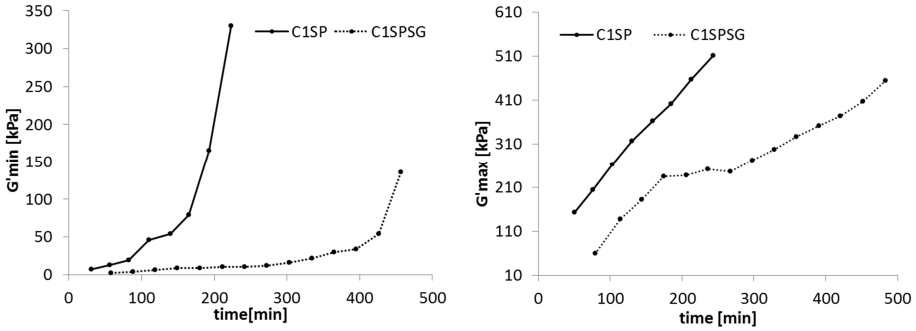

Fig.5.3 Evolution of G'_{min} (left) and G'_{max} (right) in function of time for the reference cement pastes

It can be observed for G'_{min} in Fig.5.3 that the structure development is delayed by approximately five hours if one considers the value of 50kPa as a threshold. This delay corresponds with the delay obtained in the heat flow and confirms the relation between the hydration process and the

structural evolution. For G'_{max}, a linear increase in the beginning is observed after which a small plateau of 4 cycles is reached. Finally, it continues to increase linearly. The plateau is a clear sign that over those particular cycles only the elementary amount of extra hydrates was produced to recover from the shear rate sweep.

5.1.3 Flow behavior

To quantify the flow behavior of C1SPSG, again a series of hysteresis cycles was performed. The resulting stress in function of shear rate is presented in Fig.5.4 and should be compared with Fig.4.6.

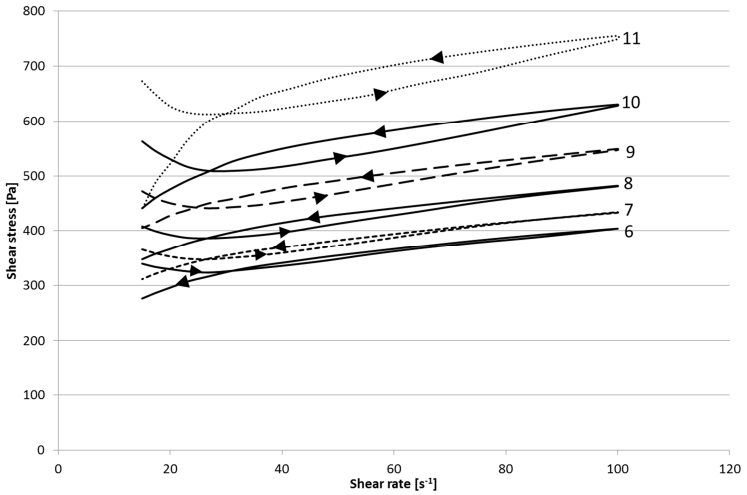

Fig.5.4 Hysteresis loops C1 with cycle numbers indicated in Table 5.1

In the case of C1SPSG, one can see six cycles above each other for increasing stress levels and increasing hydration time. These cycles were retained from a series of twelve cycles and numbered accordingly. The first five cycles were omitted because they showed only thixotropic behavior and the twelfth cycle did no longer allow a reliable shape of the curve. The number of the cycle also corresponds to the hydration time, given in Table 5.1, for which that cycle is started. The length of one entire hysteresis interval is again about 16 minutes and it is followed by a period of rest towards the next cycle.

Table 5.1 Cycle number with corresponding start time for C1SPSG

Cycle number	6	7	8	9	10	11	12
Time after water addition [min]	264	295	326	357	387	418	449

By comparing Fig.5.4 with Fig.4.6 from previous chapter, some remarkable differences can be observed:

- a series of curves can be detected for which the intersection of the accelerating and decelerating ramps decreases progressively but less fast than for C1SP.
- the acceleration loops are less shear thinning than in C1SP or are at least showing higher curvature than in C1SP
- the retarded paste allows smooth stress registration above the 500 Pa stress level. The C1SP paste was only measurable below this level. The highest cycle number (5) of C1SP is manifested around the stress level of cycle 8 in C1SPSG.
- the area enclosed by the accelerating and decelerating ramp is increasing for higher stress levels, while it is clearly decreasing for C1SP.

A comprehensive summary of all relevant parameters is presented in Fig.5.5. The series of curves showing decreasing intersection times are connected with a grey line. In chapter 4 this series was called an anti-thixotropic curve and this will be continued in this chapter. It is however noticeable that in this case the anti-thixotropic area is increasing instead of decreasing as for C1SP. The thixotropic area remains increasing as well, which seems contradictory in the light of the shear mechanism discussed for C1SP.

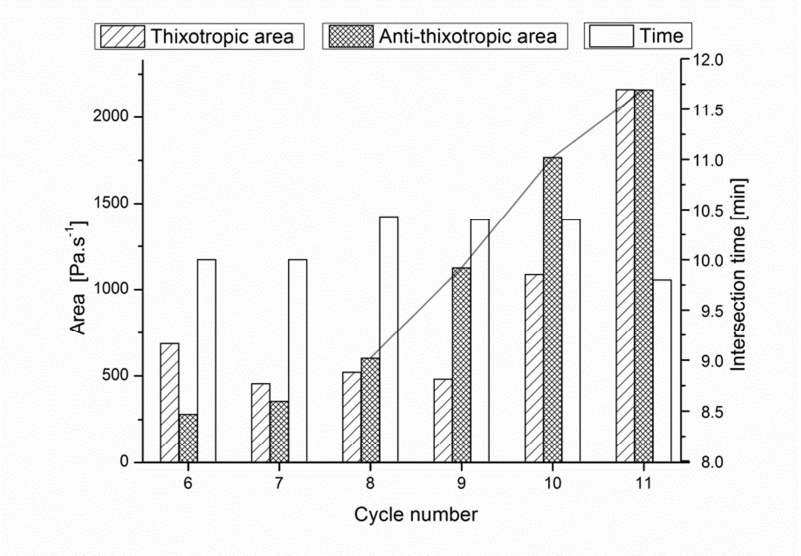

Fig.5.5 Hysteresis properties for C1SPSG

When we compare the timing in Table 5.1 for all anti-thixotropic cycles in Fig.5.4 with the heat evolution of C1SPSG in Fig.5.1, it can be observed that the heat of hydration is steadily decreasing in that specific time interval. At first sight, this observation does not agree with the increasing anti-thixotropic area in Fig.5.5 for which an increasing heat of hydration would be expected (i.e. more external hydrates). It is clear that the anti-thixotropic area evolution in the retarded system has been decoupled from the connectivity potential of the hydrates on the agglomerate surface, as observed for C1SP. Apparently, the retarder introduces a different shear mechanism that allows higher stress levels and simultaneously increasing hysteresis areas. To learn more about this mechanism, the retarder plasticizer interaction will be investigated at the submicroscopic level in the following paragraph.

5.2 At the origin of the retarder influence [7]

The first paragraph demonstrated the important delay in hydration reactions for retarder addition but also the changes in the shear mechanism in-between cement agglomerates. Therefore, the shear mechanism will first be investigated by varying the retarder dosage and

[7] This section contains parts of the published article “Plasticizing Mechanism of Sodium Gluconate Combined with PCE” in Advances in Cement Research, 2014, DOI : 10.1680/adcr.13.00087.

monitoring the viscosity evolution. After that, it will be examined how the paste viscosity is depending on the degree of hydration to distinguish the chemical from the physical effects.

5.2.1 Paste viscosity

When a freshly-mixed cement paste is left to rest, it will build up a network structure over time due to the agglomeration of the cement particles, as illustrated in chapter 3. The involved inter-particle forces originate from colloidal and contact interactions between particles, and depend on the volume fraction of these particles. As seen in chapter 4, the presence of a superplasticizer significantly influences this system.

In this paragraph, a range of SG dosages will be applied on plasticized C1 pastes and the SP dosage is half that of the other pastes in this thesis, like C1SP. This is done to magnify the effect of the SG but this will not affect the conceptual conclusions in the end of this paragraph. Here, all the pastes but the reference paste (REF) are plasticized with 0.065 % superplasticizer. The plasticized reference without sodium gluconate is abbreviated with REFSP. All other sample names (SG1, SG2, SG3) represent the plasticized paste, accompanied with a corresponding dosage of sodium gluconate (SG) as dry mass percentage of the cement weight (%C). The dosage can be found in the second column of Table 5.2.

The built-up network structure of the tested cement pastes will disappear during the start of a viscosity measurement as the shearing of the rheometer destroys it. Also this particular behavior is known as thixotropy [64]. The time needed for the shear stress to stabilize is a measure for the level of structural build-up. This was incorporated in the experiments in this section by mixing and homogenizing the cement pastes completely and leaving them for one minute to rest before starting the viscosity measurement. The stabilization time for the viscosity became then longer when more structure was built up in that one minute. This evidences a higher agglomeration rate for the cement paste.

In Table 5.2 the results of the viscosity measurements are shown as a function of the age of the cement pastes (i.e. 40 min, 6h and 19h). The time needed for the viscosity to become stabilized is expressed by t_s and the viscosity by μ. Not all samples were tested for every age. For example, all the paste mixtures hardened after 19 h except the one with the highest retardation (SG3).

Table 5.2 Viscosity and stabilization time for cement pastes in function of the retarder content

		t = 40 min		t = 6 h		t = 19 h	
name	SG[%C]	t_s[min]	μ[mPas]	t_s[min]	μ[mPas]	t_s[min]	μ[mPas]
REF	0	10	4885	11	49700	-	-
REFSP	0	9	3328	11	37250	-	-
SG1	0.03	-	-	23	12660	-	-
SG2	0.05	-	-	33	9938	-	-
SG3	0.08	3	1453	35	7125	10	32000

It is observed in Table 5.2 that the viscosity of the plasticized reference (REFSP) is lower than the unplasticized reference (REF) for the tested ages. This means that, besides enhancing the fluidity, the synthesized SP also lowers the viscosity of the cement paste. At the age of 6 h, it can be observed that the viscosity of the pastes decreases for a higher addition of sodium gluconate and this relation is expected to hold for the other ages as well. When we consider the stabilization time t_s at the age of 6 h, it is noted that it takes longer for the viscosity to become stabilized for pastes with a lower viscosity. This is not the case for the early age test, as will be discussed further in the text.

The observed differences in the viscosity can be explained by examining the material parameters that influence the rheology of the cement paste. Generally, the viscosity is determined by complex interactions between hydrodynamic, colloidal and contact forces during the movement of the suspended particles. As it is very hard to determine these forces accurately, the focus will be on the effects of sodium gluconate as a rheology modifying agent.

In all pastes, the same cement was used and the dosage of superplasticizer was maintained constant. Therefore, the initial deviations in the volume fraction of the cement particles and surface charge are expected to be negligible before sodium gluconate is added. However, the rheology of the reference paste will change as a function of time due to particle agglomeration and hydration, leading eventually to the initial setting of the cement paste.

5.2.2 Hydration rate

By adding sodium gluconate, the cement particles are impeded to hydrate as shown in the heat of hydration curves in Fig. 5.6. It can be seen that with increasing dosage of SG the acceleration period - during which hydration of C_3S is accelerated with the formation of calcium silicate hydrates and portlandite - is postponed and the so-called induction period is extended. Such effect is translated to much longer delay in the initial setting times and possibly to larger time intervals between the initial and the final setting times. Consequently, less water is consumed by these slowly hydrating pastes and more water stays available in the pore solution. From a physical point of view this means that after mixing the paste, a higher water volume is enabled to disperse the cement particles better during the viscosity measurement, leading to lower viscosities. The presence of the water excess is confirmed by the amount of bleeding water detected at the age of 6 h (Table 5.3). These differences in particle volume fraction might therefore be considered to explain the differences in viscosity.

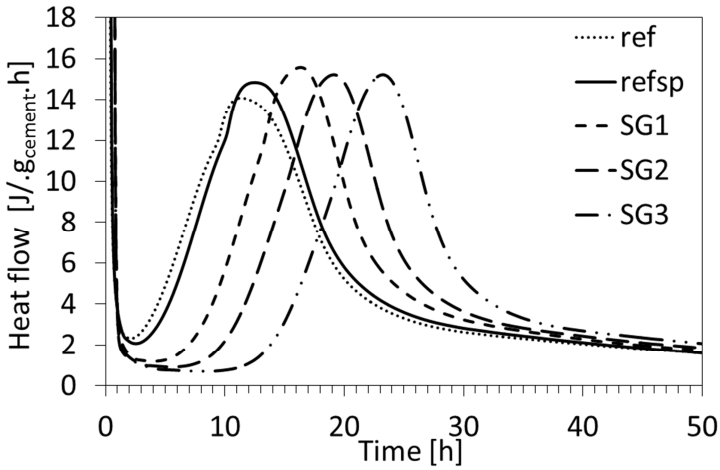

Fig.5.6 Heat of hydration curves for the pastes in Table 5.2

Table 5.3 Amount of bleeding water after 6h for the pastes in Table 5.2

name	SG [%C]	Bleeding water [vol%]
REF	0	0.00
REFSP	0	0.00
SG1	0.03	1.96
SG2	0.05	3.72
SG3	0.08	5.40

However, by adding sodium gluconate, the particle volume cannot be brought under the initial volume of the particles in the REFSP paste. This means that for the same degree of hydration (i.e. constant particle volume fraction), the SG pastes are expected to have at least the viscosity of the REFSP paste. The degree of hydration *α(t)* was determined from the calorimetric measurements as the ratio of the time-integrated heat *Q(t)* evolved at a time (t) to the total theoretical heat of hydration of cement Q_∞, according to Equation 5.1 [153]. The value of Q_∞ was calculated by means of the QXRD composition of C1 in Table 5.4. Any uncertainties on this method do not hinder a reliable comparison in-between pastes of the same cement, like in this research, for which the value of Q_∞ is constant.

$$\alpha(t) = Q(t) / Q_\infty \qquad (5.1)$$

Table 5.4 Clinker content from QXRD in Table 3.3

	C_3S	C_2S	C_3A	C_4AF
Amount (%)	39.6	15.9	4.4	10.5
Heat of hydration (J/g)	510	260	1100	410

The total heat of hydration is the quantity of heat in joules per gram of non-hydrated cement (J/g), evolved upon complete hydration. This is a theoretical value as not all the cement particles will fully hydrate. The value of the total heat was therefore estimated as the relative sum of the heat of hydration of the individual compounds (see Table 5.4) [154]. Considering the tested cement, the total heat of hydration was 335 J/g.

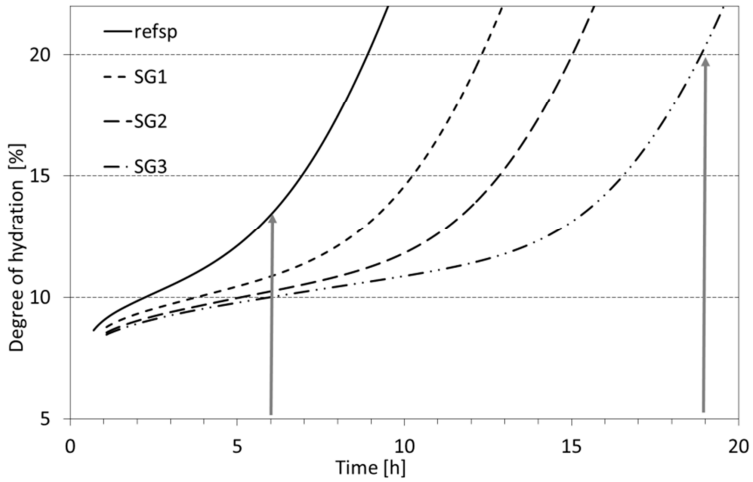

Fig.5.7 Degree of hydration for the pastes in Table 5.2

When the degree of hydration is plotted as a function of time in Fig. 5.7, it is observed that the degree of hydration for the SG3 paste at 19 h is higher than for the REFSP paste at 6 h. Interestingly, the corresponding viscosity of the SG3 paste is lower than the viscosity of the REFSP (see Table 5.2). Therefore, other effects than particle volume fraction have to be considered to explain the viscosity behavior of the pastes. In this respect, the interparticle forces will be closer examined in the following sections.

5.2.3 Interparticle forces

The interaction between flowing cement particles is influenced by attractive and repulsive forces in-between the particles. These result from the surface properties of the particles which evolve together with the ion concentrations of the pore solution and depend on the considered length scale. In this case, long range forces can be influenced by the charge of the particle surface and the presence of steric hindering polymers on the surface. The contact forces are influenced by the particle morphology, resulting from hydrated phases and organic polymers situated on the grain surface.

5.2.3.1 Long range forces

To estimate the electrostatic repulsion, the particle charge has been determined by the zeta-potential. The addition of sodium gluconate to the plasticized reference paste leads to a negative increase in potential from -2.27 mV to -2.63 mV in the case of SG3. One might doubt the significance of this small increase but the abundant SP molecules already present on the cement grain surface hinder any large change in zeta-potential. Therefore, this slightly higher zeta-potential represents a stabilization of the particles in the retarded paste, which means that the particle repulsion is higher and the particles are less tempted to coagulate. This extra repulsive inter-particle force reduces the attractive force in-between sliding particles and therefore contributes to a lower apparent viscosity.

5.2.3.2 Surface charge

One would expect that the addition of a salt to an aqueous solution increases the ionic strength of the pore solution, which would lead to a decrease in the zeta-potential. On the contrary, the opposite occurs and

this implies that the ionic strength decreases by the addition of sodium gluconate. From the ion concentrations of REFSP and SG3 in Table 5.5, one cannot make an exclusive conclusion for the ionic strength but during the zeta-potential measurement, a decrease in the conductivity was observed which could indicate a lower ionic strength. However, this has to be interpreted carefully in case of highly concentrated solutions such as cement paste. It will be investigated further in the text how the SG influences the zeta-potential.

Table 5.5 Ion concentration [ppm] of pore solutions at the paste age of 1 h

name	Ca	Fe	K	Mg	Na	S
REF	555	0.1	7325	0.025	2684	3368
REFSP	561	0.1	7300	0.014	2685	3307
SG3	572	17.8	7060	2.949	2734	3673
SP+SG	531	0.1	6925	0.020	3014	3143

From Table 5.5 it is observed that the addition of SG to the plasticized reference leads to a significant increase in concentration for the elements Fe, Mg, Na and S. The increase in sodium ions is not surprising because of the dissolved sodium gluconate. On the contrary, the increase in Fe and Mg concentrations cannot be explained but the absolute amounts are still small. Interestingly, for the addition of SG, the K concentration is lower. This can only imply the precipitation of a potassium salt for which the solution became saturated. This could have been enhanced by the increase in sodium ions, which influences the alkali balance in the pore solution [23].

The observed increase in the zeta-potential from -2.27 mV to -2.63 mV could also be explained by a chemical reaction at the grain surface such as adsorption. Surface reactive agents, like organic salts, are adsorbed on the particle surface due to their carboxylic acid group. In that case, sodium gluconate might have been adsorbed at the grain surface just like the superplasticizer. The competition for the adsorption sites between PCE superplasticizer and sulfate ions [92] also applies to carboxylic retarders and sulfate ions, because they show a similar adsorption mechanism [38]. The increase in sulfur concentration in the SG3 paste confirms the competitive adsorption between the retarder and the sulfate anion on the cement particle.

The adsorption of the organic admixtures was quantified by determination of the total organic content of the pore solution at the age of 1 h. From the results in Table 5.6 it is clear that the addition of superplasticizer increases the carbon content by a factor 10 in the paste pore solution. Addition of sodium gluconate to this extracted pore solution (SP+SG) delivers an extra 1795.4 mg/l of carbon to the pore solution. This concentration is originating solely from the carbon atoms in the sodium gluconate. When the same amount of sodium gluconate was mixed with the plasticized cement paste before extraction (SG3), the carbon concentration of this pore solution was only 110.8 mg/l. Assuming that this amount of carbon results solely from sodium gluconate, this proves that one milliliter of pore solution contains only 6 % of the available gluconate ions, which means that 94% has been adsorbed on the cement surface. Of course, the calcium affinity and the conformation free energy (ΔG) of SG is higher than for SP, inducing potential superplasticizer desorption. However, in that case, the adsorbed amount of the gluconate ion is even higher than 94% which would prove an even better adsorption of SG.

Table 5.6 Carbon content in pore solution after 1 h.

name	SG [%C]	Carbon content [mg/l]
REF	0	4
REFSP	0	42
SG3	0.08	110
SP+SG	0.08	1838

The successful adsorption of the SG ions can be explained by the nature of the cement grain surface, consisting of metal oxides and hydrated minerals. Both phases are typically hydrophilic and interact with water or other dipolar groups. Therefore, the metal oxides form good adsorption sites for the gluconate ion and for the carboxylic acid group present in the SP. Adsorption through this mechanism will be called *vertical adsorption* (tail configuration) because the head group is attached to the cement grain surface and the side chain can be thought to position itself perpendicular to the surface, although the carbon chain is very flexible (conformation V in Fig. 5.8). This theoretical mechanism is expected to be the most dominant one, because it involves a strong ionic interaction. On the other hand, the SG chain contains polar hydroxyl groups which will interact with the highly polar hydrated phases, through electrostatic forces and hydrogen-bonding interactions. By doing so, they repel water molecules from the hydrated surface and prevent further hydration, which supports the attributed coating potential of this type of retarder. We refer to this mechanism with

horizontal adsorption (train configuration) (conformation H in Fig. 5.8). Finally, in case the number of surface adsorption sites for the gluconate ion is limited, there is a possibility that the gluconate ion is contributing to a negative surface charge through formation of a double layer of gluconate ions. The ground layer adsorbs vertically to the cement surface and the upper layer orients its hydroxyl rich chain in between the chains of the adsorbed layer. The conformation is similar to the film formation with apolar interaction between the hydrocarbon chains of a surfactant [155]. Instead, there are now electrostatic forces and hydrogen-bonding interactions between the hydroxyl groups. Furthermore, calcium ions may function as bridging ions like it has been observed in chapter 2 for organic polymers. These interactions might enhance spatial stabilization of the upper layer and allow the carboxyl group to point towards the pore solution. In this way part of a double layer could be formed which will be called a capacitive layer (conformation C in Fig. 5.8).

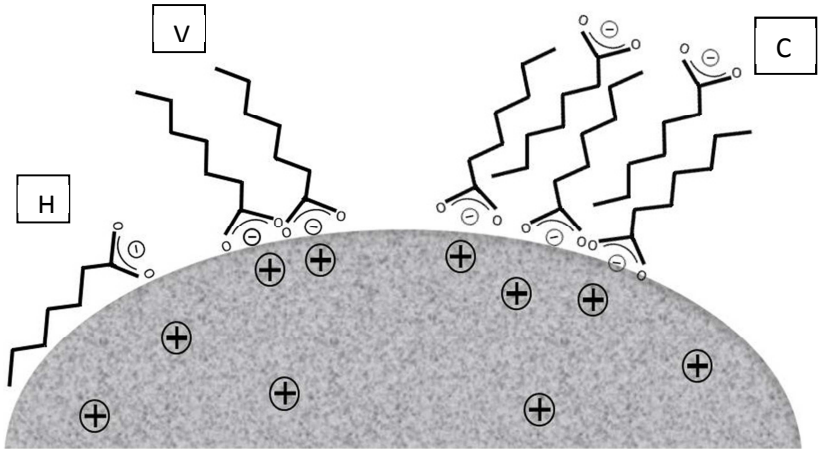

Fig.5.8 Schematic representation of potential adsorption mechanisms of the gluconate anion. The hydroxyl groups are not drawn for clarity. H: horizontal adsorption; V: Vertical adsorption; C: capacitive layer adsorption

One might wonder which mechanism is responsible for the origin of the more negative zeta potential. In the case of cement, the electrostatic charge is heterogeneously distributed over the grain surface. The net charge of the grain is then partially represented by the zeta-potential. A change in the global surface charge through adsorption would generally result from (a) the neutralization of one kind of charged sites, (b) the charge density of the adsorbed ion or (c) a specific adsorption configuration of these ions (e.g. capacitive double layer).

As the zeta-potential became more negative, one might expect neutralization of the positively charged surface sites. On the other hand, the calcium ions in pore solution show bridging capacity and could allow surface coverage of the negative surface sites as well [156]. However, the observed ion concentrations do not indicate any consumption of calcium ions by the SG.

Considering the charge density of the gluconate anion, we know that the SG has only one acid group. After ionic bonding to the surface, the anion's negative charge is neutralized and no additional charge is present in the gluconate structure. This is different for many PCE structures that are polycarboxylic salts for which the negative zeta-potential is often attributed to the presence of other deprotonated carboxylic acids in the structure [76, 157]. On the other hand, the hydroxyl groups of the gluconate ion can partially deprotonate at the highly alkaline pH (≥ 12.5) of the cement paste [36] and could provide a negative charge to the structure. This deprotonated chain might also chelate certain cations from the pore solution which would lead to a reduction of the negative charge.

In order to clarify if SG is effectively adding a negative charge to the cement grain surfaces, either through complex formation or adsorption configuration, the zeta-potential evolution was measured for SG and sodium acetate solutions with similar pH. Sodium acetate (SAc) contains also a carboxylic group but has no chain enabling complex formations or specific adsorption configurations (see Fig. 5.9).

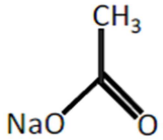

Fig.5.9 Chemical composition of sodium acetate

By titrating a constant equimolar salt solution volume to a constant volume of cement paste, the evolution of the zeta potential in function of the salt dosage was obtained. Fig. 5.10 shows the subtle difference in negative increase in zeta-potential between sodium acetate and SG. The small change in zeta-potential for both salts is due to the dominant surface coverage of the superplasticizer. Nevertheless, the added dosages of sodium gluconate resulted in the high viscosity changes observed in Table 5.2. For example, the dosage of SG3 is corresponding with 1.6 mmol of sodium gluconate in Fig. 5.10. It is also clear that after addition of 4 mmol

of salt, the absolute value of the zeta potential increased by 50% in the case of sodium acetate and only by 30 % in the case of sodium gluconate. This shows that sodium acetate is more effectively contributing to the negative surface charge.

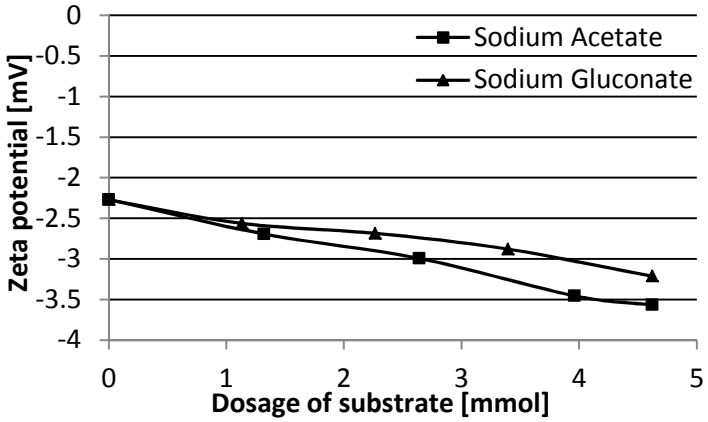

Fig.5.10 Zeta potential of plasticized OPC slurry upon addition of sodium acetate and sodium gluconate solution at pH= 13,3

Because sodium acetate is only adsorbed by charge neutralization, the zeta potential evolution of the sodium acetate paste is the maximal achievable zeta-potential to obtain through charge neutralization and without ion chelation. If all SG would have been adsorbed through vertical adsorption, the zeta-potential would at least be the same as for SAc. As this is not the case, two reasons can be found for the lower absolute value of the zeta-potential evolution. On the one hand, the zeta-potential can be lower because of chelation of certain cations which would offset the neutralization of the negative surface charge in the case of 100% vertical adsorption. On the other hand, a part of the SG ions might not be adsorbed on the positive surface sites and leave them not neutralized. This is more likely for higher concentrations of the salt, as the access to the remaining surface charges becomes more difficult. This is also observed in Fig. 5.10. Considering the lower mobility of the gluconate ion, it is unlikely that all gluconate ions are adsorbed vertically at the acetate adsorption sites. However, as all SG ions do adsorb, at least part of the SG ions have to be considered to get adsorbed horizontally. As a consequence, both adsorption mechanisms are involved in the surface adsorption of sodium gluconate and it is clear that the contribution to the positive charge neutralization becomes less effective for higher concentrations of the gluconate ion.

It is also clear from Fig. 5.10 that the hydroxyl groups do not remain deprotonated while adsorbing vertically, because that would provide a zeta-potential higher than for SAc. Several works in literature show that gluconate chelates metal cations [158, 159]. However, in order to contribute to the more negative zeta-potential, the net charge of the adsorbed gluconate complex would have to remain negative. From the experimental cation concentrations, only a decrease in the potassium ions is observed. So, it is expected that the surface shows a higher potassium density, regardless the adsorption mechanism. This will be confirmed further in the text.

Considering the specific adsorption conformation, there is no indication that the SG ion would form a capacitive layer, because this would result in a higher zeta potential than for SAc as it would provide charge neutralization of the surface and even an amount of negative charge pointed toward the solution, which the SAc cannot offer.

5.2.3.3 Steric hindering

Up to this point, it has been demonstrated that the repulsive forces in between cement particles are partly increased due to an increase in the repulsive surface charge due to SG. The net negative surface charge is the result of horizontal and vertical adsorption of negatively charged complexes of gluconate with certain cations. Besides surface charge, the steric repulsive potential of the superplasticizer side chains might also be influenced by the gluconate adsorption.

Generally, the hydrodynamic radius of the adsorbed superplasticizer polymers can be influenced by the ion concentration of the pore solution, which would affect the steric hindering potential of the superplasticizer. However, in our case, the SP adsorption mainly occurred 30 minutes earlier than the SG addition and the observed change in ionic strength is too small to be significant.

One could expect the vertical adsorption mode to be more relevant in the context of steric repulsion but the impact of the gluconate ion should remain limited in this respect because of its small length. The superplasticizer side chain length is about 14 times higher than the length of the carbon chain in the gluconate ion. However, several different

gluconate ions together are able to form a surface covering layer of a few nanometers [50, 55].

Considering the superplasticizer adsorption conformation, the SP will primarily attach to the surface with its polar carboxylic acid group. It is expected that a considerable number of PCE side chains will spread out into solution when the low polarity of the hydrocarbon part of these side chains is dominant enough to prevent surface adsorption [160]. However, the oxygen atoms in these side chains do contain some polar capacity (i.e. PEG [161]) and therefore there is potential reactivity with the gluconate ion. In the case of vertical adsorption, neighboring PCE side chains could provide spatial stabilization of the gluconate chains due to dipolar interaction, depending on the local concentration [156]. Gluconate chains that do not adsorb vertically could induce a different effectiveness towards steric repulsion, for example by raveling out the coiled mush-room like polymer conformations [43, 160]. In this respect, the gluconate ions could be considered as bridging ions, linking adsorbed polymers to each other which corresponds with the more densely packed organic layers of Plank et al. [93]. So, for both adsorption mechanisms, interaction between the SG and the superplasticizer side chains will enhance polymer entanglement over the grain surface, leading to a more homogeneous polymer layer. This way, it can be concluded that, besides the small electrostatic contribution, the steric repulsion is mainly responsible for the lower viscosities. It then remains the question how the stabilization times are determined by this mechanism. This will be investigated in the following paragraph.

5.2.4 Contact forces

A more homogeneous polymer layer on the surface of the cement particles also changes direct contact interactions. It was shown in section 4.2 that the organic polymer affects the morphology of the surface hydrates and amorphous phases can be created. This non-crystalline material in combination with the additional SG is likely to form low elastic (soft) inter-particle bridges that will disconnect easily when they are sheared directly by the viscometer instrument. As a consequence, neighboring particles will show a highly viscous capacity and delay the shear propagation into the rest of the paste volume. The viscosity stabilization time would therefore have to increase for higher polymer content. For example, immediately after addition of SG to the paste (i.e. SG3 at age 40 min in Table 5.2), we can assume that not enough time was provided to form a significant amount of soft inter-particle connections in two minutes. The stabilization time is therefore low (3 min) as there are hardly any viscous nor solid

elastic inter-particle connections. At the age of 6 h, still few elastic inter-particle connections are formed due to retardation. The viscous soft bridges could form already and are likely to be dominant over any elastic connection. This is confirmed by the stabilization time that is prolonged for higher amounts of SG as the shear propagation is hindered by the viscous connections. On the contrary, at the age of 19 h, hydration has proceeded sufficiently for elastic inter-particle connections to become dominant over the soft network connections and shear propagation occurs much faster than at 6 h. The shear behavior of the SG3 paste, at 19 h, should therefore be compared with that of the REFSP paste at 6 h. So, at this point, it is clear how a homogeneous polymer layer could explain the observed stabilization times for plasticized cement pastes with additional sodium gluconate. However, it then remains unclear how the morphology of the induced soft interparticle bridges looks like.

5.2.4.1 Morphology of the hydration products

We know from previous chapters that, besides the physical impact on the viscosity of the cement paste, superplasticizer and setting retarder will also influence the hydration process and the hydration products. The general consensus is that rapid dissolution of clinker components, in particular those of aluminate phases and alkali sulfates, leads to instant formation of ettringite within the first minutes (wetting period) in the absence of any organic admixtures [99]. In the course of the induction period, nucleation and growth of calcium silicate hydrates (C-S-H) occur via dissolution of alite (C_3S) and the pore solution becomes supersaturated with respect to calcium ions, leading to the nucleation of portlandite crystals. During this period, AFm phases start to appear and more ettringite formation results in continuous increase in the viscosity of the dispersion. The ettringite crystals are known to have a stronger influence on the setting than the other phases due to its crystal morphology and its amount which is higher than the others [99]. Some effects on the morphology of hydrates have been reported to occur by superplasticizers but the actual influence depends on the kind of the admixture [99, 162]. On the microstructural scale of the plasticized cement pastes in our case, a soft polymer network would lower the spatial density of newly hydrated phases at the grain surface, resulting in a lower particle roughness. To understand this effect, the evolution of the particle morphology in the course of hydration has been investigated using ESEM for the REFSP and SG3 paste.

After 3 hours of hydration, the surface of the cement grains in the REFSP paste have been observed to be partially covered with hydration products

(Fig. 5.11.A). A closer look at these hydration products shows the abundant presence of small polygonal crystals of 100 to 400 nm in size (Fig. 5.11.B). Next to these small crystals, elongated prismatic needles of micrometer size were observed growing at the expense of the small crystals (Fig. 5.11.C and 5.11.D). This reaction product was identified as ettringite which precipitates at the surface of C_3A to prevent fast setting. The crystals, smaller than 400 nm, are too small to bridge the space between the clinker grains and do not contribute significantly to any stiffening of the paste. However, this layer increases the particle roughness which contributes to shear resistance and might result in higher viscosities. The large needles of ettringite have inter-particle bridging capacity and contribute significantly to the cement paste viscosity [163].

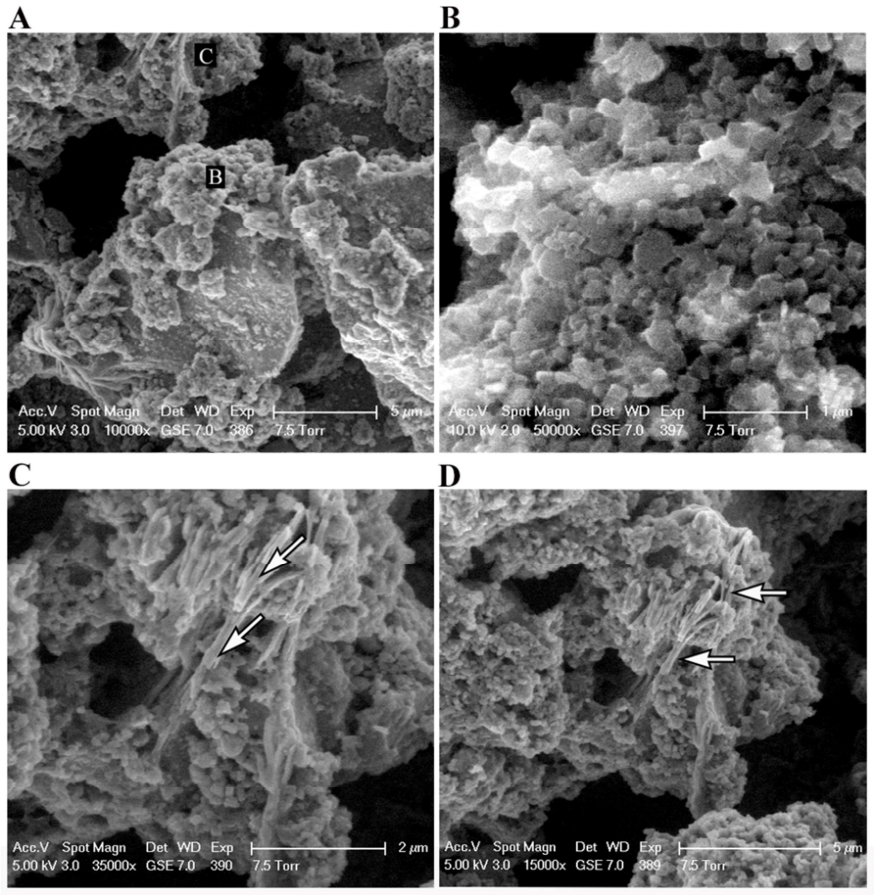

Fig.5.11 ESEM-FEG images of REEFSP at the age of 3 hours. A) global view, B) small ettringite crystals, C) large ettringite needles (close-up), D) large ettringite needles among small crystals

Regarding the SG3 paste, it was also observed that, after 3 hours, the grain surface of C_3A was partly covered with small ettringite crystals. In this case, no large ettringite needles, as observed in the REFSP, could be established at this age. However, at the earlier stage of 2 hours, shorter and thinner prismatic ettringite needles were found to be lying loosely all over the grain surface (Fig. 5.12.A) which indicates that they touched the grain surface when the pore water receded during the experiment. These observations are confirmed by the impeded ettringite formation suggested by Tenoutasse [52]. The presence of these small fine particles is in sharp contrast with the large needles growing on the grain surface of the REFSP paste. It is likely that the prevented surface connection of the fine particles is enhanced by the densified polymer layer on the grain surface in the SG3 paste. Furthermore, on the same particle, batten shaped rods were also observed as completely attached to the grain surface (Fig. 5.12.B).

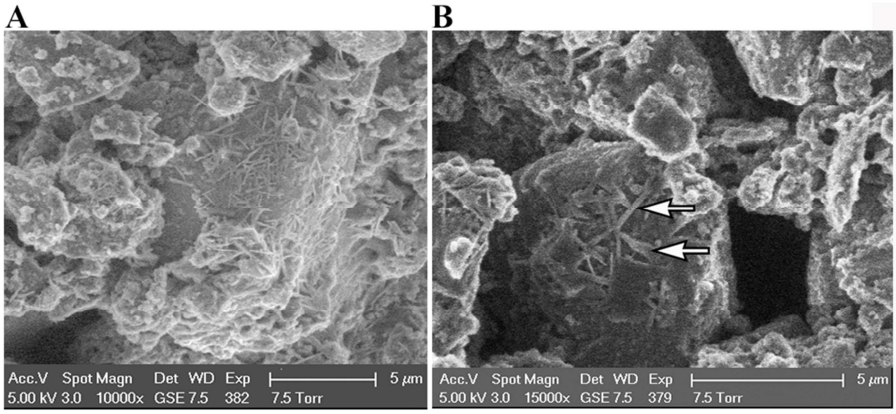

Fig.5.12 ESEM-FEG images of SG3 paste at the age of 2 hours: A) thin prismatic ettringite needles; B) batten shaped plates

During hydration of the SG3 paste at the age of 3 hours, clusters of parallel plates were observed in Fig. 5.13. These plates are approximately 0.1 µm thick and 1 µm wide. The length varies between 5 and 10 µm and the plates might be extending each other in the longitudinal direction.

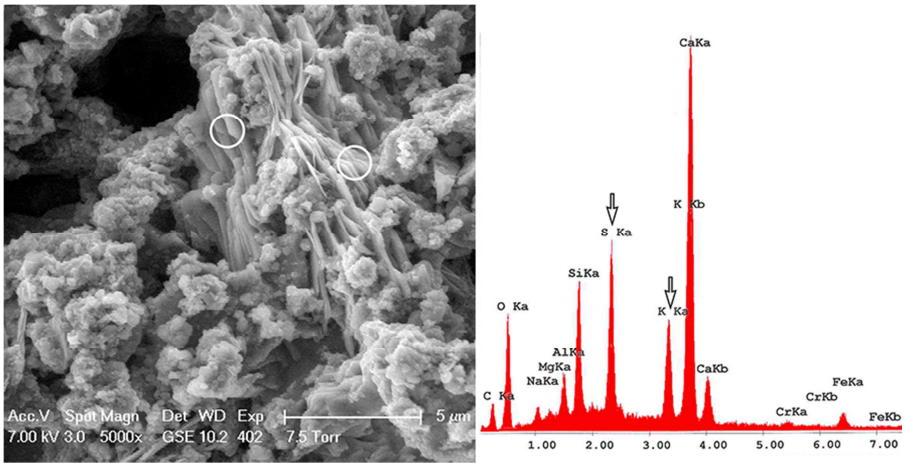

Fig.5.13 ESEM-FEG images of SG3 paste at the age of 3 hours: parallel plates (left) and EDX spectrum of the circled areas (right)

In order to determine its composition, the EDX spectrum is shown at the right in Fig. 5.13 for the circled scanned areas at the left. The corresponding elemental composition is presented in Table 5.7. It is noted that the spectrum could not be obtained for the pure mineral since the resolution is obscured by ettringite and C-S-H. Nevertheless, as can be seen from the spectrum in Fig. 5.13, the plate-like crystals contain a relatively high amount of sulfate and potassium. As mentioned before, a remarkable decrease in the potassium concentration in Table 5.5 indicated the precipitation of a potassium salt due to SG addition. Taking this into account, these plate-like crystals seem to be the syngenite mineral ($K_2Ca(SO_4)_2 \cdot H_2O$) which is in correspondence with the earlier detection of syngenite formed alongside short prisms of ettringite in a cement rich in alkalis [164]. Previous observations of syngenite show a clear batten shaped rod morphology [89, 165]. Despite different spatial conformations in literature, the plates in Fig. 5.13 have geometrical properties that are very similar to the reported syngenite rods.

Table 5.7 EDX data from parallel batten shaped rods in Fig. 5.13

Element	O	Na	Mg	Al	Si	S	K	Ca	Fe
At%	33.04	0.85	0.34	1.84	5.38	8.16	6.62	30.74	4.42

The above observations show that due to the addition of SG the particle morphology is changed in two ways. Firstly, the morphology of the outgrowing ettringite needles is changed to smaller and suspended fine

particles. The fact that the amount of large needles is smaller at the age of 3 hours is already expected to lower the shear resistance. Secondly, a flat mineral phase, similar to syngenite, has been detected at the grain surface. As pointed out before, the viscosity of cement paste is lower for higher dosages of sodium gluconate, even for pastes with a similar degree of hydration. Because the detected mineral is incorporated within the hydration products, it can therefore be expected to be less physically contributing to the shear resistance than the large ettringite rods in the unretarded paste.

So, the appearance of the soft interparticle bridges could be related with the suspended fine particles in solution. During shear, a temporarily concentration of these particles in-between large cement grains could work lubricative by deviating the inter-grain contact stress. Moreover, the described polymer layer on cement grains can also be present at the fine hydrates in solution that were dispersed by the additional SG. Together with the (non-crystalline) hydration products observed in chapter 4 all these features can constitute the nature of the soft interparticle contact “bridge”.

Summary

To conclude this section, the following findings describe the impact and mechanism of the retarder:

- For a higher dosage of sodium gluconate, the hydration kinetics of a plasticized cement paste are more delayed because of the increasing adsorption of gluconate to the cement grain surface. This confirms the attributed coating formation which impedes the further reaction of the cement surface with water.
- The excluded water volume, due to gluconate adsorption, contributes to a lower particle volume fraction of the cement which results in a lower viscosity of the retarded cement pastes.
- For cement pastes with a similar degree of hydration, the lower viscosity of the sodium gluconate paste is explained by a higher electrostatic and steric repulsion, mainly due to positive charge neutralization and a densified polymer network on the cement grain surface. The gluconate ion is generally expected to precipitate as a negatively charged complex, by means of its hydroxyl and carboxyl functional groups. The contribution to the

positive charge neutralization becomes less effective for higher concentrations of the gluconate ion.

- The gluconate anion is expected to enhance the formation of a homogeneous polymer network on the cement grain surface, which changes hydrate morphology and the inter-particle contact forces. A discussion on this network formation was useful in explaining the evolutions in the observed viscosity stabilization time.
- Sodium gluconate changes the paste morphology by reducing the amount and size of the large prismatic ettringite needles. Combined with the amorphous morphology due to SP addition and the spreading of fine hydrates in solution, the interparticle contact energy will be buffered in-between shearing cement grains which facilitates particle flow.
- From pore solution analysis and EDX spectra, a potassium rich mineral is detected with geometrical properties that are similar to syngenite. This morphological change is also expected to lower the shear resistance and the paste viscosity compared to ettringite rods.

5.3 The influence of the retarder in the agglomeration model

It was clear from the experimental observations in the first section that the anti-thixotropic area evolution in the retarded system has been decoupled from the connectivity potential of the hydrates on the agglomerate surface, as observed for C1SP. The retarder seemed to introduce a different shear mechanism that allows higher stress levels and simultaneously increasing hysteresis areas.

In section 5.2, we learned that the interaction between superplasticizer and retarder results in a densified polymer layer on the cement grain surface. It was also discussed how this layer contributed to the lower viscosities with complementary lubrication from suspended plasticized fine particles in the more retarded pastes (§ 5.2.4). Considering that the SP dosage is higher in C1SPSG, the polymer layer will also be considered in this section. From a certain degree of hydration, the elastic interparticle bridges start dominating this viscous behavior and provide a more elastic stress response.

5.3.1 Agglomeration parameters

When we introduce all parameters, obtained from the experiments in paragraph one, into the agglomeration model (Eq.4.1-4.8), we see a similar situation as in figures 4.19 and 4.20. The cumulative heat production of internal hydration products for C1SPSG is plotted in Fig.5.14. The development of these hydration products is clearly postponed and only reaches the starting level of C1SP for the considered time interval. Similarly, for the heat production of external hydrates in Fig.5.15, the maximal hydrate production reached for C1SPSG corresponds with the lower values for C1SP.

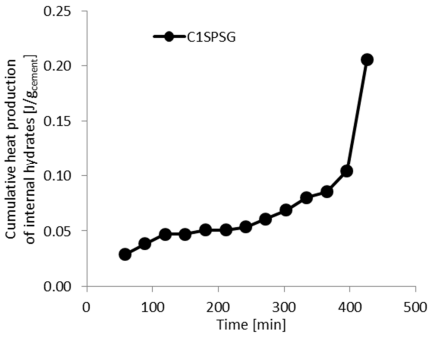

Fig.5.14 Cumulative heat production of internal hydration products for C1SPSG

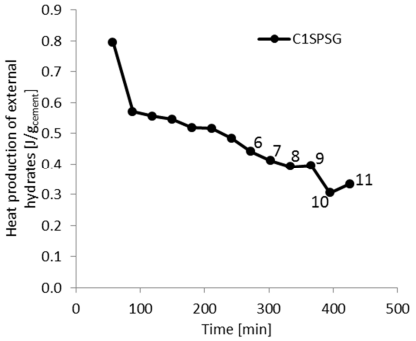

Fig.5.15 Heat production of external hydrates for C1SPSG

In Fig.5.16, the sum of the cumulative heat production for internal hydrates ($\sum Q_{int}$) and the absolute heat production of the external hydrates ($Q_{ext,i}$) is shown for C1SPSG. The entire evolution falls below the levels achieved with C1SP which again confirms the serious delay in hydration kinetics. However, both evolutions show an increase in heat production at the end of the registrable shear behavior.

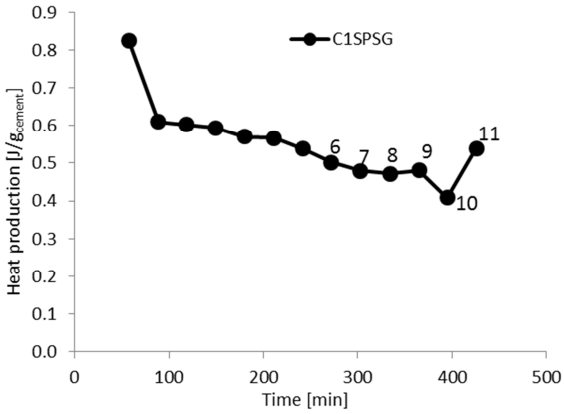

Fig.5.16 Sum of cumulative heat production for internal hydrates ($\sum Q_{int}$) and heat production of external hydrates ($Q_{ext,i}$) for C1SPSG

For the comparison between the relative change in anti-thixotropic area (ΔA_i) and hydrate production ($\Delta(\sum Q_{int,i} + Q_{ext,i})$) in Fig.5.17, a totally different situation is observed than in Fig.4.25. Similarly, the relative change in reagglomeration rate relates very differently to the hydrate production in Fig.5.18 than in Fig.4.26. As noticed before, the change in anti-thixotropic area is increasing for a decreasing heat of hydration, as confirmed in Fig.5.15. This makes the data couples appear in the bottom right quadrant instead of the top right one, which asks for a different interpretation of the micromechanical mechanism than for C1SP.

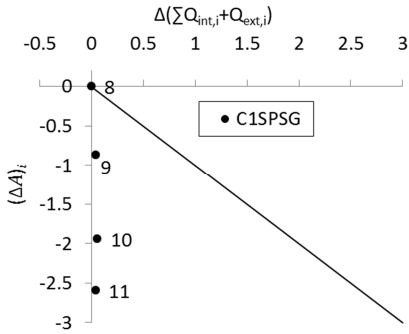

Fig.5.17 Comparison between the relative change in anti-thixotropic area (ΔA_i) and hydrate production ($\Delta(\sum Q_{int,i} + Q_{ext,i})$)

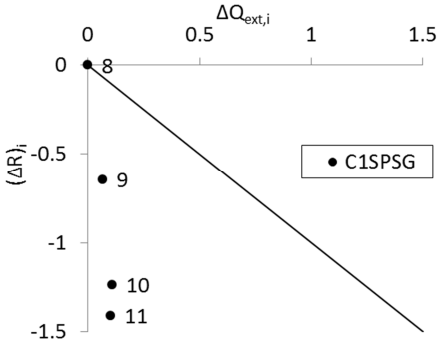

Fig.5.18 Comparison between the relative change in reagglomeration rate and hydrate production

5.3.2 Micromechanical mechanism

The fact that the anti-thixotropic area is no longer in correspondence with the hydration energy, indicates that the polymer layer changed the physical state of the paste. Earlier reports on anti-thixotropic features by Nagataki et al. suggest that these effects may be a result of the development and breakdown of a secondary structure [166]. This structure is related to gel formation and is not to be confused with the floc structure of the pre-existing paste [105]. Shaunessy mentioned that this theory is in contrast with that described by Helmuth [105, 167], for which all anti-thixotropic effects are directly related to the varying rate of breakdown and recovery of the floc structure.

In order to explain the anti-thixotropy, Helmuth states that pastes with a high degree of flocculation will be prone to a higher degree of thixotropic breakdown as opposed to a paste that has undergone intense mixing [105]. Better mixing induces better dispersion and increases the tendency to a faster structural recovery after mixing. If this recovery is superimposed upon the break-down caused by the test itself, the paste will show anti-thixotropic behavior [105]. It is indeed reasonable that the SG addition contributes to the better dispersing of the cement particles but, unlike intensified mixing, the SG will not create reactive particle surface for reagglomeration because of its retarding nature.

Despite their different approach, Nagataki and Hemulth do not necessarily have to contradict each other in the current context. Due to better dispersion of the cement particles by SG addition, it is expected from section 2.3.2 that relatively more small particles will be released out of previous agglomerates and that their polymer coverage is high [168]. Comparing with Fig.4.17b, the picture could now be represented by Fig.5.19(left). Considering only the colloidal size range particles, the increased amount of polymer within this fraction of the paste may then change its physical state to look more like a gelled material than a suspension. Upon hydration of these colloidal particles, the formation of C-S-H gel might even contribute to the gel-like state of this fraction. This idea of dispersed fine particles shows similarities with the microscopic observations in section 5.2. Fine non-colloidal hydrates have indeed been observed which is indicative for finer fractions that could not be visibly detected.

It is unlikely that the dispersion of the fine fraction will lead to an increased hydration rate as their dispersion was initiated by a retarder. If that was

not the case, the retarder would have worked as a hydration accelerator, improving the reagglomeration rate through structural recovery like Helmuth described. The retarding impact of SG is also more pronounced for these newly spread fine particles because they have hardly been submerged in the initial mixing water. Therefore, these fine unreacted particles are expected to remain unhydrated longer than some particle surface areas of large particles. Furthermore, the heat of hydration of these fine particles in the interstitial solution is not expected to follow the main hydration evolution on the cement grain surface because their local chemical environment is the fluctuating pore solution and not the dense hydrate layer at the grain surface.

Any increased content of fine particles in the interstitial solution will have an obstructing effect on the mobility of water films within agglomerates [169, 170]. Together with newly formed hydrates on the grain surface, the fixation of the interstitial solution hinders the movement of particles within SPSG agglomerates as illustrated in Fig.5.19(right). In this way, the SPSG agglomerates are more stable than the SP agglomerates which is counterintuitive. Of course, this solution effect should be clearly distinguished from the direct hydrate bridges in-between particles and it should be noted that it concerns agglomerates near the initial setting time for both pastes.

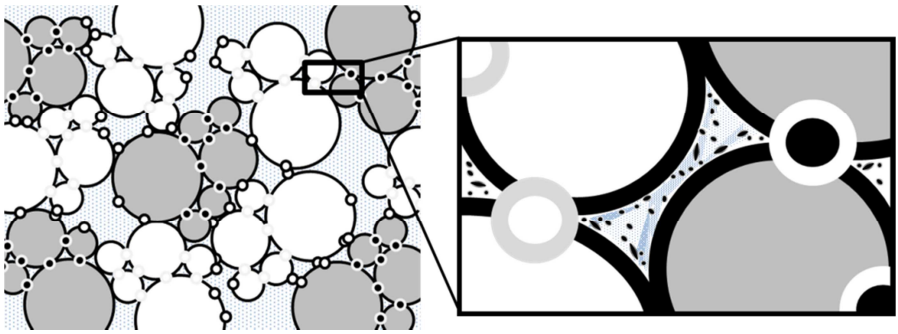

Fig.5.19 Nuclei and fine hydrates in SPSG pore solution (left) obstructing the mobility of water films (right)

Suppose the strength of a hydrate bridge is similar within the SP and SPSG paste for equally large agglomerates. Then, the additional solution effect would have to result in a higher stress increase within the acceleration ramp for the SPSG paste compared to the SP paste. This is actually confirmed by the difference in shear thinning tendency. In section 5.1, we observed a less strong shear thinning effect for the SPSG paste compared to the SP paste, also for the earliest cycles with small anti-thixotropic area.

So, it is now clear why the stability of equally large agglomerates could be higher for the SPSG combination than for SP solely. Still, the higher agglomerate stability does not explain the increasing anti-thixotropic area due to SG addition.

One possible manner for the small sized fraction to gain influence over time, is that it remains excluded from co-agglomerating with the other volume fractions due to its low hydration rate. The recently established tendency for polymers to attach on the small particles implies that the hydration rate is more impeded than for the polymer layer on larger particles [168]. Of course, reagglomeration in-between other particles could then still occur for large particles with surface sites where the polymer layer is thin or easily abraded by shear. Experimental observations are needed to confirm the continuous exclusion of the fine plasticized fraction, but it would allow the fraction to remain isolated around these agglomerates in the interstitial solution. In that case, the importance of this small particle fraction in the flow behavior of the paste would rise, as it increasingly suspends the newly formed agglomerates.

Besides the growing impact of the fine particles, it then remains the question by which means this material contributes to a higher stress response in the decelerating ramps of Fig.5.4 compared to the accelerating ramps.

Besides hindering the agglomerate break-up, the interstitial solution of the SPSG paste is also a source of slowly hydrating nuclei and some amorphous hydration products. Eventually, at some point in the hydration process, the polymer cover on these small particles will become ineffective and the hydration activity within the gel-like material will increase. It is expected that this is enhanced during shear. For example, the freshly broken agglomerates and hydrating small particles will show the most attraction to each other at the maximum shear rate in cycles 9, 10 and 11 of Fig. 5.4.

The rate of co-agglomeration of the fine fraction is likely to depend on the size range of the particles that have been isolated. It is possible that during cycle 9, the largest particles of the fine fraction show hydrate activity and therefore contribute to reagglomeration. The limited number of this group of particles causes the reagglomeration to be rather modest. For the remaining fine particles, their increasing number might be indicative for the higher anti-thixotropic area during cycle 10 and 11. Thereby, the small fraction is consumed more and more as the polymer layer is consumed due to hydration. The steady consumption of suspending water will increase

the friction in-between agglomerates, particularly at high shear rates. This is indeed confirmed by the strong reduction in shear thinning (or higher curvature) for higher stress levels in the acceleration ramps of cycles 9-11.

New experimental techniques should be developed to confirm the isolation and the hydrating properties of the fine fraction in cement paste. It was mentioned in section 2.4 that the current methods show important limitations in visualizing the particles in the environment of a real cement paste. Other techniques provide a rather indirect probing of the flocculation state. Perhaps, future progress with the recently applied FBRM method might show some potential in elucidating this matter.

Despite the lack of experimental proof for the hydrate activity of the fine fraction, other aspects of the increasing anti-thixotropic area can be investigated. For example, for C1SP, it was noted that the decreasing intersection time is a result of the agglomerates becoming too big to respond gently to the applied shear stress. They suffer so much particle friction that they disrupt the shear plane, even aborting further stress registration. It is remarkable that in Fig.5.5, the cycles 8 to 10 show an almost constant value for the intersection time while the agglomerates are as large as for C1SP, according to the stress levels. During these cycles, the reagglomerated clusters seem to remain greatly intact during one cycle in Fig.5.4 until the minimum shear stress in the acceleration ramp is achieved again. The fact that the intersection time does not decrease for these cycles suggests that the reagglomeration is not hindered by increasing friction. This could be caused by the postponed water consumption, which would physically facilitate the particle movement. On the other hand, the water should be steadily consumed already for achieving these high agglomerate sizes and stress levels.

At this point, it is useful to address the ball-bearing effect of an increased amount of small particles that lower the friction during shearing of the agglomerates. In the same physical way, the relatively high presence of polymer within the fine fraction could increase its compressibility, allowing the shear energy to be spatially distributed more easily. Both aspects are illustrated in Fig.5.20 and Fig.5.21 and would contribute to the smooth stress registration and the achieved stress levels that are higher for SPSG than for SP paste. This ball-bearing mechanism could work complementary in lowering the particle friction when the water consumption is finally accelerated.

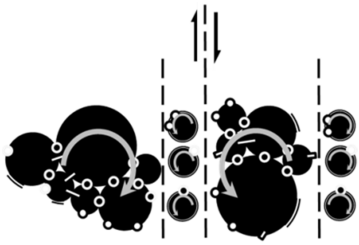

Fig.5.20 Shear induced rotation of agglomerates and ball-bearing fine particles

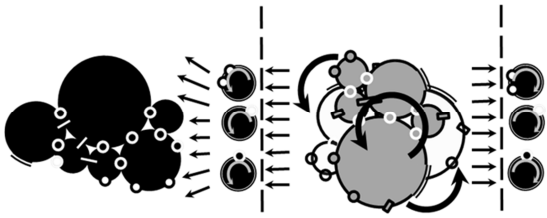

Fig.5.21 Agglomerate rotation (grey) leads to lateral stresses which are spatially distributed by plasticized fine particles.

Towards cycle 11, the intersection time is lowered but the anti-thixotropic area still increases compared to cycle 10. This means that little water and polymer is available for lowering the friction and a consecutive intercalation of all remaining nuclei from the pore solution is pending. The latter contributes to the high reagglomeration during this cycle and, therefore, even in cycle 11, the reagglomeration mechanism is still not similar to the one described for C1SP.

So, it is no use seeking correlations in Fig.5.18 between the value of the connectivity potential (*x*-axis) and the reagglomeration (*y*-axis), as the above discussion has shown that the rheology is dominated by the increased amount of polymer and plasticized fine particles in-between agglomerates instead of the elastic contact forces like for C1SP. However, the diagram still allows to see the dominance of this polymer layer evolve in function of time.

5.3.3 Agglomeration diagram

Compiling all above observations considering the agglomeration model, it can now be extended towards the diagram in Fig.5.22 for the reagglomeration rate. Data points located at the bisectors in quadrants I and III represent cement pastes for which the shear behavior is dominated by the elastic inter-agglomerate hydrate bridges. For example, for increasing reductions in external hydrate energy in C1SP, the reductions in reagglomeration rate increase proportionally in function of hydration time. When the data points would deviate from the bisector in function of time (or agglomerate size), different mechanisms can be behind it. Data points deviating to sectors A would require an admixture combination that contributes in connecting the agglomerates during shear. Contrarily, data

points in sectors B would include some weakening of the inter-agglomerate bridges by another kind of admixture combination.

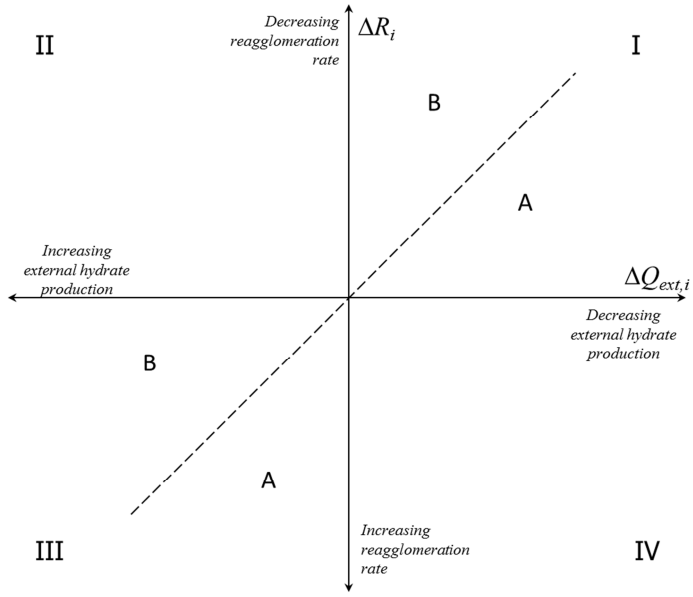

Fig.5.22 Agglomeration diagram

In contrast, the quadrants II and IV show no particular correlation with the x-axis, because there would be a reverse relation between the external hydrate energy and the reagglomeration rate. Therefore, these systems do not show the elastic response of hydrate interactions and can only exist if the shear behavior is dominated by another mechanism, like the polymer layer and plasticized fine particles in-between agglomerates. However, it can be learned from the vertical position of the data point to what extent the reagglomeration rate is accelerated during hydration. Towards the end of the cycles the difference will decrease and it is even possible that data points will move back towards the *x*-axis as the influence of the polymer layer is diminished. This could have been observed for C1SPSG but the elastic hydrate interaction interfered so fast that no smooth stress registration was possible any longer.

For the systems in quadrant II, an admixture combination would be required that lowers the reagglomeration rate, even for increasing hydrate bridges. These admixtures cannot be retarders, as the hydrate production increases, and they would need to prevent contact in-between fresh inter-agglomerate hydrates.

It is clear that, with the diagram in Fig.5.22, an instrument is provided to estimate the origin of the rheological behavior when no information on the admixtures is known. It is also possible to effectively communicate the combined effect of different known admixtures, different dosages and hydration time on the rheology of the cement paste. In this respect, the diagram, as an extension of the agglomeration model, contains most of the relevant information considering combined admixture effects.

Summary

So, in summary of this section, SG induced another reagglomeration behavior as found for C1SP: The reagglomeration rate accelerated while the hydration rate decreased. This was related with the intervention of the polymer in-between particles, as found in the previous section, and was further detailed concerning SG: First, the presence of a fine particle fraction in the suspending liquid due to a plasticizer addition (like SG) was apparent from literature [46, 71]. These fine particles are capable of reinforcing the agglomerate stability [169], which was also observed by the increased curvature of the acceleration ramps of C1SPSG, compared to C1SP. Furthermore, it was proposed that this fine fraction would remain available in the liquid by its exclusion from co-agglomeration. This would be enhanced by the relatively high polymer content on the particle surface of this fine fraction, which has been pointed out in literature very recently for superplasticizers [168]. The gradual consumption of this polymer layer and the disruption of it, during shear, would then be responsible for the gradual incorporation of the fine particles during the reagglomeration process. The increasing anti-thixotropic area indicates an increasing effect of this particle incorporation and it is therefore suggested that the finest particles of the fine fraction are agglomerated last of all because they show the highest polymer adsorption and they are high in number. Once their polymer layer is consumed and their surface shows hydrate activity, this also means that most of the suspending water is consumed, which corresponds with higher particle friction and the observed decreasing intersection time. The agglomeration diagram is a useful tool in quantifying all these different effects of admixture combinations on the cement paste rheology.

Chapter summary

In this chapter, the retarder was found to induce further delay in hydration kinetics and structure development of the plasticized cement paste. For a

higher SG addition, the cement paste showed a lower viscosity and a weaker shear propagation.

Through indirect analysis of the interparticle forces, the lower viscosity was attributed to (1) the change in volume fraction due to the postponed water consumption, (2) a slightly higher electrostatic repulsion, mainly due to positive charge neutralization on the cement grain surface, (3) increased steric repulsion caused by a densification of the polymer layer on the particle surface and (4) a morphological change of ettringite and related phases. All these factors contribute to the observed lower viscosity upon retarder addition.

The reduced shear propagation was attributed to a change in the interparticle connections. On the one hand, the densified polymer layer increases the steric repulsion but, on the other hand, the nature of the suspending liquid can also contribute. It was already demonstrated in chapter 4, with thermodynamics and mineralogy, how the SP influenced the hydrate composition. It was shown that, besides ettringite, also monosulfate or amorphous ettringite could form at the grain surface and it was indicated that their morphology is likely to change the mechanical particle interaction. For SG in this chapter, the hydrate composition and morphology have been investigated with environmental scanning electron microscopy. The addition of SG also showed some particular changes in the hydrate morphology at the grain surface but also a better dispersion of fine hydrates in the suspending liquid. Therefore, it can be concluded that SG simulated the SP interference in the hydrate formation and that small hydrates and possibly amorphous phases are spread out through the pore solution. In this way, these fine hydrates remain longer in the suspending liquid, before co-agglomeration, where they can lubricate the particle contact during shear. In this way, further SG addition will cause a decrease in paste viscosity and a higher delay in shear propagation.

The same mechanism was able to explain the observed increase in reagglomeration rate because the postponed co-agglomeration of the fine fraction can increase the anti-thixotropic area over time. To this end, it is suggested that the finest particles of the fine fraction are agglomerated last of all due to their high polymer coverage. Once their surface shows hydrate activity, higher particle friction might be expected to decrease the intersection time. All these separate effects are concisely represented in the extended agglomeration diagram.

Chapter 6 - The influence of accelerator on the retarded plasticized cement paste rheology

In the two previous chapters, a conceptual understanding has been given on the relation between agglomeration and hydrate formation. The combined effects of the superplasticizer and retarder showed a particular reagglomeration behavior which was analyzed quantitatively with an extended agglomeration model. In this chapter, one more admixture will be added to the retarded plasticized system. It concerns a hydration accelerator and, parallel to the fourth and fifth chapter, the influence of the accelerator will first be estimated by three kinds of experiments. In the second section, the focus will be on the origin of the accelerator influence in order to understand the observed behavior. In the final sections, all findings are integrated in the agglomeration model that was developed in the last sections of the previous chapters. In this way, the model is further extended for the additional interference of accelerating admixtures.

6.1 Experiments

In these experiments, the cement paste (C1SPSG) and one accelerator will be combined. The accelerator is calcium nitrate, abbreviated with 'CN' and the pastes are prepared according to the mixing procedure in section 3.1.3. They contain 0.13% SP, 0.03% SG and 2% CN. The final paste will be referred to as C1SPSGCN.

6.1.1 Hydration kinetics

The hydration kinetics of the reference, the plasticized, the retarded and accelerated cement paste is represented by isothermal calorimetric measurements. The absolute heat of hydration can be observed in Fig.6.1 and the cumulative heat in Fig.6.2 for all the admixture containing pastes and the reference paste. It is clear that the accelerator compensates the delay in the hydration kinetics induced by SG, as the first small peak in the heat flow is even above the level of the reference paste during the induction period. Furthermore, the main hydration peak is also overlapping with the reference paste without exceeding its maximum value. The fast increase in the cumulative heat of hydration in Fig.6.2 is caused by the first small peak in Fig.6.1. So, the accelerated paste shows the highest hydration rate of all pastes, but remains comparable with the reference in terms of total heat production during the first 50 hours.

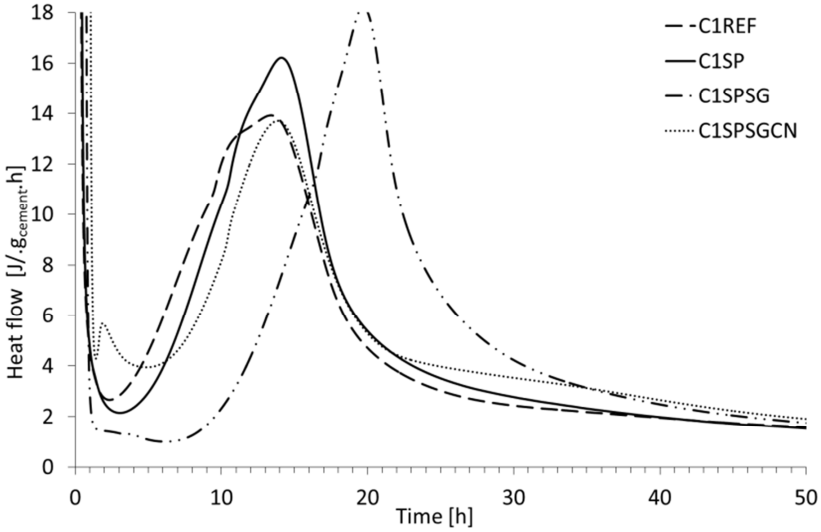

Fig.6.1 Heat flow for all admixtures

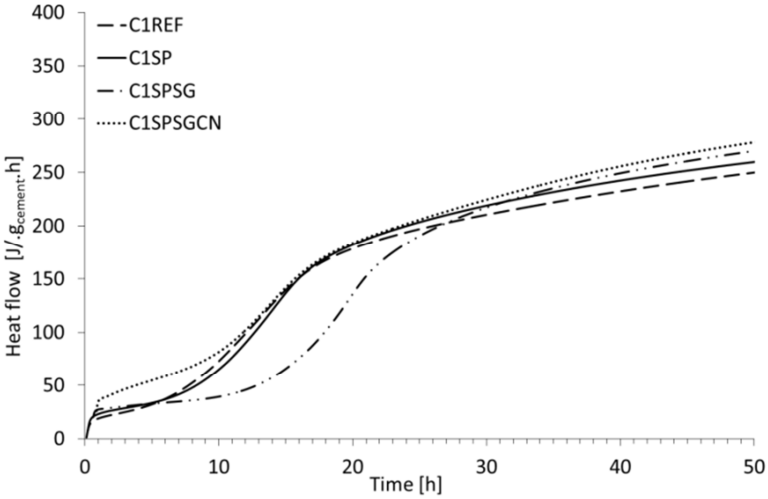

Fig.6.2 Cumulative heat production for all admixtures

6.1.2 Structure development

The storage modulus was measured for all the setting pastes according to the prescribed oscillatory procedure (see section 3.2.1). The minimal and maximal storage moduli were collected for the plasticized paste with and without retarder-accelerator combination. Furthermore, the C1SPCN paste (plasticized paste without retarder and with accelerator) is also plotted for use in the next section. The evolution of the minimal storage modulus (G'_{min}) in function of time is given in Fig.6.3 at the left and the maximal storage modulus (G'_{max}) at the right.

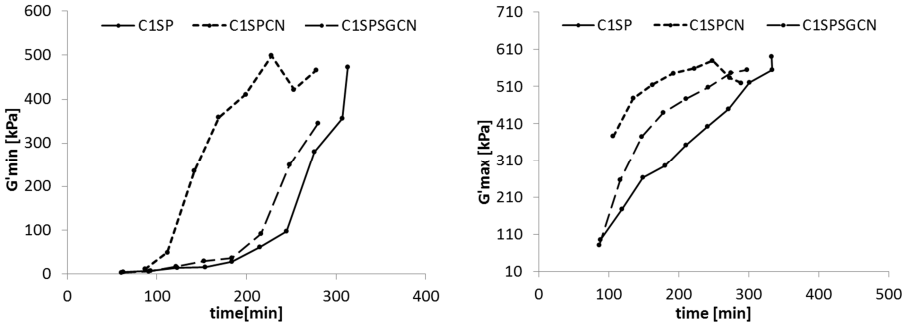

Fig.6.3 Evolution of G'_{min} (left) and G'_{max} (right) in function of time

Comparing Fig.5.3 with Fig.6.3, shows that the accelerator addition has compensated the delay in structure development created by SG. The G'_{min} evolution of C1SPSGCN closely follows the evolution for C1SP during the

first five cycles after which the accelerated paste shows a slightly faster network build-up. For G'_{max}, a similar faster structure development is observed, apart from the distinct difference in cycle 2 to 5. Considering C1SPCN, the highest modulus is noted more than an hour sooner than for the C1SP paste, which illustrates the accelerating potential of the CN dosage for an unretarded paste. After the maximum value, a small drop is observed for both moduli. This might be related with a low rheometer registration accuracy at these high stress levels or a significant interference of some hydration product but this will not be addressed here.

6.1.3 Flow behavior

A series of hysteresis cycles was performed on the C1SPSGCN paste and the observed stress in function of shear rate is presented in Fig.6.4 and should be compared with Fig.4.6 and 5.4.

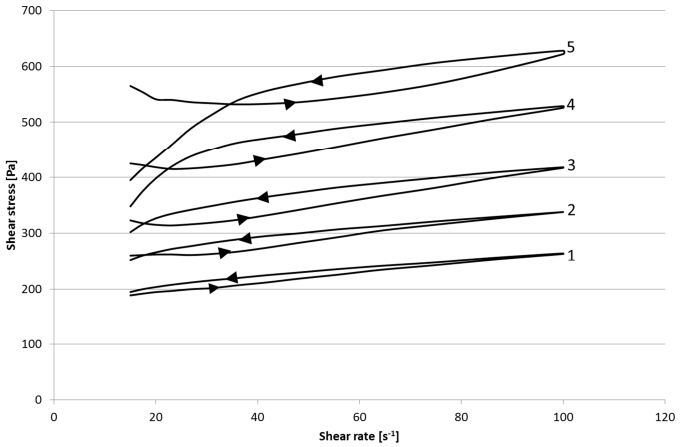

Fig.6.4 Hysteresis loops C1SPSGCN with cycle numbers indicated in Table 6.1

In contrast to C1SP and C1SPSG, the case of C1SPSGCN shows immediate anti-thixotropic behavior and decreasing intersection times. For cycle one, the hysteresis loop did not even close, indicating a high rate of agglomeration that could be related with the first small peak of hydration in Fig.6.1. The following cycles show an increasing hysteresis area and a decreasing intersection time. The sixth cycle is omitted because it showed no longer reliable stress registration due to the accelerated stiffening of the paste. The number of the cycles in Fig.6.4 corresponds to the hydration time for which the cycle started in Table 6.1. The length of one entire hysteresis interval is again about 16 minutes and it is followed by a period of rest towards the next cycle.

Table 6.1 Cycle number with corresponding start time for C1SPSGCN

Cycle number	1	2	3	4	5
Time after water addition [min]	59	86	112	139	166

The quantified characteristics of Fig.6.4 are summarized in Fig.6.5. It is clear how the anti-thixotropic area increases continuously for a decreasing intersection time. In the meantime, the thixotropic area gradually increases due to the steeper deceleration ramp in the hysteresis loops. From this figure, the reagglomeration properties seem similar to the case of C1SPSG in the sense that the agglomeration rate seems to increase over time and for shorter intersection times. Moreover, the agglomeration increases during a generally decreasing hydration rate, which again indicates that the connectivity potential of the surface hydrates is not dominant in agglomeration. This phenomenon will be investigated further for the C1SPSGCN combination.

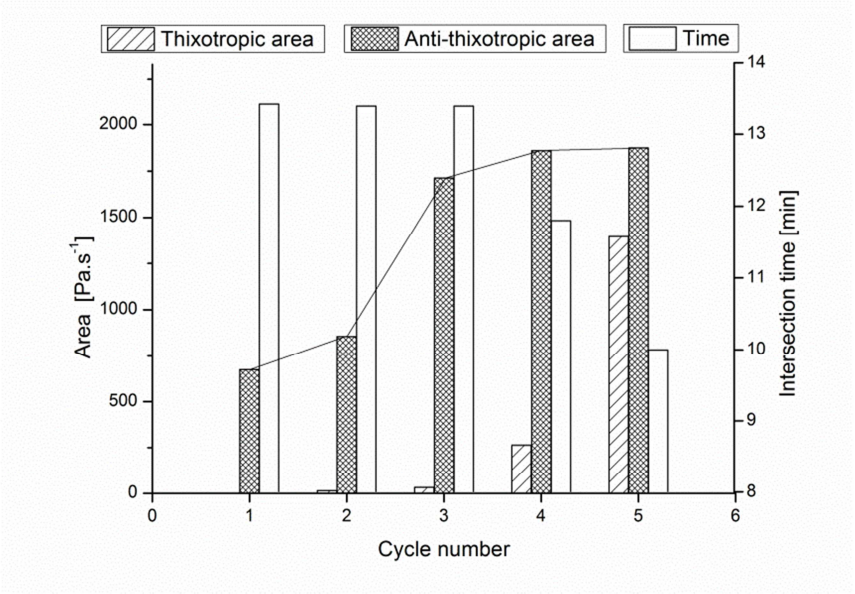

Fig.6.5 Hysteresis properties for C1SPSGCN

6.2 At the origin of the accelerator influence on retarded paste

It is remarkable in Fig.6.3 that G'_{max} of C1SPSGCN is differing strongly from C1SP while G'_{min} is partly overlapping. This means that, for this overlapping region, the agglomerate size (G'_{min}) does not increase in correspondence with the accumulating stress response (high G'_{max}). This means that the stress contributing structure is not incorporated into the agglomerate growth and, therefore, other than particle contact bridges should be investigated. This phase reinforces the strength of the network structure in the paste but it is too weak to overcome the strain sweep in-between the time sweeps.

To identify the origin of this behavior, the G' evolution of C1SPCN was incorporated in Fig.6.3. It can be observed that the evolution of G'_{min} is more or less corresponding to the evolution of G'_{max}: the difference with C1SP is immediately very pronounced for both measures. In order to quantify this correspondence the ratio of G'_{max} over G'_{min} is plotted in Fig.6.6 and is called the *elastic ratio*. It can be seen that the elastic ratio of C1SPSGCN evolves in a similar way but rather isolated from C1SP and C1SPCN, while the latter partly overlap with each other. From this, it is clear that the addition of CN to the plasticized system strengthens the paste structure in a way more similar to the mechanism observed in C1SP.

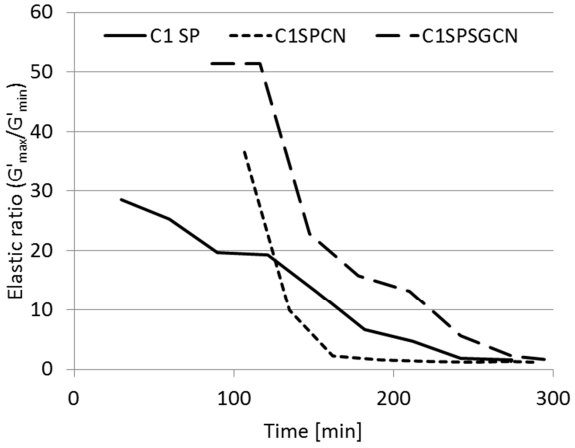

Fig.6.6 Comparison of the elastic ratio for the addition of CN

From the previous chapters, it was found that the agglomeration rate evolves proportionally with the hydrate production for C1SP and that instead, for C1SPSG, the polymer interactions are creating another regime.

From the analogical evolution in elastic ratio of C1SP and C1SPCN, it seems that CN interferes with these original mechanisms. Therefore, the stress contributors in the C1SPSGCN paste should be searched in the physical and chemical state of the interstitial volume.

An example of the interstitial volume contributing to agglomeration is found for the viscosity modifying agent hydroxymethyl ethyl cellulose [114]. The authors attributed the reagglomeration potential to the three-dimensional gel network generated by the admixture and the elastic ratio was found to increase for higher admixture dosage. In the case of CN, the admixture properties are not particularly suited to form a gel-network itself. However, in combination with the interstitial hydrate nuclei and particles from chapter 5, the calcium interaction might initiate similar behavior. Please note that this path differs from chapter 5 in a way that the interstitial volume is now no longer used as a supplier of agglomerative nuclei but rather as a strengthening structure itself. This possibility will be investigated in the following paragraphs.

The family of calcium salt accelerators has been investigated on its efficiency and resulted in a ranking that can be seen below [171]. The sequence distinguished the cations and anions that are most effective in accelerating the hydration of OPC and C_3S.

$$Ca^{2+} > Sr^{2+} > Ba^{2+} > Li^{+} > K^{+} > Na^{+} \approx Cs^{+} > Rb^{+}$$

$$Br^{-} \approx Cl^{-} > SCN^{-} > I^{-} > NO_3^{-} > ClO_4^{-}$$

Only inconclusive correlations could be found between these ionic rankings and the diffusivity of ions, pH of the solution, or the solubility of calcium hydroxide [171]. However, the series shows significant similarities with the Hofmeister (lyotropic) series, which describes the ability of ions to affect the flocculation of hydrophilic colloids [171]. This means that the more accelerating ions are better capable of flocculating the C-S-H on C_3S particle surface. As a consequence, the flocculated C-S-H contains larger pores that create accessible pathways for ion diffusion and consecutive hydration. A schematic representation has been made by Juenger et al. in Fig.6.7 [171].

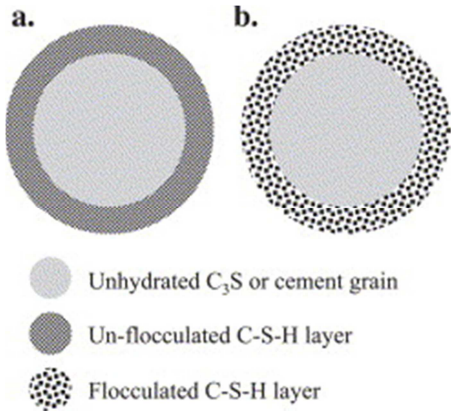

Fig.6.7 Effects of accelerating ions on flocculation of C-S-H,
(a) unflocculated system, (b) flocculated C-S-H [171]

Although the supposed structure has not been observed directly due to experimental limitations, the concept of the flocculated C-S-H is promising. The enhanced diffusion of water into the hydrating particle and calcium and silica ions away from the particle would definitely increase the rate of the hydration. Indirect evidence comes from surface area measurements that confirm a more open or less dense C-S-H formation in presence of $CaCl_2$ [172]. The honeycomb morphology seen by electron microscopy is also indirectly indicating a more open microstructure [171, 173].

The above proposed mechanism mainly relates to the *inner* C-S-H which is said to be formed within the dissolving grain volume. This consideration is appropriate for the cited study using soft X-ray microscopy because the outer C-S-H was not fully identified. However, the concept of ions that flocculate C-S-H may also concern the interstitial phase formation. Actually, the denser inner product is expected to have a lower porosity than the outer product [174]. Moreover, a calcium salt accelerator does not only enhance the C-S-H formation within and on the particle surface [17], in recent research it also seems to encourage the homogeneous nucleation of C-S-H in the interstitial volume [59].

Assuming that the outer C-S-H flocculates and the fact that homogeneous nucleation in the interstitial volume is encouraged by the accelerating admixtures, the network structure of the volume may be represented by Fig.6.8 in the case of CN addition. The network structure may not take place in the entire interstitial volume but only tide areas between agglomerates would comply to provide additional stress resistance.

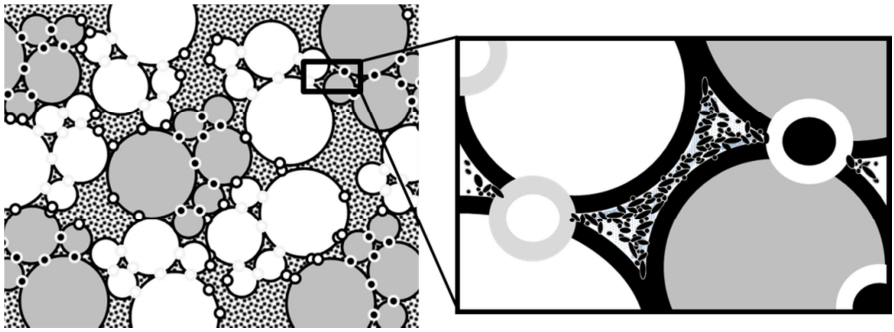

Fig.6.8 Agglomerate network with flocculated C-S-H in the interstitial volume

The question then remains if the flocculated C-S-H network, with wider pores, would be able to support the particles better than any deflocculated C-S-H. After all, this suggested structure should contribute to the stress development in a way that G'_{max} increases faster relative to G'_{min}.

Today, it is hardly possible to visualize or probe the mentioned C-S-H phase in-between the agglomerates because of the nano-scale and the amorphous nature of the phase, not to mention the experimental needs [174]. This makes it hard to find out more about the mechanical performance of this phase. However, intuitively, it seems possible that a porous coagulated network is more rigid than loosely attached C-S-H foils. Considering this possibility, some arguments will follow which support this higher strength assumption of flocculated C-S-H, without drawing premature conclusions:

- At the molecular scale, all C-S-H is constituted by polymerized silicate sheets held together by water and calcium ions [175]. It was found that, for higher water/calcium ratios in C-S-H gels, the structural water molecules weaken the stiffness and the cohesive force by replacing the ionic–covalent calcium bond with unstable H-bond connections [176]. Increasing the number of calcium ions by accelerator addition in pore solution could reduce the H-bond replacement.
- A viscoelastic investigation confirms the importance of interlayer water and argued that the structural water allows the sliding of C-S-H sheets in function of time, causing stress relaxation [177, 178]. Similarly, for more cohesion and friction of solid nano-grains, an improvement of the strength of the C-S-H matrix would be expected [179].

- Furthermore, it was supported with small-angle neutron scattering surface area data, that $CaCl_2$ increases the packing density of the initial C-S-H product [180, 181]. The increased packing density could be interpreted as interpenetration of elementary C-S-H globules defined by Jennings, which is suggested as an element in strength development as it reduces the number of large gel pores [182].

Assuming the flocculated C-S-H forms indeed a more rigid network, the concept of an evolving interstitial contribution to the stress is then schematically visualized in Fig.6.9. Initially, the agglomerate network in a paste at rest behaves like for C1SPSG (Fig.6.9 (a)). The corresponding mechanism will have no time to develop in the C1SPSGCN paste because the CN is added already 12 minutes after the SG. Due to the calcium addition by the CN, the interstitial volume shows some network activity as in Fig.6.8 to increase the G'_{max} evolution (Fig.6.9 (b)). For an increasing number of low strength connections in-between the particles, the paste structure's stress response will increase. Finally, when shear is applied, the interstitial network is disrupted and not solid enough to be incorporated in the agglomerate volume (Fig.6.9(c)).

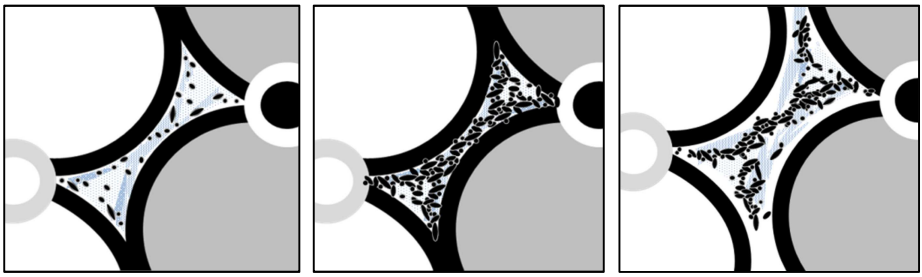

(a) fine nuclei and hydrates in SPSG volume, at rest

(b) interstitial soft network formation due to Ca^{2+}, at rest

(c) partly disrupted soft network, under shear

Fig.6.9 Interstitial network formation and disruption in agglomerated cement paste

Summary

To conclude, considerable evidence is available for the accelerator calcium ion to flocculate the initially formed C-S-H sheets in the interstitial paste volume. Considering a constant volume of C-S-H, this would automatically lead to a more porous network of the C-S-H, as free water is excluded from between the sheets. It is proposed that the elastic response of this porous network is higher due to the more rigid structure of the flocculated C-S-H. In this way, the network would be contributing to the storage modulus

development while, under shear, it does not have to remain intact. It is expected that, at some point during hydration, the disrupted C-S-H network will be sufficiently strong to be also partly incorporated in the agglomerate formation. At that point, the evolution of G'_{min} and G'_{max} would again show qualitative similarities, as seen for accelerated pastes without SG. Moreover, the addressed mechanical activity of the interstitial volume corroborates the assumed chemical activity of the fine nuclei spread out in the C1SPSG paste.

6.3 The influence of the accelerator in the agglomeration model

6.3.1 Agglomeration parameters

All parameters, obtained from the experiments in the first section, are introduced into the agglomeration model (Eq.4.1-4.8). The cumulative heat production of internal hydration products for C1SPSGCN is plotted in Fig.6.10. The development of these hydration products is comparable with C1SP but clearly much faster than C1SPSG (i.e. Fig.4.20 and Fig.5.14). Similarly, for the heat production of external hydrates in Fig.6.11, C1SPSGCN produces about twice as much heat as C1SP and manifolds more heat than for C1SPSG.

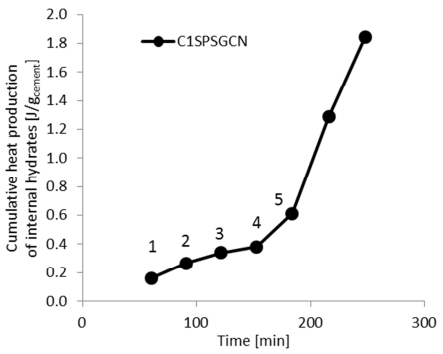

Fig.6.10 Cumulative heat production of internal hydration products for C1SPSGCN

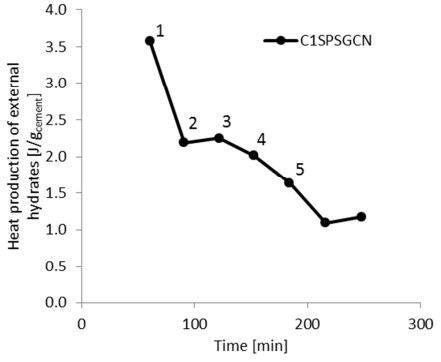

Fig.6.11 Heat production of external hydrates for C1SPSGCN

In Fig.6.12, the sum of the cumulative heat production for internal hydrates ($\sum Q_{int}$) and the absolute heat production of the external hydrates

($Q_{ext,i}$) is shown for C1SPSGCN. The entire evolution is situated above the levels achieved with C1SP and C1SPSG, while the shape of the curve has most resemblance with the C1SP curve (Fig.4.23).

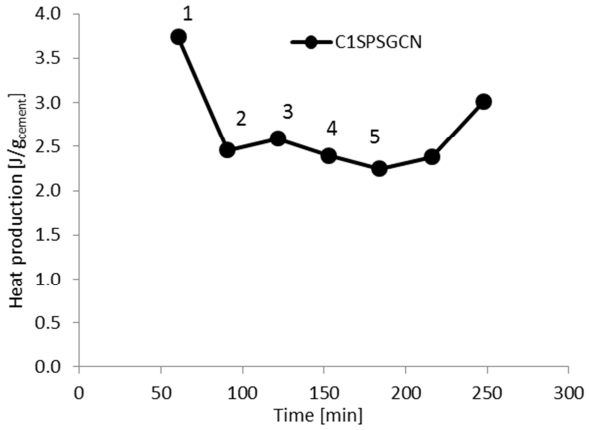

Fig.6.12 Sum of cumulative heat production for internal hydrates ($\sum Q_{int}$) and heat production of external hydrates ($Q_{ext,i}$) for C1SPSGCN

For the comparison between the relative change in anti-thixotropic area (ΔA_i) and hydrate production ($\Delta(\sum Q_{int,i} + Q_{ext,i})$) in Fig.6.13, some qualitative similarity might be observed compared with Fig. 5.17. In contrast, the relative change in reagglomeration rate in Fig.6.14 relates very differently to the hydrate production than in Fig.5.18.

It is observed that the data points in Fig.6.13 and 6.14 appear again in the fourth quadrant as for C1SPSG. This suggests that the agglomeration rate is not controlled by the surface connectivity that is represented by the changes in hydrate production in the x-axis. However, as it was also suggested for C1SPSG, data points that evolve back towards the *x*-axis represent a decreasing effectivity of the polymer layer towards the growing agglomerate size. This phenomenon can be detected in Fig.6.14 where cycle 3,4 and 5 seem to evolve gradually in the direction of the *x*-axis while only a stagnation can be observed in Fig.6.13.

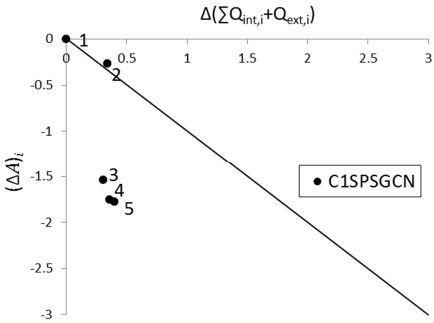

Fig.6.13 Comparison between the relative change in anti-thixotropic area (ΔA_i) and hydrate production ($\Delta(\sum Q_{int,i} + Q_{ext,i})$)

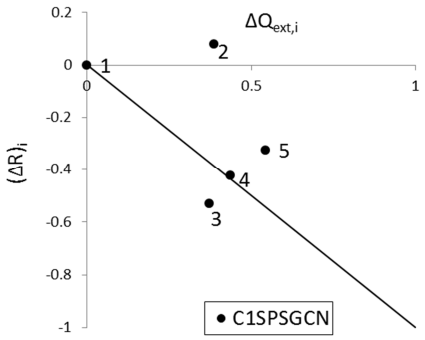

Fig.6.14 Comparison between the relative change in reagglomeration rate and hydrate production

In contrast to the strongly accelerating agglomeration rate in Fig.5.18, the C1SPSGCN paste shows a deceleration in agglomeration rate over hydration time. This results from a similar evolution for the increasing hysteresis area in Fig.5.5 and 6.5 and the generally higher intersection time for C1SPSGCN. The latter is in turn related with the agglomerate strength, thus it is expected that the CN addition creates stronger agglomerates, close to setting, than in the case of retarder and plasticizer only.

6.3.2 Micromechanical mechanism

The micromechanical mechanism behind the decelerating agglomeration rate can be related to the concepts discussed in section 2 of this chapter. More specifically, the high elastic ratio for cycle 1 and 2 is resembled by the low *y*-values of cycle 2 in Fig.6.13 and 6.14. Similarly, the decreasing elastic ratios for cycles 3 to 5 are in accordance with decreasing dominance of the non-elastic agglomerate interactions observed in the change in agglomeration rate in Fig.6.14 for cycle 3 to 5.

The observations on the change in reagglomeration rate in Fig.6.14 decreasing for cycle 3 to 5 could be considered to be indicative for a lowering stress contribution of the interstitial volume. In fact, it is to be expected that the structuring interstitial volume is gradually consumed in the agglomerate growth according to its floc strength. As a consequence, the aggregation rate or incorporated amount of interstitial C-S-H will be higher in the presence of calcium. In this respect, the sudden intrusion of calcium ions into the plasticized layer on fine nuclei seems to be

immediately high in cycle 3 and lower in cycle 5. This hydrate consumption pattern is the reverse from the one for the fine nuclei in cycle 9-11 of the C1SPSG paste. This finding indicates that, for C1SPSGCN, the vertical position of cycle 3 in Fig.6.14 would be further from the *x*-axis if less calcium was present. Furthermore, the evolution of cycle 3 to 5 would look more like cycle 9 to 11 in Fig.5.18. The contrasting decrease of cycles 3 to 5 in Fig.6.14 is only as steep as the amount of calcium ions that is available to accelerate the interstitial C-S-H aggregation and incorporation.

6.3.3 Summarized agglomeration diagram

To summarize the developed agglomeration model, the data points of all admixture combinations are given in the diagrams in Fig.6.15 and 6.16. At the left, the change in amount of agglomeration (ΔA_i) is plotted for comparison with the change in agglomeration rate (ΔR_i) at the right. The data points are accompanied with the abbreviation of the last added admixture in the paste name (e.g. C1SPSG).

Fig.6.15 shows the relation between the change in agglomerate stability in the *x*-axis and the change in amount of agglomeration in the *y*-axis. The agglomerate stability is related with the G'_{min} evolution or the curvature of the acceleration ramp but, as might be expected, this stability is hard to correlate with the enclosed hysteresis area, incorporated in *y*-axis. Therefore, this figure might only prove useful when it is considered in addition to Fig.6.16.

The agglomeration diagram in Fig.6.16 shows the relation between the change in agglomerate connectivity potential in the *x*-axis and the change in agglomeration rate in the *y*-axis. Only for SP, the change in hydrate activity of the agglomerate surface showed proportional influence on the agglomeration rate. This becomes relevant when one compares the functionality of experimental superplasticizers for example. Suppose an unknown superplasticizer causes the data points to move away from the *x*-axis for the same changes in external hydrate activity as the reference. This would mean that the product causes greater reductions in the reagglomeration rate by weakening the inter-particle bonds. Then, one could already assume that the unknown polymer exerts a slightly better repulsion than the reference but that it does not change the hydration rate. If the polymer functionality would be known, then the diagram could also allow quantifying the sensitivity of arbitrary cements towards the polymer weakening.

So, for the SP cases, a quantitative judgment of the admixture performance can be made because the reagglomeration rate can be related with the

external hydrates. Fig.6.16 shows that a different situation is obtained for the extra addition of hydration controlling admixtures. For both the retarder and the accelerator, the diagram shows an increase in the reagglomeration rate in the fourth quadrant. For SG, the increments in reagglomeration rate increase over time, while for CN a decrease occurs. This observation leads to a discussion on the fundamental mechanisms behind these results. The micromechanical mechanism is explained by the activity of the interstitial volume, containing fine particles and nuclei. In the case of the retarder, these particles are steadily exposed to water and gradually consumed in the agglomerates. In case of the accelerator, the fine particles are hydrating more suddenly when calcium is added, which empowers the particle incorporation from the start and makes it slow down over time.

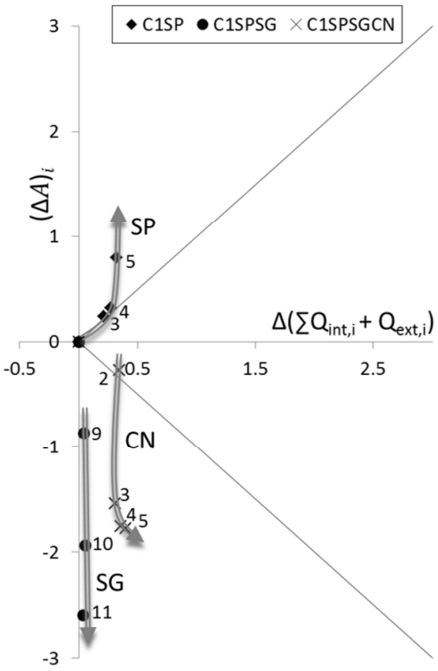

Fig.6.15 Influence of different admixture combinations on the amount of agglomeration

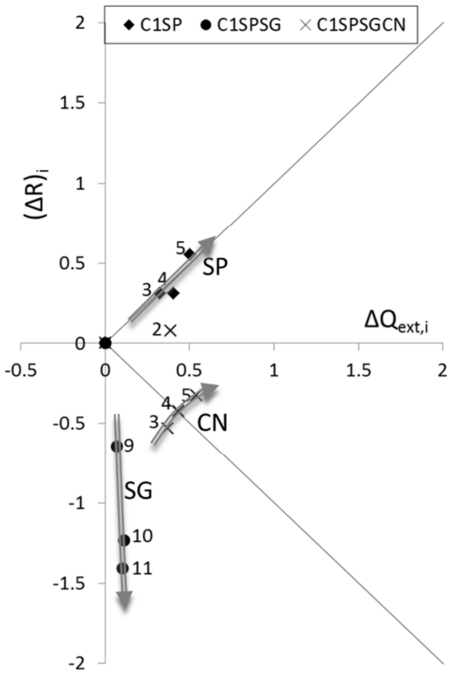

Fig.6.16 Influence of different admixture combinations on the reagglomeration rate

For the C1SPSGCN paste, it is now possible to assess the functionality of another accelerator dosage or type. Considering the hysteresis loops, for example, upon addition of extra calcium ions, the increase in anti-thixotropic area over the different hysteresis cycles will occur sooner but

the increment in-between the consecutive cycles is expected to diminish. For unchanged intersection times, this would result in a lower increment of the reagglomeration rate in Fig.6.16 and, therefore, the CN curve would shift towards the *x*-axis. In a similar way, the slope of the new CN curve is expected to decrease compared to the one pictured in Fig.6.16.

When the dosage of retarder would increase for the current C1SPSGCN paste, the CN curve in Fig.6.16 would move away from the *x*-axis because the CN dosage would be less effective in flocculating the fine hydrates. This causes a low initial increment in reagglomeration in the first hysteresis cycle and a high relative difference with the following cycles. In this way, ΔR_i increases. The retarder would also induce a higher delay in hydration kinetics which would cause the hydration rate to decrease and to show lower decrements. This way, the CN curve would move away from the *x*-axis and towards the *y*-axis.

The above examples demonstrate the possibilities of the agglomeration diagram. However, the utility of the diagram should be extended by experimental verification of the mentioned examples. This will reinforce or mitigate the use of some of the fundamental concepts that have been applied in this work. A coherent relation between all these concepts would improve our knowledge on the fundamental mechanisms and would greatly contribute to a bottom-up understanding of cement paste rheology for combined admixtures.

Chapter summary

In this chapter, the accelerator compensated the delay in hydration kinetics and structure development, induced by the retarder. The elastic ratio was used to identify a change in the micromechanical mechanism compared to the C1SPSG paste. The stress contribution was attributed to the interstitial volume of the C1SPSGCN paste where the calcium ions interacted with the fine particles, described in chapter 5. Based on the Hofmeister analogy, this interstitial structure was identified as flocculated C-S-H nano-particles in solution, creating a porous network. Several arguments were collected that indicate a higher rigidity of this porous coagulated network compared to C-S-H sheets with a lower calcium content. It was suggested that the interstitial structure reinforced the hydrate bridges during rest by forming a high number of low strength connections that break upon shearing. Towards the final cycles, this network structure is supposed to be compact and rigid enough to be incorporated in the agglomerate growth. In a way, the existence of the

interstitial network evolution could explain the transition in particle interaction from retarded to merely plasticized cement pastes.

With the incorporation of the model parameters for the accelerated paste, the agglomeration model confirmed that the calcium ions somehow reduce the dominance of the plasticized fine particles in the agglomeration kinetics. The model also indicates that this occurs at a different rate than for SG by having the data-points evolve towards the *x*-axis. It is argued that the C-S-H flocculation is addressed immediately by the calcium addition resulting in a fast consumption of the interstitial fine particles. This is the reverse of the case for SP and retarder only. Furthermore, the interstitial volume does no longer only provide hydrating fine particles but it also forms an irregular soft structure itself for which the growing mechanical impact is in correspondence with the observed agglomeration rate. The stronger fine structure is expected to be easily incorporated in the growing agglomerates during the last hysteresis cycles.

Chapter 7 - Conclusions

The scope of this thesis is to perform fundamental research on the physico-chemical interactions between cement and concrete admixtures. The aim is to assess the micromechanical impact of combined admixtures on cement paste rheology.

The bibliographical research has demonstrated the difficulties and complexity of cement paste rheology. It has been reported how the cement/admixture compatibility shows significant variations for different cement properties and what the impact of the admixture type is. The cement particle agglomeration was put at the center of discussion in this thesis for two reasons. First, to identify potential rheological mechanisms to elaborate our conceptual understanding, and second, to channel the rheological influence of combined admixtures towards these mechanisms.

7.1 Identified mechanisms

The physical and chemical aspect of admixture interaction was caught by performance of three kinds of experiments on cement paste. By studying the hydration kinetics, the structure development and the flow behavior, the macroscopic impact of the admixture additions was quantified.

Concerning the superplasticizer impact on cement paste, it was observed that the hydration reactions were delayed and different rheological behavior was initiated for the same cements of different batches. For the cement with a higher share of cubic aluminate phase, the SP was found to change the morphology of ettringite, which interfered with the dissolution behavior of the sulfate carrying phases and with the dissolution rate of C_3A. The thermodynamic modelling indicated the presence of temporarily

monosulfate due to the higher availability of aluminate ions. This morphology of the hydrates is an essential element in the mechanical interaction between particles and is, therefore, related with the observed differences in rheology.

For the combination of SP and retarder, the latter clearly induced a delay in hydration kinetics and structure development. From the shear rheology, it was observed that the micromechanical mechanism became partly dominated by the polymer on the particle surface. The impact of the retarder was attributed to (1) the change in volume fraction due to the postponed water consumption, (2) a slightly higher electrostatic repulsion, mainly due to positive charge neutralization on the cement grain surface, (3) increased steric repulsion caused by a reinforcement of the polymer layer on the particle surface and (4) a morphological change of ettringite and related phases. All these factors contribute to the observed lower viscosity upon retarder addition. It was also concluded that SG simulated the SP interference in the hydrate formation and that small hydrates remain longer in the suspending liquid, before co-agglomerating, where they can lubricate the particle contact during shear. In this way, further SG addition will cause a decrease in paste viscosity and a higher delay in shear propagation.

In the final stage, the SP was combined with a retarder and an accelerator. This accelerator compensated the delay in the hydration kinetics and structure development induced by the retarder. The storage modulus evolution identified a change in the micromechanical mechanism responsible for the agglomerate growth. It was concluded that the interstitial volume showed an increased structure forming activity compared with the SP retarder combination. Based on literature, this interstitial structure was identified as flocculated C-S-H nano-particles in solution, creating a porous network. The presence of the accelerator led to an extra interstitial structure which indirectly diminished the effect of the polymer layer. In this way, the interstitial network evolution explains the transition in particle interaction from retarded to merely plasticized cement pastes.

7.2 Conceptual modelling

The precarious balance between the hydrate morphology and the admixture adsorption showed to be arduous to model. The chemical interactions on this nano-scale influence the physical properties of the

grain surface and thus also the inter-particle mechanics. The challenge of working on this small scale was circumvented by addressing the global chemical activity of the grain surface through a series of model parameters based on the observed hydration kinetics, structure development and flow behavior. Through the definition of internal and external hydrates, a concept was founded to describe the connection mechanism of flowing agglomerates in function of the C-S-H production.

In the case of superplasticizer addition only, a consistent proportional relation was found between changes in the chemical activity on the agglomerate surface and the changes in reagglomeration rate of those agglomerates under shear. It was observed that, from a certain threshold agglomerate size, the shear stress of all tested cements increased towards a level for which the structural build-up mechanism is dominant over the structural break-down. This was called the start of anti-thixotropic series as soon as the intersection time monotonously decreased. During that anti-thixotropic period, the decrement in reagglomeration changed proportionally with the changing amount of internal and external hydrates. Generally, the cumulative amount of C-S-H within the agglomerates influenced the agglomerate stability or size and the amount of external C-S-H determined the reagglomeration rate. If the observed proportionality can be obtained for other cements, one might consider the possibility to predict the further heat evolution of these cements solely from the rheological behavior.

On the one hand, the added dosage of SP was required to obtain smooth stress registration, on the other hand, its impact on the interparticle connectivity is small enough to let hydrate formation dominate the connectivity potential. This demonstrates that, for one particular cement/SP combination, a rheometrical procedure can be found that relates the rheological behavior with the underlying micromechanical mechanism.

For the combination of superplasticizer and retarder, the micromechanical mechanism shows major differences with the one for superplasticizer only. A reverse relation was found between the hydrate formation rate and the agglomeration rate. This implies that the polymer layer on the cement particles is more active in the agglomeration kinetics than for SP alone. The observation of higher increments in agglomeration rate over time led to the conclusion that a small fraction of hydrates was temporally excluded from agglomerate incorporation. To that end, this fraction is expected to remain in the interstitial volume between agglomerates, which is

supported by the refinement of the particle size distribution upon retarder addition, as reported in literature. This fraction is gradually activated due to the increasing consumption of the dense polymer layer during hydration. The remaining admixtures in solution keep the fine particles separated as long as possible and conserve the gradual uptake of the slowly hydrating particles. In this way, the postponed activity of this fraction can cause an increasing increment of agglomerate connectivity over time.

For the extra addition of the accelerator, the agglomeration model shows to what extent the calcium ions in the interstitial solution reduce the polymer layer dominance in the agglomeration kinetics. It is argued that the C-S-H flocculation is addressed immediately by the calcium and that this results in another kind of interstitial volume than in the case of SP and retarder only. This volume does no longer solely provide slowly hydrating fine particles but it forms an irregular soft structure itself, that reinforces the stress buildup but breaks upon shearing. Its effect on the agglomeration rate seems to decrease over time while the corresponding effect of the retarder increased due to the postponed hydration.

7.3 Original contributions

In this thesis, the rheological consequences of the use of three combined admixtures in cement paste have been investigated thoroughly. The existing knowledge on combined admixtures has focused mostly on only two kinds of admixtures and never on three of them. Moreover, no studies were found to describe the influence of three combined admixtures on cement paste rheology. In this work, a new rheological perspective has been explored to contribute to the existing but limited knowledge on cement particle agglomeration in rheological models.

Insights have been gained on the superplasticizer interaction with the cement hydrates through thermodynamic modelling and mineralogy. These techniques have been used before, for long hydration times [135, 138], but now they have been applied to identify the different rheological performance of two similar cements at very young age. This led to the conclusion that the superplasticizer can change the hydrate morphology to such an extent that the interparticle contact forces are modified.

Furthermore, the adsorption mechanism and repulsive functionality of sodium gluconate have been clarified by physico-chemical analysis. The

particular working mechanism in combination with a superplasticizer has only been remotely described in literature without identification of the electrostatic or steric nature of the repulsive functionality. Here, it was found that the sodium gluconate densified the polymer layer at the cement grain surface which contributes to the steric stabilization of the cement paste. An additional electrostatic effect and the induced changes in particle morphology are also demonstrated.

In current research, the agglomeration mechanism is still hard to incorporate in rheological models [8]. Therefore, an attempt was made to extend the understanding of the agglomeration mechanism and to describe the effects with measurable parameters in an agglomeration model. The original contribution of the agglomeration model comes from the relation between the agglomeration rate and the indirectly measured agglomerate connectivity. By defining the internal and external hydrates in a cement particle agglomerate, a new research perspective is created in order to incorporate the agglomeration mechanism into future micromechanical models.

The difficulties in building a sound agglomeration model are partly related with the lacking experimental techniques to study the particular phenomenon. To that end, an original mechanism is proposed in this work to explain the observed agglomeration behavior upon combined admixture addition. The little evidence from literature about the dispersion of fine particles due to plasticizer interference is applied to assume an agglomerative contribution from the interstitial volume. On the one hand, the retarder creates a source of slowly hydrating nuclei and particles in that volume while, on the other hand, these particles are expected to coagulate due to accelerator addition. In the latter case, the interstitial volume can also deliver a contribution to the stress resistance of the cement paste.

7.4 Outlook

During this work, some boundaries to the current understanding of cement paste rheology have been met and ask for further research on the topic. These topics are summarized as follows:

Further research still needs to be done concerning the change in particle size distribution upon admixture addition. The challenge to visualize the

fine particle fraction within the high volume fraction of cement paste is enormous, especially because altering the suspending solution may also affect the targeted size fractions. Similarly, research on the agglomeration state would benefit if the appropriate technique is developed to investigate the particle level without disturbing its environment. A promising research possibility is the focused beam reflectance measurement [112].

Subsequent to the above challenge, the impact of admixtures on the flocculation state could lead to conclusive proof of the theories proposed in this work. Visually demonstrating the difference in morphology of the interstitial structure for the retarder and for the accelerator with retarder, would reinforce some hypotheses made in this research. Moreover, the applicability of these new techniques in other fields of suspension rheology would be very helpful.

In attendance of the above technique it is still a viable research path to examine the performance of the interstitial network itself by mechanical probing. With techniques like atomic force microscopy some major improvements might be made in the structural properties of the interstitial network. Using synthesized C-S-H, could allow changing the chemical environment of the structure and relate it with the impact of calcium ions for example.

Considering the agglomeration diagram as a tool for technological research would require the validation of this diagram for other cements. In this respect, further exploration would be needed in order to establish a particular mix procedure for which the different cements can be compared. For now, the mix procedure chosen was fruitful for one cement to perform as described within the agglomeration diagram. If the mix procedure would change, the rheological performance would no longer be the same but it might allow another cement of the same type to start performing similar to the first cement. So the relativity of this technique requires the sound determination of a good reference that can be used to qualify admixture combinations for different cements.

The relations that have been obtained in the agglomeration diagram should be supported and verified by experimental evidence. For example, the three tests that have been applied should be repeated for several dosages of accelerator to testify that the data points would indeed move in the theoretically predicted direction. Similarly, for a fixed dosage of accelerator, the dosage of retarder or superplasticizer should be varied. In this way, the ability of the diagram to provide a useful comparative tool in

scientific research would be confirmed and quantitative estimates could be rightfully deduced.

Appendix A

Ion concentrations [ppm] for all four cement pastes in function of hydration time

C1REF	4	22	50	120	150	220	260
Ca^{2+}	895.87	361.50	281.07	344.23	278.28	256.92	319.67
Al^{3+}	0.47	0.43	0.56	0.38	0.37	0.32	0.30
Si^{4+}	4.47	4.12	4.01	3.20	3.60	2.66	3.14
Fe^{3+}	0.48	0.19	0.17	0.07	0.06	0.08	0.04
K^{+}	5873.70	7560.70	7189.60	8251.90	8070.20	7425.60	8129.90
Mg^{2+}	0.17	0.06	0.06	0.06	0.02	0.04	0.01
Na^{+}	1944.60	2596.90	2550.60	2955.00	2911.70	2699.20	2970.90
S^{6+}	3809.60	3865.40	3505.40	3864.00	3766.10	3515.20	3851.50

C2REF	4	21	50	120	150	220	250
Ca^{2+}	928.34	475.58	475.38	405.73	430.25	405.54	421.45
Al^{3+}	0.36	0.44	0.55	0.53	0.65	0.41	0.46
Si^{4+}	2.15	3.69	2.98	3.86	2.94	2.06	2.54
Fe^{3+}	0.97	0.49	0.23	0.12	0.14	0.11	0.13
K^{+}	5680.50	9116.10	10118.60	9818.80	9563.20	9429.30	9739.70
Mg^{2+}	0.13	0.05	0.02	0.01	0.03	0.02	0.04
Na^{+}	2421.80	3330.00	3751.70	3629.70	3543.00	3548.60	3672.60
S^{6+}	3896.20	4753.20	4954.40	4485.70	4367.90	4385.70	4592.70

C1SP	4	22	50	120	150	250	310
Ca^{2+}	895.87	397.20	393.24	407.28	421.16	369.96	384.72
Al^{3+}	0.47	0.26	0.39	0.28	0.44	0.26	0.30
Si^{4+}	4.47	2.07	2.23	2.14	2.51	2.05	1.97
Fe^{3+}	0.48	0.14	0.14	0.05	0.16	0.06	0.06
K^{+}	5873.70	9321.60	8944.20	9008.20	9056.70	9093.90	9001.40
Mg^{2+}	0.17	0.01	0.03	0.01	0.05	0.03	0.01
Na^{+}	1944.60	3267.90	3177.30	3264.30	3274.10	3312.30	3297.30
S^{6+}	3809.60	4668.50	4261.90	4152.20	4190.00	4220.90	4207.80

C2SP	4	22	50	120	145	250	295
Ca^{2+}	928.34	534.29	459.23	537.36	489.63	490.93	418.06
Al^{3+}	0.36	0.51	0.62	0.44	0.49	0.43	0.51
Si^{4+}	2.15	4.42	3.00	1.31	1.84	1.83	2.28
Fe^{3+}	0.97	0.61	0.27	0.09	0.12	0.09	0.14
K^{+}	5680.50	9889.60	9894.40	10063.60	10250.40	10107.80	10052.40
Mg^{2+}	0.13	0.05	0.04	0.01	0.03	0.02	0.04
Na^{+}	2421.80	3561.40	3688.40	3940.40	3851.40	4031.30	3869.10
S^{6+}	3896.20	5091.90	4712.20	4740.80	4666.70	4890.40	4702.40

Appendix B

Saturation indexes for portlandite, jennite and tobermorite

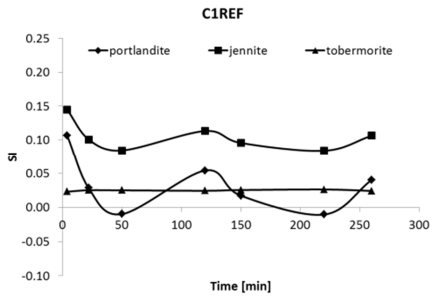

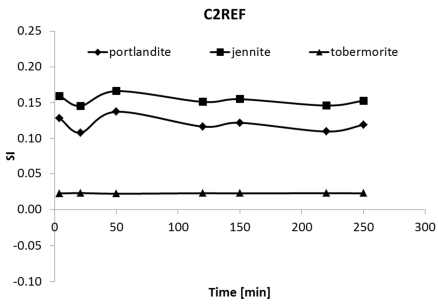

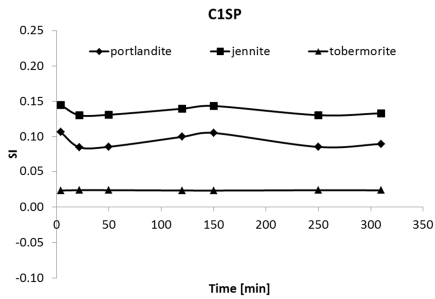

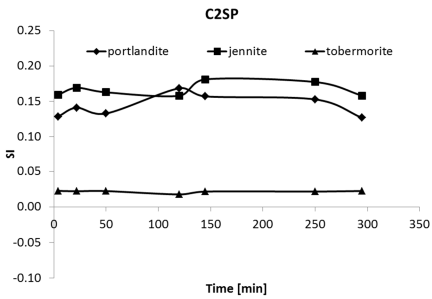

References

1. Flatt, R.J., N. Roussel, and C.R. Cheeseman, *Concrete: An eco material that needs to be improved.* Journal of the European Ceramic Society, 2012. **32**(11): p. 2787-2798.
2. Flatt, R.J., N. Martys, and L. Bergström, *The Rheology of Cementitious Materials.* MRS Bulletin, 2004. **29**(05): p. 314-318.
3. Kenai, S. and R. Bahar, *Evaluation and repair of Algiers new airport building.* Cement and Concrete Composites, 2003. **25**(6): p. 633-641.
4. Jennings, H.M. and J.W. Bullard, *From electrons to infrastructure: Engineering concrete from the bottom up.* Cement and Concrete Research, 2011. **41**(7): p. 727-735.
5. Roussel, N., et al., *Steady state flow of cement suspensions: A micromechanical state of the art.* Cement and Concrete Research, 2010. **40**(1): p. 77-84.
6. Kitaoji, H., et al., *Flow simulation of fresh concrete cast into wall structure by viscoplastic divided space element method.* Transactions of the Japan Concrete Institute, 1996. **16**: p. 45-52.
7. Roussel, N., et al., *Computational modeling of concrete flow: General overview.* Cement and Concrete Research, 2007. **37**(9): p. 1298-1307.
8. Flatt, R.J., *Towards a prediction of superplasticized concrete rheology.* Materials and Structures, 2004. **37**: p. 289-300.
9. Wallevik, O.H. and J.E. Wallevik, *Rheology as a tool in concrete science: The use of rheographs and workability boxes.* Cement and Concrete Research, 2011. **41**(12): p. 1279-1288.

10. Wallevik, Ó., *Description of Fresh Concrete by Using the Two-point Workability Apparatus (NTH/BML report 83.414)*, 1983, NTNU Trondheim: Norway.
11. Taylor, H.F.W., *Cement chemistry 2nd edition*. 1997: Thomas Telford Publishing.
12. Hewlett, P.C.E., *LEA'S Chemistry of Cement and Concrete*. 4th ed, ed. P.C. Hewlett. 1998: Arnold London.
13. Bullard, J.W., et al., *Mechanisms of cement hydration.* Cement and Concrete Research, 2011. **41**(12): p. 1208-1223.
14. Juiland, P., et al., *Dissolution theory applied to the induction period in alite hydration.* Cement and Concrete Research, 2010. **40**: p. 831-844.
15. Barret, P. and D. Ménétrier, *Filter dissolution of C3S as a function of the lime concentration in a limited amount of lime water.* Cement and Concrete Research, 1980. **10**(4): p. 521-534.
16. Barret, P., D. Ménétrier, and D. Bertrandie, *Mechanism of C3S dissolution and problem of the congruency in the very initial period and later on.* Cement and Concrete Research, 1983. **13**(5): p. 728-738.
17. Garrault, S. and A. Nonat, *Hydrated Layer Formation on Tricalcium and Dicalcium Silicate Surfaces: Experimental Study and Numerical Simulations.* Langmuir, 2001. **17**(26): p. 8131-8138.
18. Gauffinet, S., et al., *Observation directe de la croissance d'hydrosilicate de calcium sur des surfaces d'alité et de silice par microscopie à force atomique.* Comptes Rendus de l'Académie des Sciences - Series IIA - Earth and Planetary Science, 1998. **327**(4): p. 231-236.
19. Jennings, H.M., *A model for the microstructure of calcium silicate hydrate in cement paste.* Cement and Concrete Research, 2000. **30**(1): p. 101-116.
20. Minard, H., et al., *Mechanisms and parameters controlling the tricalcium aluminate reactivity in the presence of gypsum.* Cement and Concrete Research, 2007. **37**(10): p. 1418-1426.
21. Scrivener, K.L., *The development of microstructure during the hydration of Portland cement*, in *Imperical College of Science, Technology, and Medicine*1984, University of London.
22. Gallucci, E., P. Mathur, and K. Scrivener, *Microstructural development of early age hydration shells around cement grains.* Cement and Concrete Research, 2010. **40**(1): p. 4-13.
23. Taylor, H.F.W., *Cement Chemistry*. 1990: Academic Press limited, London.

24. Stark, J., B. Möser, and F. Bellman, *Hydration von Portlandzement*, in *Lehrbrief des F.A. Finger-Institutes für Baustoffkunde* 2004, Bauhaus-Universität Weimar.
25. Kubens, S., *Interaction of cement and admixtures and its effect on rheological properties*, in *F.A. Finger Institut für Baustoffkunde*2010, Bauhaus-Universität Weimar: Cuvillier Verlag, Göttingen 2010.
26. Stark, J. and B. Wicht, *Zement und Kalk: Der Baustof als Werkstoff*. 2000, Finger-Institut für Baustoffkunde der Bauhaus-Universität Weimar: Birkhauser.
27. Spiratos, N., et al., *Superplasticizers for Concrete: Fundamentals, Technology and Practice*. 2006, Quebec: Marquis.
28. Jiang, S., B.-G. Kim, and P.-C. Aïtcin, *Importance of adequate soluble alkali content to ensure cement/superplasticizer compatibility.* Cement and Concrete Research, 1999. **29**(1): p. 71-78.
29. Vladu, C.M., C. Hall, and G.C. Maitland, *Flow properties of freshly prepared ettringite suspensions in water at 25 °C.* Journal of Colloid and Interface Science, 2006. **294**(2): p. 466-472.
30. Sarkar, S.L. and X. Aimin, *Preliminary study of very early hydration of superplasticized C3A+gypsum by environmental SEM.* Cement and Concrete Research, 1992. **22**(4): p. 605-608.
31. Gartner, E.M., J.F. Young, and I.J. Damidot, *Hydration of portland cement*. 2nd ed. Structure and Performance of Cements, ed. J. Bensted and P. Barnes. 2002, New York.
32. Matović, V., et al., *The origin of syngenite in black crusts on the limestone monument King's Gate (Belgrade Fortress, Serbia) – the role of agriculture fertiliser.* Journal of Cultural Heritage, 2012. **13**(2): p. 175-186.
33. Aïtcin, P.-C., et al., *Retardation effect of superplasticizer on different cement fractions.* Cement and Concrete Research, 1987. **17**(6): p. 995-999.
34. Jansen, D., et al., *Change in reaction kinetics of a Portland cement caused by a superplasticizer — Calculation of heat flow curves from XRD data.* Cement and Concrete Research, 2012. **42**(2): p. 327-332.
35. Chen, W.F., *Handbook of Structural Engineering*. 2010: Taylor & Francis.
36. Plank, J., et al., *Synthesis and performance of methacrylic ester based polycarboxylate superplasticizers possessing hydroxy terminated poly(ethylene glycol) side chains.* Cement and Concrete Research, 2008. **38**(10): p. 1210-1216.

37. Winnefeld, F., et al., *Effects of the molecular architecture of comb-shaped superplasticizers on their performance in cementitious systems.* Cement and Concrete Composites, 2007. **29**(4): p. 251-262.
38. Plank, J. and C. Winter, *Competitive adsorption between superplasticizer and retarder molecules on mineral binder surface.* Cement and Concrete Research, 2008. **38**(5): p. 599-605.
39. Ferrari, L., et al., *Multi-method approach to study influence of superplasticizers on cement suspensions.* Cement and Concrete Research. **41**(10): p. 1058-1066.
40. Houst, Y.F., et al., *Design and function of novel superplasticizers for more durable high performance concrete (superplast project).* Cement and Concrete Research, 2008. **38**(10): p. 1197-1209.
41. Zingg, A., et al., *Interaction of polycarboxylate-based superplasticizers with cements containing different C3A amounts.* Cement and Concrete Composites, 2009. **31**(3): p. 153-162.
42. Schröfl, C., M. Gruber, and J. Plank, *Preferential adsorption of polycarboxylate superplasticizers on cement and silica fume in ultra-high performance concrete (UHPC).* Cement and Concrete Research, 2012. **42**(11): p. 1401-1408.
43. Kjeldsen, A.M., R.J. Flatt, and L. BergstrÃ¶m, *Relating the molecular structure of comb-type superplasticizers to the compression rheology of MgO suspensions.* Cement and Concrete Research, 2006. **36**(7): p. 1231-1239.
44. Janowska-Renkas, E., *The effect of superplasticizers' chemical structure on their efficiency in cement pastes.* Construction and Building Materials, 2013. **38**(0): p. 1204-1210.
45. Ferrari, L., et al., *Multi-method approach to study influence of superplasticizers on cement suspensions.* Cement and Concrete Research, 2011. **41**(10): p. 1058-1066.
46. Zingg, A., et al., *The microstructure of dispersed and non-dispersed fresh cement pastes -- New insight by cryo-microscopy.* Cement and Concrete Research, 2008. **38**(4): p. 522-529.
47. Nocuń-Wczelik, W. and P. Czapik, *Use of calorimetry and other methods in the studies of water reducers and set retarders interaction with hydrating cement paste.* Construction and Building Materials, 2013. **38**(0): p. 980-986.
48. Chiang, W.-S., et al., *Microstructural changes of globules in calcium–silicate–hydrate gels with and without additives determined by small-angle neutron and X-ray scattering.* Journal of Colloid and Interface Science, 2013. **398**(0): p. 67-73.

49. Edmeades, R.M. and P.C. Hewlett, *Cement Admixtures*, in *Lea's Chemistry of Cement and Concrete (Fourth Edition)*. 2003, Butterworth-Heinemann: Oxford. p. 841-905.
50. Cheung, J., et al., *Impact of admixtures on the hydration kinetics of Portland cement.* Cement and Concrete Research, 2011. **41**(12): p. 1289-1309.
51. Casu, B., et al. *Interaction of aluminates with carbohydrates and aldonates*. in *Proceedings of the 7th International Congress on the Chemistry of Cement*. 1980. Paris.
52. Tenoutasse, N. and N.B. Singh, *Effect of glucose and calcium gluconate on the hydration of Portland cement.* Indian J. Technol., 1978. **16** (5): p. 184-189.
53. Recalde Lummer, N. and J. Plank, *Combination of lignosulfonate and AMPS®-co-NNDMA water retention agent—An example for dual synergistic interaction between admixtures in cement.* Cement and Concrete Research, 2012. **42**(5): p. 728-735.
54. Li, G., et al., *Effects of two retarders on the fluidity of pastes plasticized with aminosulfonic acid-based superplasticizers.* Construction and Building Materials, 2012. **26**(1): p. 72-78.
55. Perez, J.-P., *The mechanism of action of sodium gluconate on the fluidity and set of Portland cement*, in *12th International Congress of the Chemistry of Cement*2007: Montreal.
56. Hanehara, S. and K. Yamada, *Rheology and early age properties of cement systems.* Cement and Concrete Research, 2008. **38**(2): p. 175-195.
57. Justnes, H. and E.C. Nygaard. *The mechanism of calcium nitrate as set accelerator for cement*. in *10th International Congress on the Chemistry of Cement*. 1997. Gothenburg.
58. Justnes, H. and B.G. Petersen. *Counteracting Plasticizer Retardation of Cement Setting with Calcium Nitrate*. in *International Conference on Innovations and Developments in Concrete Materials and Construction*. 2002. Dundee, Scotland.
59. Nicoleau, L., *Accelerated growth of calcium silicate hydrates: Experiments and simulations.* Cement and Concrete Research, 2011. **41**(12): p. 1339-1348.
60. Hu, C. and F. de Larrard, *The rheology of fresh high-performance concrete.* Cement and Concrete Research, 1996. **26**(2): p. 283-294.
61. Roshavelov, T., *Prediction of fresh concrete flow behavior based on analytical model for mixture proportioning.* Cement and Concrete Research, 2005. **35**(5): p. 831-835.

62. Chidiac, S.E. and F. Mahmoodzadeh, *Plastic viscosity of fresh concrete - A critical review of predictions methods.* Cement and Concrete Composites, 2009. **31**(8): p. 535-544.
63. Ferraris, C.F. and F.d. Larrard, *Testing and modelling of fresh concrete rheology*, 1998, National Institute of Standards and Technology: Gaithersburg, MD 20899.
64. Roussel, N., et al., *The origins of thixotropy of fresh cement pastes.* Cement and Concrete Research, 2012. **42**(1): p. 148-157.
65. Flatt, R.J., *Interparticle forces and superplasticizers in cement suspensions*, in *Département de matériaux*1999, École polytechnique fédérale de Lausanne: Lausanne.
66. Nachbaur, L., et al., *Dynamic mode rheology of cement and tricalcium silicate pastes from mixing to setting.* Cement and Concrete Research, 2001. **31**(2): p. 183-192.
67. Van Damme, H., *Colloidal chemo-mechanics of cement hydrates and smectite clays: cohesion vs. swelling*, in *Encyclopedia of surface and Colloidal Science*. 2002, Marcel Dekker Inc: New York. p. 1087-1103.
68. Prieve, D.C. and M.A. Bevan, *Effect of physisorbed polymers on the interaction on latex particles and their dispersion stability*, in *Polymers in Particulate Systems: Properties and Applications*, V.A. Hackley, P. Somasundaran, and J.A. Lewis, Editors. 2001, Marcel Dekker: New York. p. 1-26.
69. Mueller, A., U. Stark, and S. Erfurt. *The Early Stage of Cement Hydration: Measurement of the Particle Size Distribution at Different Times*. in *12 th ICCC*. 2007. Montreal, Canada.
70. Lilkov, V., E. Dimitrova, and S. Gaidardzhiev, *Microscopic and laser granulometric analyses of hydrating cement suspensions.* Cement and Concrete Research, 1999. **29**(1): p. 3-8.
71. Autier, C., et al., *Mesostructure evolution of cement pastes with addition of superplasticizers highlighted by dispersion indices.* Powder Technology, 2013. **249**(0): p. 282-289.
72. Holzer, L., *Cryo-FIB-nanotomography for quantitative analysis of particle structures in cement suspensions.* Journal of Microscopy, 2007. **227**(3): p. 216-228.
73. Fantinel, F., et al., *Complexation of Polyacrylates by Ca2+ Ions. Time-Resolved Studies Using Attenuated Total Reflectance Fourier Transform Infrared Dialysis Spectroscopy.* Langmuir, 2004. **20**: p. 2539-2542.
74. Plank, J., B. Sachsenhauser, and J. de Reese, *Experimental determination of the thermodynamic parameters affecting the adsorption behaviour and dispersion effectiveness of PCE*

superplasticizers. Cement and Concrete Research, 2010. **40**(5): p. 699-709.
75. Bouhamed, H., S. Boufi, and A. Magnin, *Dispersion of alumina suspension using comb-like and diblock copolymers produced by RAFT polymerization of AMPS and MPEG.* Journal of Colloid and Interface Science, 2007. **312**(2): p. 279-291.
76. Plank, J. and B. Sachsenhauser, *Experimental determination of the effective anionic charge density of polycarboxylate superplasticizers in cement pore solution.* Cement and Concrete Research, 2009. **39**(1): p. 1-5.
77. Flatt, R.J. and Y.F. Houst, *A simplified view on chemical effects perturbing the action of superplasticizers.* Cement and Concrete Research, 2001. **31**(8): p. 1169-1176.
78. Zingg, A., *Cement-superplasticizer interaction: Link between macroscopic phenomena and microstructural data of the early cement hydration*, 2008, Swiss federal institute of technology Zurich.
79. Plank, J., et al., *Fundamental mechanisms for polycarboxylate intercalation into C3A hydrate phases and the role of sulfate present in cement.* Cement and Concrete Research, 2010. **40**(1): p. 45-57.
80. Plank, J., et al., *Fundamental mechanisms for polycarboxylate intercalation into C3A hydrate phases and the role of sulfate present in cement.* Cement and Concrete Research. **40**(1): p. 45-57.
81. de Gennes, P.G., *Polymers at an interface; a simplified view.* Advances in Colloid and Interface Science, 1987. **27**(3–4): p. 189-209.
82. Kauppi, A., K.M. Andersson, and L. BergstrÃ¶m, *Probing the effect of superplasticizer adsorption on the surface forces using the colloidal probe AFM technique.* Cement and Concrete Research, 2005. **35**(1): p. 133-140.
83. Flatt, R.J. and P. Bowen, *Yodel: A Yield Stress Model for Suspensions.* Journal of the American Ceramic Society, 2006. **89**(4): p. 1244-1256.
84. Garrault, S., et al., *Study of C-S-H growth on C3S surface during its early hydration.* Materials and Structures, 2005. **38**(4): p. 435-442.
85. Garrault-Gauffinet, S. and A. Nonat, *Experimental investigation of calcium silicate hydrate (C-S-H) nucleation.* Journal of Crystal Growth, 1999. **200**(3–4): p. 565-574.
86. Uchikawa, H., D. Sawaki, and S. Hanehara, *Influence of kind and added timing of organic admixture on the composition, structure*

and property of fresh cement paste. Cement and Concrete Research, 1995. **25**(2): p. 353-364.
87. Yoshioka, K., et al., *Adsorption characteristics of superplasticizers on cement component minerals.* Cement and Concrete Research, 2002. **32**(10): p. 1507-1513.
88. Neubauer, C.M., M. Yang, and H.M. Jennings, *Interparticle Potential and Sedimentation Behavior of Cement Suspensions: Effects of Admixtures.* Advanced Cement Based Materials, 1998. **8**(1): p. 17-27.
89. Plank, J. and C. Hirsch, *Impact of zeta potential of early cement hydration phases on superplasticizer adsorption.* Cement and Concrete Research, 2007. **37**(4): p. 537-542.
90. Zingg, A., et al., *Adsorption of polyelectrolytes and its influence on the rheology, zeta potential, and microstructure of various cement and hydrate phases.* Journal of Colloid and Interface Science, 2008. **323**(2): p. 301-312.
91. Basile, F., et al., *Effect of the gypsum state in industrial cements on the action of superplasticizers.* Cement and Concrete Research, 1987. **17**(5): p. 715-722.
92. Yamada, K., S. Ogawa, and S. Hanehara, *Controlling of the adsorption and dispersing force of polycarboxylate-type superplasticizer by sulfate ion concentration in aqueous phase.* Cement and Concrete Research, 2001. **31**(3): p. 375-383.
93. Plank, J., C. Schröfl, and M. Gruber, *Use of a supplemental agent to improve flowability of ultra-high performance concrete*, in *9th CANMET/ACI Conference on superplasticizers and other chemical admixtures in concrete*, T.C. Holland, P.R. Gupta, and V.M. Malhotra, Editors. 2009: Seville. p. 1-16.
94. Wu, Y., et al. *Effect of sodium gluconate on polynaphthalene sulfonate adsorption*. Advances in Cement Research, 2011. **23**, 249-254.
95. Yang, H., B.-q. Ma, and H.-b. Tan *Effect of competitive adsorption between sodium gluconate and naphthalene-based superplasticiser on fluidity of cement paste*. Magazine of Concrete Research, 2013. **65**, 1212-1218.
96. DELVO. *http://www.basf-admixtures.com/en/sustainability/eco_friendly/delvo_hca/Pages/default.aspx*. 2008.
97. Kinney, F.D., *Reuse of Returned Concrete by Hydration Control: Characterization of a New Concept*, in *Third CAN-MET/ACI Conference Superplasticizers and Other Chemical Admixtures in Concrete*1989, ACI: Ottawa, Canada. p. pp. 19-40.

98. Hanehara, S. and K. Yamada, *Interaction between cement and chemical admixture from the point of cement hydration, absorption behaviour of admixture, and paste rheology.* Cement and Concrete Research, 1999. **29**(8): p. 1159-1165.
99. Gartner EM, et al., *Hydratation of Portland cement.*, in *Structure and Performance of Cements*, Bensted J and B. P, Editors. 2002, Spon Press. Taylor and Francis Group: London. p. 57-113.
100. Damidot, D.A., D. Sorrentino, and D. Guinot, *Factors influencing the nucleation and growth of the hydrates in cementitious systems: an experimental approach*, in *2nd Int. RILEM Symposium 'Why does cement set, An interdisciplinary approach*2000, Rilem Publications. p. 161-197.
101. Jolicoeur, C., et al. *Progress in understanding the functional properties of superplasticizers in fresh concrete*. in *4th CANMET/ACI International Conference on Superplasticizers and Other Chemical Admixtures*. 1994. Montreal: ACI.
102. Nunes, S., et al., *Rheological characterization of SCC mortars and pastes with changes induced by cement delivery.* Cement and Concrete Composites, 2011. **33**.
103. Flatt, R.J., et al., *The role of adsorption energy in the sulfate-polycarboxylate competition*, in *Ninth ACI Internation Conference on Superplasticizers and Other Chemical Admixtures in Concrete*2009, ACI: Sevilla, Spain. p. 153-164.
104. Jarvis, P., et al., *A review of floc strength and breakage.* Water Research, 2005. **39**(14): p. 3121-3137.
105. Shaughnessy Iii, R. and P.E. Clark, *The rheological behavior of fresh cement pastes.* Cement and Concrete Research, 1988. **18**(3): p. 327-341.
106. Struble, L. and G.-K. Sun, *Viscosity of Portland cement paste as a function of concentration.* Advanced Cement Based Materials, 1995. **2**(2): p. 62-69.
107. Bentz, D., *Cement hydration: building bridges and dams at the microstructure level.* Materials and Structures, 2007. **40**(4): p. 397-404.
108. Schramm, G., *Introduction to Practical Viscometry*. 1981: Haake.
109. Khayat, K., M. Saric-Coric, and F. Liotta, *Influence of Thixotropy on Stability Characteristics of Cement Grout and Concrete.* ACI Materials Journal, 2002. **99**(3).
110. Yang, M., C.M. Neubauer, and H.M. Jennings, *Interparticle potential and sedimentation behavior of cement suspensions:*

Review and results from paste. Advanced Cement Based Materials, 1997. **5**(1): p. 1-7.
111. Chatterji, S., *On the properties of freshly made Portland cement paste. Part 2. sedimentation and strength of flocculation.* Cement and Concrete Research, 1988. **18**(4): p. 615-620.
112. Ferron, R.D., et al., *Aggregation and breakage kinetics of fresh cement paste.* Cement and Concrete Research, 2013. **50**(0): p. 1-10.
113. Yim, H.J., J.H. Kim, and S.P. Shah, *Cement particle flocculation and breakage monitoring under Couette flow.* Cement and Concrete Research, 2013. **53**(0): p. 36-43.
114. Betioli, A.M., et al., *Effect of HMEC on the consolidation of cement pastes: Isothermal calorimetry versus oscillatory rheometry.* Cement and Concrete Research, 2009. **39**(5): p. 440-445.
115. Banfill, P.F.G. and D.C. Saunders, *On the viscometric examination of cement pastes.* Cement and Concrete Research, 1981. **11**(3): p. 363-370.
116. Barnes, H.A., *Thixotropy—a review.* Journal of Non-Newtonian Fluid Mechanics, 1997. **70**(1–2): p. 1-33.
117. Petkova, V. and V. Samichkov, *Some influences on the thixotropy of composite slag Portland cement suspensions with secondary industrial waste.* Construction and Building Materials, 2007. **21**(7): p. 1520-1527.
118. Grzeszczyk, S. and L. Kucharska, *The influence of alkalis on rheological properties of fresh cement pastes.* Cement and Concrete Research, 1988. **18**(1): p. 1-8.
119. Gaskin, A.J. *Chemistry of Cement Proceedings of the Fourth International Symposium* in *Chemistry of Cement*. 1960. Washington: U.S. Department of Commerce.
120. Roussel, N., *Understanding the rheology of concrete*. 2012, Cambridge: Woodhead Publishing Limited.
121. Jiang, S.P., J.C. Mutin, and A. Nonat, *Studies on mechanism and physico-chemical parameters at the origin of the cement setting. I. The fundamental processes involved during the cement setting.* Cement and Concrete Research, 1995. **25**(4): p. 779-789.
122. Grzeszczyk, S. and L. Kucharska, *Hydrative reactivity of cement and rheological properties of fresh cement pastes.* Cement and Concrete Research, 1990. **20**(2): p. 165-174.
123. Bonen, D. and S.L. Sarkar, *The superplasticizer adsorption capacity of cement pastes, pore solution composition, and parameters affecting flow loss.* Cement and Concrete Research, 1995. **25**(7): p. 1423-1434.

124. Vikan, H., et al., *Correlating cement characteristics with rheology of paste.* Cement and Concrete Research, 2007. **37**(11): p. 1502-1511.
125. Ovarlez, G., et al., *Flows and heterogeneities with a vane tool : Magnetic resonance imaging measurements.* Journal of Rheology, 2011. **55**(2): p. 197.
126. Cheng, D.C.-H. and F. Evans, *Phenomenological characterization of the rheological behaviour of inelastic reversible thixotropic and antithixotropic fluids.* British Journal of Applied Physics, 1965. **16**(11): p. 1599.
127. Roussel, N., *A thixotropy model for fresh fluid concretes: Theory, validation and applications.* Cement and Concrete Research, 2006. **36**(10): p. 1797-1806.
128. Schultz, M.A. and L.J. Struble, *Use of oscillatory shear to study flow behavior of fresh cement paste.* Cement and Concrete Research, 1993. **23**(2): p. 273-282.
129. Saasen, A., et al., *Oscillating rheometer measurements on oilfield cement slurries.* Cement and Concrete Research, 1991. **21**(1): p. 109-119.
130. Papo, A. and B. Caufin, *A study of the hydration process of cement pastes by means of oscillatory rheological techniques.* Cement and Concrete Research, 1991. **21**(6): p. 1111-1117.
131. Banfill, P.F.G., R.E. Carter, and P.J. Weaver, *Simultaneous rheological and kinetic measurements on cement pastes.* Cement and Concrete Research, 1991. **21**(6): p. 1148-1154.
132. Matschei, T., *Thermodynamics of Cement Hydration*, in *Department of Chemistry*2007, University of Aberdeen: Aberdeen.
133. Damidot, D. and F.P. Glasser, *Investigation of the CaO-Al2O3-SiO2-H2O system at 25 °C by thermodynamic calculations.* Cement and Concrete Research, 1995. **25**(1): p. 22-28.
134. Reardon, E.J., *An ion interaction model for the determination of chemical equilibria in cement/water systems.* Cement and Concrete Research, 1990. **20**(2): p. 175-192.
135. Lothenbach, B. and F. Winnefeld, *Thermodynamic modelling of the hydration of Portland cement.* Cement and Concrete Research, 2006. **36**(2): p. 209-226.
136. Matschei, T., B. Lothenbach, and F.P. Glasser, *Thermodynamic properties of Portland cement hydrates in the system CaO–Al2O3–SiO2–CaSO4–CaCO3–H2O.* Cement and Concrete Research, 2007. **37**(10): p. 1379-1410.

137. Lothenbach, B., et al., *Hydration of a low-alkali CEM III/B–SiO2 cement (LAC).* Cement and Concrete Research, 2012. **42**(2): p. 410-423.
138. Winnefeld, F. and B. Lothenbach, *Hydration of calcium sulfoaluminate cements — Experimental findings and thermodynamic modelling.* Cement and Concrete Research, 2010. **40**(8): p. 1239-1247.
139. Lothenbach, B., *Thermodynamic equilibrium calculations in cementitious systems.* Materials and Structures, 2010. **43**(10): p. 1413-1433.
140. Rothstein, D., et al., *Solubility behavior of Ca-, S-, Al-, and Si-bearing solid phases in Portland cement pore solutions as a function of hydration time.* Cement and Concrete Research, 2002. **32**(10): p. 1663-1671.
141. http://gems.web.psi.ch/. Gibbs Energy Minimization Software for Geochemical Modeling.
142. Lothenbach, B., et al., *Thermodynamic modelling of the effect of temperature on the hydration and porosity of Portland cement.* Cement and Concrete Research, 2008. **38**(1): p. 1-18.
143. Brown, P.W. and J.V. Bothe *The stability of ettringite*. Advances in Cement Research, 1993. **5**, 47-63.
144. Clark, B.A. and P.W. Brown, *The formation of calcium sulfoaluminate hydrate compounds: Part I.* Cement and Concrete Research, 1999. **29**(12): p. 1943-1948.
145. Thomas, J.J., et al., *Effect of hydration temperature on the solubility behavior of Ca-, S-, Al-, and Si-bearing solid phases in Portland cement pastes.* Cement and Concrete Research, 2003. **33**(12): p. 2037-2047.
146. Jawed, I. and J. Skalny, *Alkalies in cement: A review: II. Effects of alkalies on hydration and performance of Portland cement.* Cement and Concrete Research, 1978. **8**(1): p. 37-51.
147. Prince, W., M. Espagne, and P.C. Aïtcin, *Ettringite formation: A crucial step in cement superplasticizer compatibility.* Cement and Concrete Research, 2003. **33**(5): p. 635-641.
148. Vernet, C., *Mécanismes chimiques d'interactions ciment-adjuvant*, in *Service Physico-chimie du Ciment*1995, GTC Spa: Guerville.
149. Aïtcin, P.C., *High-performance concrete*. 2011: CRC Press.
150. Uchikawa, H., et al., *Effect of admixture on hydration of cement, adsorptive behavior of admixture and fluidity and setting of fresh cement paste.* Cement and Concrete Research, 1992. **22**(6): p. 1115-1129.

151. Locher, F.W., *Cement. Principles of Production and Use*. 2006, Düsseldorf: Vbt Verlag Bau U. Technik.
152. Vikan, H., *Rheology and Reactivity of Cementitious Binders with Plasticizers*, in *Materials Science and Engineering*2005, NTNU: Norwegian.
153. De Schutter, G., *Hydration and temperature development of concrete made with blast-furnace slag cement.* Cement and Concrete Research, 1999. **29**(1): p. 143-149.
154. Lawrence, P., M. Cyr, and E. Ringot, *Mineral admixtures in mortars: Effect of inert materials on short-term hydration.* Cement and Concrete Research, 2003. **33**(12): p. 1939-1947.
155. Jolicoeur, C. and M.-A. Simard, *Chemical admixture-cement interactions: Phenomenology and physico-chemical concepts.* Cement and Concrete Composites, 1998. **20**(2–3): p. 87-101.
156. Hunter, R.J., *Foundations of Colloid Science*. 2nd ed. 2001: Oxford.
157. Plank, J. and G. Bassioni, *Adsorption of Carboxylate Anions on a CaCO3 Surface.* Zeitschrift für Naturforschung 2007. **62b**: p. 1277-1284.
158. Gyurcsik, B., *Carbohydrates as ligands: coordination equilibria and structure of the metal complexes.* Coordination chemistry reviews, 2000. **203**(1): p. 81.
159. Phadungath, C., *Effect of sodium gluconate on the solubility of calcium lactate.* Journal of dairy science, 2011. **94**(10): p. 4843.
160. Flatt, R.J., et al., *Conformation of adsorbed comb copolymer dispersants.* Langmuir, 2008. **25**(2): p. 845-855.
161. Rudan-Tasic, D. and C. Klofutar, *Apparent Specific Volume and Apparent Specific Refraction of Some Poly(oxyethylene) Glycols in 1,4-Dioxane and Benzene Solutions at 298.15 K.* Monatshefte für Chemie, 2004. **135**(10): p. 1209-1224.
162. Prince, W., M. Edwards-Lajnef, and P.C. Aïtcin, *Interaction between ettringite and a polynaphthalene sulfonate superplasticizer in a cementitious paste.* Cement and Concrete Research, 2002. **32**(1): p. 79-85.
163. Rößler, C., et al., *Influence of hydration on the fluidity of normal Portland cement pastes.* Cement and Concrete Research, 2008. **38**(7): p. 897-906.
164. Aïtcin, P.C., *Binders for Durable and Sustainable Concrete*. 2008: Taylor & Francis Group.
165. Rößler, C., et al., *Influence of hydration on the fluidity of normal Portland cement pastes.* Cement and Concrete Research, 2008. **38**(7): p. 897-906.

166. Nagataki, S. and S. Kawano, in *Seventh Intl. Congress on the Chem. of Cement*1980: Paris.
167. Helmuth, R.A. in *Seventh Intl. Congress on the Chem. of Cement* 1980. Paris.
168. Ferrari, L., et al., *Impact of particle size on interaction forces between ettringite and dispersing comb-polymers in various electrolyte solutions.* Journal of Colloid and Interface Science, 2014. **419**(0): p. 17-24.
169. Gaskin, A.J. in *4th Intl. Symp. Chem. Cement*. 1966. Washington, DC.
170. Roy, D.M. and K. Asaga, *Rheological properties of cement mixes: III. The effects of mixing procedures on viscometric properties of mixes containing superplasticizers.* Cement and Concrete Research, 1979. **9**(6): p. 731-739.
171. Juenger, M.C.G., et al., *A soft X-ray microscope investigation into the effects of calcium chloride on tricalcium silicate hydration.* Cement and Concrete Research, 2005. **35**(1): p. 19-25.
172. Garci Juenger, M.C. and H.M. Jennings, *The use of nitrogen adsorption to assess the microstructure of cement paste.* Cement and Concrete Research, 2001. **31**(6): p. 883-892.
173. Young, J.F., R.L. Berger, and F.V. Lawrence Jr, *Studies on the hydration of tricalcium silicate pastes III. Influence of admixtures on hydration and strength development.* Cement and Concrete Research, 1973. **3**(6): p. 689-700.
174. Nguyen, D.-T., et al., *Microindentation creep of monophasic calcium–silicate–hydrates.* Cement and Concrete Composites, 2014. **48**(0): p. 118-126.
175. Björnström, J., et al., *Accelerating effects of colloidal nano-silica for beneficial calcium–silicate–hydrate formation in cement.* Chemical Physics Letters, 2004. **392**(1–3): p. 242-248.
176. Hou, D., et al., *Calcium silicate hydrate from dry to saturated state: Structure, dynamics and mechanical properties.* Acta Materialia, 2014. **67**(0): p. 81-94.
177. Alizadeh, R., J.J. Beaudoin, and L. Raki, *Viscoelastic nature of calcium silicate hydrate.* Cement and Concrete Composites, 2010. **32**(5): p. 369-376.
178. Pellenq, R.J.-M., et al., *A realistic molecular model of cement hydrates.* Proceedings of the National Academy of Sciences, 2009. **106**(38): p. 16102-16107.
179. Venkovic, N., L. Sorelli, and F. Martirena, *Nanoindentation study of calcium silicate hydrates in concrete produced with effective*

microorganisms-based bioplasticizer. Cement and Concrete Composites, (0).

180. Scherer, G.W., J. Zhang, and J.J. Thomas, *Nucleation and growth models for hydration of cement.* Cement and Concrete Research, 2012. **42**(7): p. 982-993.
181. Thomas, J.J., A.J. Allen, and H.M. Jennings, *Hydration Kinetics and Microstructure Development of Normal and $CaCl_2$-Accelerated Tricalcium Silicate Pastes.* J. Phys. Chem. C, 2009. **113**(46): p. 19836-19844.
182. Jennings, H.M., *Refinements to colloid model of C-S-H in cement: CM-II.* Cement and Concrete Research, 2008. **38**(3): p. 275-289.

List of publications

Articles in internationally reviewed academic journals

Lesage, K., Cizer, Ö., Desmet, B., Vantomme, J., De Schutter, G., Vandewalle, L. (2014). Plasticizing Mechanism of Sodium Gluconate Combined with PCE. Advances in Cement Research, DOI : 10.1680/adcr.13.00087.

Lesage, K., Cizer, Ö., Desmet, B., Vantomme, J., De Schutter, G., Vandewalle, L. (2014). Rheological characterization of the influence of hydration on agglomeration kinetics in cement paste. Materials and Structures, under review.

Onisei, S., Lesage, K., Blanpain, B., Pontikes, Y., Synthesis of inorganic polymers from a Fe-silicate precursor, in preparation.

Papers at international scientific conferences

Lesage, K., Cizer, Ö., Vandewalle, L., Desmet, B., Deschutter, G., Vantomme, J. (2013). Effects of combined chemical admixtures on cement paste rheology. In Roussel, N. (Ed.), Proceedings of the 7th International Conference on Self-Compacting Concrete (on cd-rom). International Conference on Self-Compacting Concrete. Paris, France, 2-4 September 2013 (pp. 1-6). Paris: IFSTTAR.

Lesage, K., Andries, J., Vandewalle, L. (2013). Air-void characterisation of self-compacting concrete. In Roussel, N. (Ed.), Proceedings of the 7th International Conference on Self-Compacting Concrete (on cd-rom).

International Conference on Self-Compacting Concrete. Paris, France, 2-4 September 2013 (pp. 1-6). Paris: IFSTTAR.

Lesage, K., Cizer, Ö., Vandewalle, L., Desmet, B., Deschutter, G., Vantomme, J. (2013). Influence of sodium gluconate on cement paste viscosity. . American Conference on the Design and Use of Self-Consolidating Concrete. Chicago, 12-15 May 2013.

Lesage, K., Nullens, S., Vandewalle, L., Van Itterbeeck, P. (2013). Mechanical behaviour of self compacting concrete at young ages. Conference on Advances in Cement and Concrete Technology in Africa. South Africa, 28-31 January 2013.

Lesage, K., Cizer, Ö., Vandewalle, L., Desmet, B., De Schutter, G., Vantomme, J. (2012). Calcium nitrate counteracting PCE superplasticizer retardation. In Malhotra, V. (Ed.), Superplasticizers and Other Chemical Admixtures in Concrete. International conference on superplasticizers and other chemical admixtures in concrete. Prague, October 2012 (art.nr. SP-288.06) (pp. 89-100). US: American Concrete Institute.

Lesage, K., Cizer, Ö., Vandewalle, L., Desmet, B., Deschutter, G., Vantomme, J. (2012). Effect of PCE on the rheology of cement paste. In Russell, M. (Ed.), 32nd Cement and Concrete Science Conference 2012. Cement and Concrete Science Conference. Belfast, 17-18 September 2012 (pp. 234-238). UK: Queen's University of Belfast.

Lesage, K., Cizer, Ö., Vandewalle, L., Desmet, B., Deschutter, G., Vantomme, J. (2011). Influence of Plasticizer Type on Hydration Kinetics of Self-Compacting Concrete. In Zaragoza, A. (Ed.), López Agüí, J. (Ed.), Palomo, Á. (Ed.), Proc. of the 13th Int. Congr. on the Chemistry of Cement (XIII ICCC), ISBN CD 84-7292-400-0. International Congress on the chemistry of cement. Madrid, 3-8 July 2011.

Desmet, B., Group, S., Vantomme, J., De Schutter, G., Lesage, K., Vandewalle, L. (2010). Parametric Study of the Effects of the Composition on the Setting of Self-Compacting Mortar, using Continuous Ultrasonic Monitoring. Design, Production and Placement of Self-Consolidating Concrete. SCC2010. Montreal, 26-29 September 2010 Springer.

Van Itterbeeck, P., Cauberg, N., Parmentier, B., Vandewalle, L., Lesage, K. (2010). Evaluation of the Cracking Potential of Young Self-Compacting Concrete. Design, Production and Placement of Self-Consolidating Concrete. SCC2010. Montreal, 26-29 September 2010 Springer.

Van Itterbeeck, P., Cauberg, N., Parmentier, B., Vandewalle, L., Lesage, K. (2010). Eurocode 2 Predictions vs. Mechanical Properties of Self-Compacting Concrete. Design, Production and Placement of Self-consolidating Concrete.. SCC2010. Montreal, 26-29 September 2010 Springer.